



UNIVERSIDADE ESTADUAL DE CAMPINAS
FACULDADE DE ENGENHARIA MECÂNICA
E INSTITUTO DE GEOCIÊNCIAS

PEDRO MARCELO ADRIAN HERBAS

**ADVANCED PRODUCTION DATA ANALYSIS IN
NATURALLY FRACTURED RESERVOIRS**

**(ANÁLISE AVANÇADA DE DADOS DE PRODUÇÃO
EM RESERVATÓRIOS NATURALMENTE
FRATURADOS)**

CAMPINAS
2015

PEDRO MARCELO ADRIAN HERBAS

**ADVANCED PRODUCTION DATA ANALYSIS IN
NATURALLY FRACTURED RESERVOIRS**

**(ANÁLISE AVANÇADA DE DADOS DE PRODUÇÃO EM
RESERVATÓRIOS NATURALMENTE FRATURADOS)**

Dissertation presented to the Mechanical Engineering Faculty and Geosciences Institute of the University of Campinas in partial fulfillment of the requirements for the degree of Master in Petroleum Sciences and Engineering in the area of [Reservoirs and Management](#).

Dissertação apresentada à Faculdade de Engenharia Mecânica e Instituto de Geociências da Universidade Estadual de Campinas como parte dos requisitos exigidos para a obtenção do título de [Mestre](#) em Ciências e Engenharia de Petróleo na área de [Reservatórios e Gestão](#).

Orientador: Profa. Dra. Rosângela Barros Zanoni Lopes Moreno

Este exemplar corresponde à versão final da dissertação defendida pelo aluno [Pedro Marcelo Adrian Herbas](#), e orientado pelo Profa. Dra. Rosângela Barros Zanoni Lopes Moreno.



Assinatura do Orientador

CAMPINAS
2015

Agência(s) de fomento e nº(s) de processo(s): CAPES, 33003017

Ficha catalográfica
Universidade Estadual de Campinas
Biblioteca da Área de Engenharia e Arquitetura
Elizangela Aparecida dos Santos Souza - CRB 8/8098

A84a Adrian Herbas, Pedro Marcelo, 1983-
Advanced production data analysis in naturally fractured reservoirs / Pedro
Marcelo Adrian Herbas. – Campinas, SP : [s.n.], 2015.

Orientador: Rosângela Barros Zanoni Lopes Moreno.
Dissertação (mestrado) – Universidade Estadual de Campinas, Faculdade
de Engenharia Mecânica e Instituto de Geociências.

1. Reservatórios. 2. Reservatórios - Fratura. 3. Rochas carbonáticas. 4.
Poços de petróleo - Testes. I. Moreno, Rosângela Barros Zanoni Lopes, 1966-.
II. Universidade Estadual de Campinas. Faculdade de Engenharia Mecânica.
III. Título.

Informações para Biblioteca Digital

Título em outro idioma: Análise avançada de dados de produção em reservatórios
naturalmente fraturados

Palavras-chave em inglês:

Reservoirs

Reservoirs - Fracture

Carbonate rocks

Área de concentração: Reservatórios e Gestão

Titulação: Mestre em Ciências e Engenharia de Petróleo

Banca examinadora:

Rosângela Barros Zanoni Lopes Moreno [Orientador]

Osvair Vidal Trevisan

Álvaro Marcello Marco Peres

Data de defesa: 16-12-2015

Programa de Pós-Graduação: Ciências e Engenharia de Petróleo

UNIVERSIDADE ESTADUAL DE CAMPINAS
FACULDADE DE ENGENHARIA MECÂNICA
E INSTITUTO DE GEOCIÊNCIAS
DISSERTAÇÃO DE MESTRADO ACADÊMICO

ADVANCED PRODUCTION DATA ANALYSIS IN
NATURALLY FRACTURED RESERVOIRS

Autor: Pedro Marcelo Adrian Herbas

Orientador: Profa. Dra. Rosângela Barros Zanoni Lopes Moreno

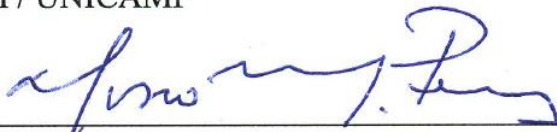
A banca examinadora composta pelos membros abaixo aprovou esta dissertação:



Profa. Dra. Rosângela Barros Zanoni Lopes Moreno, Presidente
DE / FEM / UNICAMP



Prof. Dr. Osvair Vidal Trevisan
DE / FEM / UNICAMP



Dr. Álvaro Marcello Marco Peres
Consultor Independente

Campinas, 16 de dezembro de 2015.

DEDICATION

This work is dedicated to:

The Lord for giving me the life, caring, guidance, and all blessings received.

My dear parents Julio Adrian and Clery Herbas, who are both models of the person I hope to become.

My beloved life's companion Diana Torrez, who always encouraged, supported and believed in me.

Freddy Espinoza, Jaime Soria, Edgar Sagarnaga, Luis Cruz and R. Marcelo Michel who encourage me to continue with the next step in academic life.

My teachers and mentors.

My friends.

ACKNOWLEDGEMENTS

I would like to thank University of Campinas for providing me the opportunity to conduct this research.

I would especially like to thank my advisor Dr. Rosângela Barros Zanoni Lopez Moreno for guiding me in this research and sharing her knowledge and experience with me.

I would also like to thank Dr. Osvaldo Trevisan, Dr. Denis Schiozer and Dr. Álvaro Peres for serving as members of my advisory committee and for their valuable comments on this work.

I would like to thank Dr. Blasingame, Dr. Mattar and Dr. Anderson for their comments and suggestions about this work.

Thanks to Diana Torrez, Robison Saalfeld and Kelly Quispe for listening, arguing and sharing opinions about my work.

I greatly appreciate all those people who have helped me along the way, this experience would have been worse off without your support: Alice Kiyoka Obata, Michelle Cristina Fulaneto, Giselle A. Moreira Palermo, Délcio Antonio R. da Silva.

I would like to thank CAPES for providing the funding of my studies and to the government of Brazil for their support to scientific research.

Finally, I would like to thank “YPFB Corporacion” who was the provider of the field data for the analysis of the methods proposed.

Thank you

“Opportunity is missed by most people because it is dressed in overalls and looks like work....”

Thomas A. Edison,

ABSTRACT

In recent years there has been an increasing interest in the use of Advanced Production Data Analysis (APDA) methods for dynamic reservoir description. These methods analyze available daily production data, reducing the need of well testing operations, avoiding production loss, with accuracy comparable to Pressure Transient Analysis (PTA). Different APDA models have been proposed for homogeneous, coalbed methane and shale gas reservoirs. Nevertheless, production from naturally fractured reservoirs, such as Carbonates or Siliciclastic, is still being analyzed as homogeneous systems with current APDA techniques.

This work presents the analytical derivation of two APDA methods (Dynamic Material Balance and Blasingame Type Curves) based on the dual porosity model, to analyze daily production of Naturally Fractured Reservoirs (NFR). Both interporosity flow models between matrix and fractures, pseudosteady-state and transient (slabs and spheres), were evaluated. The development was based on long-time approximate solutions of diffusivity equation for constant flow rate in a closed system with no-flow boundary. These approximations were compared with the exact solution given in Laplace space, inverted to time domain applying the Gaver-Stehfest algorithm.

The validation of the derived methods was made using synthetic production and flowing pressure data, generated by a numerical simulator, and real field data from a gas-condensate naturally fractured reservoir. Results confirmed that naturally fractured reservoirs with pseudosteady-state interporosity flow could present two boundary-dominated behaviors (fracture and total systems). Fracture permeability and wellbore skin are functions of ω and λ variables. Fractured reservoirs with transient interporosity flow between matrix and fracture system, can be analyzed using current APDA techniques developed for homogeneous systems.

Key Word: Advanced Production Data Analysis, Naturally Fractured Reservoirs, Pseudosteady-State radial flow, Material Balance time.

RESUMO

Nos últimos anos tem havido um interesse crescente no uso dos métodos de Análise Avançada de Dados de Produção (AADP) para a descrição dinâmica do reservatório. A partir destes métodos analisam-se dados de produção diárias disponíveis, reduzindo a necessidade de operações de teste de poço, evitando perda de produção e com uma exatidão comparável à Análise de Transiente de Pressão. Diferentes modelos AADP têm sido propostos para reservatórios de óleo e gás homogêneos, de metano em camadas de carvão e de gás de xisto. No entanto, a produção de reservatórios naturalmente fraturados, tais como rochas carbonáticas ou siliciclásticas, ainda está sendo analisada como sistemas homogêneos utilizando métodos AADP atuais.

Este trabalho apresenta a derivação analítica de dois métodos de AADP (Balanço de materiais dinâmico e curvas tipo de Blasingame) baseados no modelo de dupla porosidade, para analisar a produção diária de reservatórios naturalmente fraturados. Foram avaliados a transferência matriz-fratura pseudo-permanente e transiente (camadas e esferas). O desenvolvimento foi baseado nas soluções aproximadas de longo tempo da equação da difusividade em sistemas de dupla porosidade, para vazão constante em reservatórios fechados sem fluxo na fronteira. As aproximações foram comparadas com a solução exata, dada pela inversa da solução no espaço Laplace, obtida utilizando o algoritmo de Gaver-Stehfest.

A validação foi feita usando dados de produção e pressão de fluxo sintéticos, gerados por um simulador numérico, e dados reais de campo de um reservatório de gás-condensado naturalmente fraturado. Os resultados confirmaram que reservatórios naturalmente fraturados com fluxo interporoso pseudo-permanente podem apresentar dois comportamentos dominado pelos limites do reservatório (fraturas y sistema total). A permeabilidade da fratura e o dano do poço são dependentes variáveis ω e λ . Reservatórios fraturados com fluxo interporoso transiente podem ser analisados utilizando técnicas de AADP atuais desenvolvidas para sistemas homogêneos.

Palavras Chave: Análise Avançada de Dados de Produção, Reservatórios Naturalmente Fraturados, Fluxo Radial Pseudo-Permanente, Tempo de Balanço de Materiais.

TABLE OF CONTENTS

1. INTRODUCTION.....	29
1.1. Background of this research.....	29
1.2. Objectives	30
1.3. Organization of the dissertation	30
2. PRODUCTION DATA ANALYSIS	33
2.1. Classification of Production Data Analysis	33
2.2. Production Data Analysis in Homogeneous Reservoirs	34
2.3. Production Data Analysis in NFR	46
3. PRESSURE TRANSIENT ANALYSIS IN NFR	49
3.1. Pseudosteady-state Interporosity flow Model.....	49
3.2. Transient Interporosity flow Model.....	53
4. DEVELOPMENT OF ADVANCED PRODUCTION DATA ANALYSIS FOR NFR ..	57
4.1. Definition of Dimensionless Variables.....	58
4.2. Long-Time Approximations for Dual Porosity Model	58
4.3. Material Balance Time in Naturally Fractured Reservoirs	62
4.4. Derivation of Production Data Analysis Methods for NFR.....	63
4.5. Considerations for Gas-Condensate Reservoirs.....	72
5. VALIDATION OF THE METHODS.....	73
5.1. Reservoir Simulation Model	73
5.2. Field Case Study: Devonian Gas-Condensate Field	82
5.3. Discussion of the Results	93
6. SUMMARY AND CONCLUSIONS	97
6.1. Summary	97
6.2. Conclusions.....	98
6.3. Recommendations for Future Work.....	99

LIST OF FIGURES

Figure 2.1 – Composite of analytic and empirical type curves (After Fetkovich 1987)	35
Figure 2.2 – $\Delta p/q_o$ vs. t_c curves for cases simulated analytically (After Blasingame and Lee 1986).....	36
Figure 2.3 – Fetkovich-McGray type curves (After Palacio and Blasingame 1993)	38
Figure 2.4 – Converting constant rate and constant BHP to equivalent rate liquid data, radial case (After Agarwal et al. 1999).....	39
Figure 2.5 – Bounded rectangular reservoir with multiple wells located at arbitrary positions within the reservoir (After Marhaendrajana and Blasingame 2000)	40
Figure 2.6 – Inverse productivity index plot (After Mattar and Anderson 2005)	42
Figure 2.7 – Typical Cartesian plot of dry-gas normalized pseudo-pressure vs. dry gas material balance pseudo-time for a constant rate gas condensate well during boundary-dominated flow regime (After Arablo et al. 2007).....	46
Figure 2.8 – Effect of a constant storativity ratio on behavior of the solution in NFR (After Gerami et al. 2007)	47
Figure 3.1 – Idealization of the heterogeneous porous medium (After Warren and Root).....	50
Figure 3.2 – Limiting forms of naturally fractured reservoir pressure behavior (After Mavor and Cinco Ley)	51
Figure 3.3 – Idealization of a heterogeneous porous medium – Kazemi (Slabs) and De Swan (Spheres).....	54
Figure 4.1 – Comparison of approximate solutions for a dual porosity finite reservoir and PPS interporosity flow, produced at constant rate. $r_{eD} = 100$; $\omega = 0.01$; $\lambda = 1 \times 10^{-6}$	59
Figure 4.2 – Comparison of approximate solutions for a dual porosity finite reservoir and transient interporosity flow, produced at constant rate. $r_{eD} = 100$; $\omega = 0.01$; $\lambda = 1 \times 10^{-6}$	61
Figure 4.3 – Comparison of diffusivity solutions for dual porosity system between constant flow rate ($1/P_{wDf}$) and constant flowing pressure (q_{Df}). $r_{eD} = 100$; $\omega = 0.1$; $\lambda = 1 \times 10^{-4}$	63
Figure 4.4 – Inverse productivity plot for Dual Porosity System.....	66
Figure 4.5 – Material balance plot for dual porosity system.	68
Figure 4.6 – Decline type curves for dual porosity systems. $r_{eD} = 100$; $\lambda = 1 \times 10^{-4}$	70

Figure 5.1 – Production history plot. Constant gas flow rate.	75
Figure 5.2 – Inverse productivity plot for dual porosity system. Constant gas flow rate.	75
Figure 5.3 – Blasingame type curves for dual porosity system. Constant gas flow rate. $r_{eD} = 12000$ and $\lambda = 6E-8$	76
Figure 5.4 – Total compressibility and storativity ratio vs. pressure.	78
Figure 5.5 – Production history plot. Variable oil flow rate.	80
Figure 5.6 – Inverse productivity plot for dual porosity system. Variable oil flow rate.	81
Figure 5.7 – Blasingame type curves for dual porosity system. Variable oil rate case. $\omega = 0.1$ and $\lambda = 5E-8$	81
Figure 5.8 – Structural map. Field case study.	83
Figure 5.9 – Longitudinal section of the reservoir. Field case study.	84
Figure 5.10 – Gas production flow rate of all four wells.	85
Figure 5.11 – Bottomhole Pressure History. Well X-3.	87
Figure 5.12 – Diagnostic plot: Gas flow rate and BHP vs. time. Well X-3.	87
Figure 5.13 – Diagnostic plot: Pressure-rate plot. Well X-3.	88
Figure 5.14 – Inverse productivity plot for dual porosity system. Well X-3.	89
Figure 5.15 – Material balance plot for dual porosity system. Well X-3.	90
Figure 5.16 – Blasingame type curves for dual porosity system. Well X-3. $r_{eD} = 1E5$ and $\lambda = 6E-8$	91
Figure D.1 – Decline type curves for dual porosity systems. $r_{eD} = 100$; $\lambda = 1 \times 10^{-4}$	118
Figure D.2 – Decline type curves for dual porosity systems. $r_{eD} = 100$; $\omega = 0.1$	119
Figure D.3 – Decline type curves for dual porosity systems. $\omega = 0.1$; $\lambda = 1 \times 10^{-4}$	119

LIST OF TABLES

Table 2.1 – Production Analysis Methods	34
Table 5.1 – Reservoir and fluid properties for the simulated example: Gas reservoir	74
Table 5.2 – General production information	74
Table 5.3 – Match point for dual porosity system type curve: Constant gas flow rate	77
Table 5.4 – Results of DMB and type curve methods: Constant gas flow rate.....	77
Table 5.5 – Reservoir and fluid properties for the simulated example: Oil reservoir	79
Table 5.6 – General Production Information.....	79
Table 5.7 – Variable Oil Flow Rate Schedule.....	80
Table 5.8 – Match point for dual porosity system type curve: Variable oil flow rate.....	82
Table 5.9 – Results of DMB and type curve methods: Variable oil flow rate.	82
Table 5.10 – Reservoir and fluid properties for the real field case study.....	86
Table 5.11 – Match point for dual porosity system type curve. Well X-3.	91
Table 5.12 – Determination of the total Original Gas-in-Place: DMB method.	92
Table 5.13 – Results of DMB and type curve methods. Real field case study.....	92

LIST OF ACRONYMS

APDA	Advanced Production Data Analysis
BP	British Petroleum
BHP	Bottomhole Pressure
CMB	Conventional Material Balance
CVD	Constant Volume Depletion
DMB	Dynamic Material Balance
GE	Gas Equivalent
NFR	Naturally Fractured Reservoir
NPI	Normalized Pressure Integral
OGIP	Original Gas-in-Place
OOIP	Original Oil-in-place
PDA	Production Data Analysis
PI	Productivity Index
PSS	Pseudosteady-state
PTA	Pressure Transient Analysis
PVT	Pressure, Volume and Temperature

LIST SYMBOLS

α	Shape Factor of the model
β_D	Multi-well interaction coefficient
ρ_{gsc}	Molar density of gas component at standard conditions (lb/cf)
ρ_{gsc}	Molar density of condensate component at standard conditions (lb/cf)
ϕ	Effective Porosity in homogeneous system
ϕ_f	Fracture Porosity in heterogeneous system
ϕ_m	Matrix Porosity in heterogeneous system
λ	Interporosity flow coefficient
γ	Euler's constant = 0.577216..
η	Diffusivity (ft ² /s)
π	Pi constant = 3.14159..
ψ_i	Initial pseudo-pressure (psi ² /cp)
ψ_{wf}	Flowing bottomhole pseudo-pressure (psi ² /cp)
$\bar{\psi}$	Average pseudo- pressure of total system (psi ² /cp)
τ	Dummy variable
μ	Fluid viscosity at average pressure (cp)
ω	Storativity Ratio
A	Area of the reservoir (ft ²)
b	Exponential decline
b_{pss}	Inverse productivity index for oil (psi ² /cp / STBday) – single well system
$b_{pss\ mw}$	Inverse productivity index for oil (psi ² /cp / STBday) – multi-well system
$b_{a\ pss}$	Inverse productivity index for gas (psi ² /cp / Mscf/day)
\tilde{b}_{pss}	Inverse productivity index in NFR for oil (psi ² /cp / STB/day)
$\tilde{b}_{a\ pss}$	Inverse productivity index in NFR for gas (psi ² /cp / Mscf/day)
B	Fluid volumetric factor (cf/scf)
C_A	Reservoir shape factor
c	Fluid compressibility (psi ⁻¹)

c_e	Effective compressibility (psi-1)
c_t	Total compressibility (psi-1)
c_g	Gas compressibility (psi-1)
c_g^*	Two-phase gas compressibility (psi-1)
c_p	Effective pore compressibility (psi-1)
c_m	Total matrix compressibility (psi-1)
c_f	Total fracture compressibility (psi-1)
D_i	Initial decline rate (1/day)
e	Neperian number = 2,718281...
$f(u)$	Interporosity flow function
$G\omega$	Original Gas-in-place of the fracture system (scf)
G	Original Gas-in-place of the total system (fracture + matrix) (scf)
G^*	Total Original Gas-in-place including condensate equivalent (scf)
G_p	Cumulative gas production (scf)
G_p^*	Total cumulative gas production including condensate equivalent (scf)
h	Net thickness (ft)
I_o	Modified Bessel function, first kind, zero order
I_1	Modified Bessel function, first kind, first order
k	Effective permeability (md)
K_o	Modified Bessel function, second kind, zero order
K_1	Modified Bessel function, second kind, first order
K_2	Modified Bessel function, second kind, second order
m_a	Invers productivity plot slope for gas in homogeneous system (psi/scf)
n	Number of moles (lb/gmol)
n_i	Initial moles-in-place (lb/gmol)
n_p	Cumulative mole production (lb/gmol)
N	Original Oil-in-place or Original Condensate-in-place (STB)
N_p	Cumulative oil production or Cumulative condensate production (STB)
P	Pressure (psia)
\bar{P}	Average pressure of total system (psi)
P_{sc}	Standard condition Pressure (14.65 psia)
ΔP	Pressure drop (psia)

P_p	Normalized pseudo-pressure (psia)
P_D	Dimensionless pressure
P_{wD}	Dimensionless pressure at the wellbore
P_{wDf}	Fracture dimensionless pressure at the wellbore
$\overline{P_{wDf}}$	Fracture dimensionless pressure at the wellbore in Laplace domain
P_{Di}	Dimensionless pressure integral
q_o	Oil flow rate (STB/d)
q_g	Total gas flow rate (MMscf/d)
$q(t)$	Flow rate at a time t (STB/d)
q_i	Initial flow rate (STB/d)
q_D	Dimensionless flow rate for homogeneous system
q_{Df}	Dimensionless flow rate for heterogeneous system
q_{Dd}	Decline curve dimensionless flow rate for homogeneous system
q_{Ddf}	Decline curve dimensionless flow rate for heterogeneous system
QN	Normalized cumulative gas production (scf)
R	Instantaneous gas to condensate ratio (scf/STB)
R_v	Vaporized oil in gas phase (STB/MMscf)
R_s	Solution gas-oil ratio (scf/STB)
r_m	Sphere matrix radius (ft)
r_w	Wellbore radius (ft)
r_{wa}	Effective wellbore radius (ft)
r_e	Reservoir drainage radio (ft)
r_D	Dimensionless wellbore radius
r_{eD}	Dimensionless drainage radius
S_{gi}	Initial gas saturation
s	Skin damage
t	Time (day)
t_a	Pseudo-time for gas (day)
t_c	Material balance time for oil (day) – single well system
$t_{c\ tot}$	Total material balance time for oil (day) – multi-well system
t_{ca}	Material balance pseudo-time for gas (day)

t_{ca}^*	Two-phase material balance pseudo-time for gas (day)
$t_{ca\ pss}$	Pseudosteady-state material balance pseudo-time (day)
t_D	Dimensionless time for homogeneous system
t_{Dd}	Dimensionless decline time for homogeneous system
t_{DA}	Dimensionless time based on drainage area
$t_{ca,Dd}$	Dimensionless decline material balance pseudotime for homog. system
t_{caDA}	Dimensionless time based on drainage area and material balance pseudotime
t_{Ddf}	Dimensionless decline time for heterogeneous system
T	Reservoir temperature (°R)
T_{sc}	Standard Condition Temperature (520 °R)
u	Laplace space variable
$x_{wD,k}$	Position of the well in “x” axis
$y_{wD,k}$	Position of the well in “y” axis
Z	Compressibility factor

Sub-Index

c	Condensate
cr	Constant rate
d	Dew (pressure)
f	Fracture system
g	Gas
i	Initial
j, k	Well index
l	Liquid
m	Matrix
o	Oil
rg	Gas relative permeability
ro	Oil relative permeability
tp	Two-phase
v	Vapor
wf	Flowing well or flowing bottomhole

1. INTRODUCTION

1.1. Background of this research

Naturally fractured reservoirs are generally characterized as very heterogeneous systems due to the presence of different porous media and the interactions between them. They are typically subdivided in Carbonates (matrix, fracture and vugs) and Siliciclastic rocks (matrix and fracture). Analysis of International Energy Agency, BP and Schlumberger indicate that approximately around 60 % of the world's proven oil reserves and 40% of the world's gas reserves. Another important characteristic of naturally fractured reservoirs is their high productivity wells due to the fracture network in the reservoir. Therefore, an early estimation of the hydrocarbon-in-place and a good characterization of this type of reservoir are very important.

The estimation of the hydrocarbon-in-place and reserves are crucial to determine the economic viability of any field development project. Different methods are applied with this purpose depending on the quantity and quality of information available. The material balance method is widely accepted as a more reliable technique compared to volumetric estimations. This technique requires the average reservoir pressure history, generally obtained from build-up tests, which usually require to shut-in the well. In practice, this data can be scarce or non-existent for many reasons such as operational problems, production demand (especially in off-shore fields), high water flow rate, and more that render unfeasible the shut-in of a well.

Nevertheless, daily production data such as flowing pressures and flow rates are usually available. This data is related to reservoir depletion once the pressure drop reaches the reservoir boundaries in a closed system, known as pseudosteady-state flow regime. This information can be used as an alternative input to estimate the hydrocarbon-in-place, as demonstrated by several Advanced Production Data Analysis (PDA) methods such as: NPI method, Blasingame type curve, Agarwal-Gardner type curve and Dynamic Material Balance. These methods were developed considering a homogeneous reservoir and the relevance in naturally fractured reservoirs have not been fully evaluated yet.

The complexity of naturally fractured reservoirs (NFR) makes very difficult to make a production forecast, creating a high degree of uncertainty for field development. Several mathematical models have been proposed for well testing; however the dual porosity model is still the most used in the industry today. Most of the research has been focused on transient reservoir flow regime, using high quality data from a planned well test. In contrast, the use of available daily production data for NFR characterization would represent a significant improvement in the state-of-the art of Production Data Analysis.

1.2. Objectives

The objectives of this work are:

- To derive advanced production data analysis methods based on the dual porosity model, considering pseudosteady-state and transient interporosity flows.
- To present a methodology to interpret production data of naturally fractured reservoirs.
- To validate the derived methods using numerical reservoir simulation and real field data.

1.3. Organization of the dissertation

Chapter I introduces the background of advanced production data analysis as a tool for reservoir characterization and establishes the objectives of this research.

Chapter II presents a literature review of production data analysis techniques divided in two sub-sections: homogeneous reservoirs and naturally fractured reservoirs. The first sub-section describes the main contribution to production data analysis, differentiating the traditional methods from the modern or advanced methods. The second sub-section highlights few studies made in naturally fractured reservoirs. We also present the basic assumptions of all this methods and their classification.

In Chapter III introduces the dual porosity model as the physical model selected for our research. The literature review focuses on long-time approximate solutions of diffusivity

equation for dual porosity and closed reservoir system. They were divided in the two best-known fluid transfer models: pseudosteady-state and transient interporosity flow.

In Chapter IV presents the derivation of production data analysis for naturally fractured reservoirs, based on the long-time approximate solutions. We first compared different time domain approximate solutions with Laplace domain exact solution for constant rate and closed boundary reservoirs. Based on the selected approximations, we derived two advanced production data analysis methods: dynamic material balance and Blasingame type curves.

The validation of the modified methods is presented in Chapter V. For this purpose, synthetic data generated by commercial simulator, and real field data were analyzed. With the data available we generated three cases study: oil field case, gas field case and gas-condensate real field case. This last one corresponds to a gas-condensate naturally fractured reservoir producing from Devonian sandstones.

The last Chapter VI, presents a brief summary of the main topics included in the dissertation, to contextualize the conclusion of the work. Additionally, some recommendations are presented for future investigation.

Finally, additional detailed information of chapter IV is presented in appendixes as follows:

- Appendix A: Diffusivity solution for dual porosity model and pseudosteady-state interporosity flow and no-flow outer boundary.
- Appendix B: Diffusivity solution for dual porosity model and transient interporosity flow and no-flow outer boundary.
- Appendix C: Development of dynamic material balance for naturally fractured reservoirs
- Appendix D: Development of Blasingame type curves for naturally fractured reservoirs

2. PRODUCTION DATA ANALYSIS

This chapter gives an introduction of production data analysis and presents a literature review and some fundamentals of advanced production data analysis techniques. The review is divided in homogeneous reservoirs and naturally fractured reservoirs.

Production Data Analysis (PDA), is known as the procedure to process and interpret the daily production data of wells for obtaining parameters of such well or reservoirs. They can be used to forecast the most probable well life, evaluate well production in the future, and determine the multi-well communication relation and infill potential (Sun 2015).

Although, this research line demonstrated poor development compared with Pressure Transient Analysis (PTA), in the last years there were numerous advances especially related to unconventional reservoirs such as coalbed methane and shale gas reservoirs.

2.1. Classification of Production Data Analysis

According to Mattar and Anderson (2003), PDA is the main area that includes: **traditional production data analysis** and **modern or advanced production data analysis**. The first group includes Arps and Fetkovich methods which considers constant bottomhole pressure and analyze flow rate data. The second group, which is the focus of this work, is characterized because they were developed for variable rate/variable pressure production and they analyze bottomhole pressure along with flow rates. The best-known methods that belong to this group are NPI, Blasingame type curve, Agarwal-Garner type curve and dynamic material balance.

These authors also classified PDA into two major categories based on the use of type curve technique: the **type curveless** and **type curve** methods. Although the type curveless methods are also referred as specialized plotting techniques in pressure transient analysis, in this work we maintained the original terms. In **Table 2.1** it is presented the main methods of each category which will be described in the next section.

Table 2.1 – Production Analysis Methods

Categories	Method	Year
Type Curveless Analysis	Arps (Decline Curve Analysis)	1945
	Dynamic Material Balance	2005
Type Curve Analysis	Fetkovich	1973
	NPI (Normalized Pressure Integral)	1989
	Blasingame	1993
	Agarwal-Garner	1999

2.2. Production Data Analysis in Homogeneous Reservoirs

Arps (1945) made a review of empirical methods previously used in petroleum industry, based on oil wells behavior. He classified them into three main types: Exponential, hyperbolic and harmonic decline. These relations can be summarized in the following equation:

$$\frac{q(t)}{q_i} = \frac{1}{[1 + bD_it]^{\frac{1}{b}}} \dots\dots\dots (2.1)$$

Where:

$b = 0$ (for exponential decline)

$0 < b < 1$ (for hyperbolic decline)

$b = 1$ (for harmonic decline)

Fetkovich (1973) established theoretical fundamentals of Arps work, defining type curves that provide information of type of flow regime and reservoir forecast. He introduced the idea of log-log type curve analysis to production analysis for both transient and pseudosteady-state reservoir flow regimes, based on dimensionless variables. Unfortunately, a unique match was often difficult to achieve because the curves exhibit approximately the same shape.

$$q_{Dd} = \frac{q(t)}{q_i} = q_D \left[\ln \left(\frac{r_e}{r_w} \right) - \frac{1}{2} \right] \dots\dots\dots (2.2)$$

$$t_{Dd} = D_i t = \frac{t_D}{\frac{1}{2} \left[\left(\frac{r_e}{r_w} \right)^2 - 1 \right] \left[\ln \left(\frac{r_e}{r_w} \right) - \frac{1}{2} \right]} \quad (2.3)$$

Where:

$$q_D = \frac{141.3 q(t) \mu B}{kh(P_i - P_{wf})} \quad (2.4)$$

$$t_D = \frac{0.00634 kt}{\phi \mu c_t r_w^2} \quad (2.5)$$

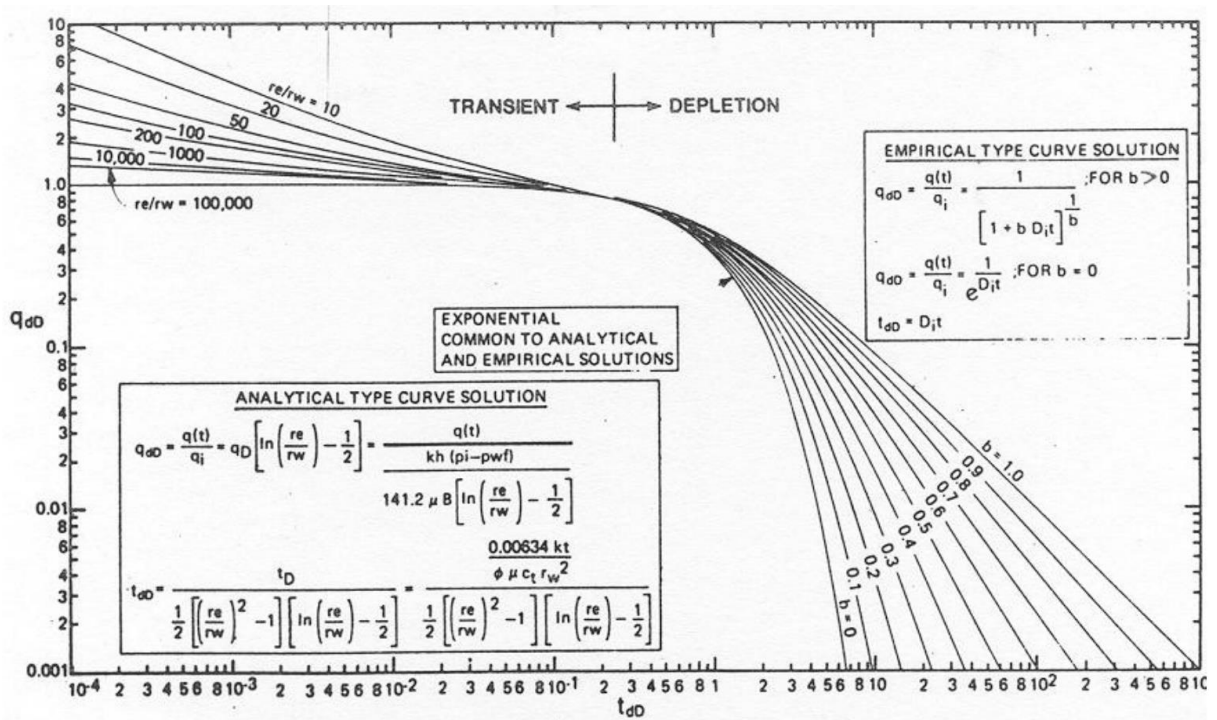


Figure 2.1 – Composite of analytic and empirical type curves (After Fetkovich 1987)

Today, these methods are considered conventional techniques. The analysis is based on flow rate decline data, assuming a constant bottomhole flowing pressure condition (constant BHP). Nevertheless this flowing condition is not always achieved.

Blasingame and Lee (1986) proposed a semi-analytical method to estimate the drainage area and reservoir shape, using “variable rate” production data, when the pressure transient has reached the outer boundary. They established a straight line relation (**Eq. 2.6**) based by defining the “material balance time” (**Eq. 2.7**) and the normalized pressure drop (**Eq. 2.8**). The new time function let to take into account for changing operating conditions.

The variable-rate solution was validated using analytical derivation and numerical reservoir simulation generating different flow rate schedule as presented in **Fig. 2.2**.

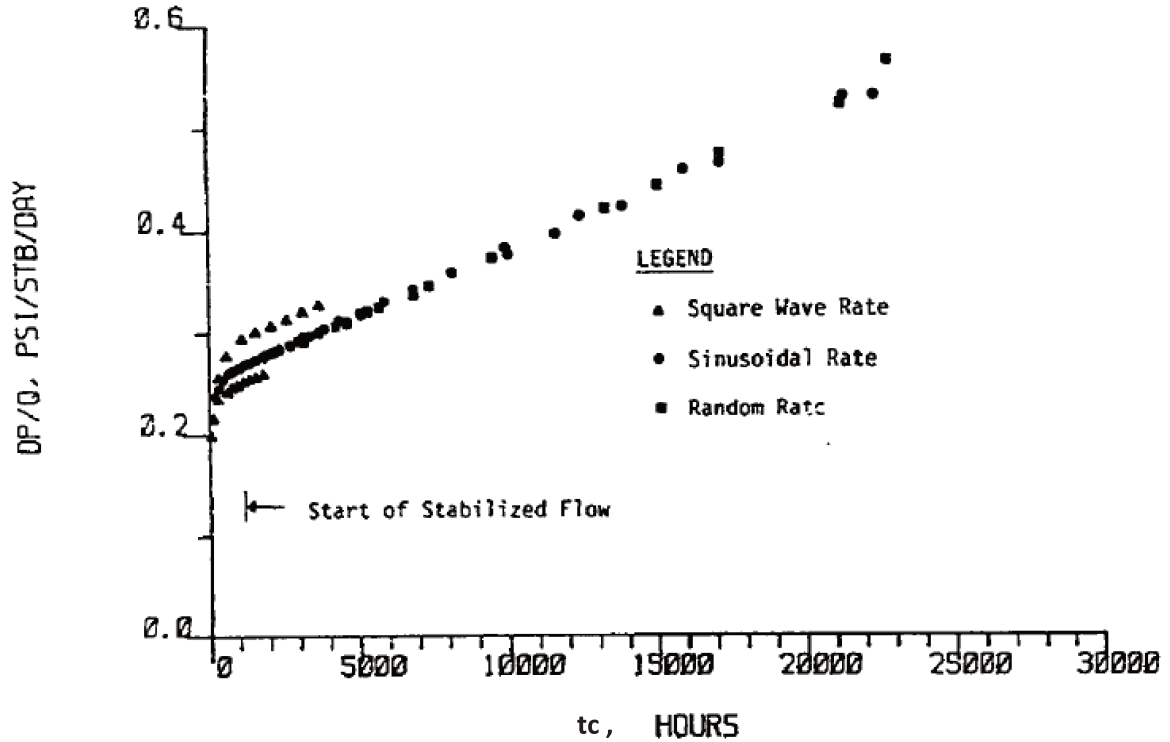


Figure 2.2 – $\Delta p/q_o$ vs. t_c curves for cases simulated analytically (After Blasingame and Lee 1986)

$$\frac{\Delta P}{q_o} = \frac{(P_i - P_{wf})}{q_o} \cong \frac{1}{N c_{ti}} t_c + 141.2 \frac{B\mu}{kh} \left[\frac{1}{2} \ln \left(\frac{4}{e^\gamma} \frac{A}{C_A r_{wa}^2} \right) \right] \dots\dots\dots (2.6)$$

Where:

$$t_c = \frac{1}{q_o} \int_0^t q_o(\tau) d\tau = \frac{N_p}{q_o} \dots\dots\dots (2.7)$$

$$\frac{\Delta P}{q_o} = \frac{(P_i - P_{wf})}{q_o} \dots\dots\dots (2.8)$$

Blasingame et al. (1989) introduced a set of integral type curves for homogeneous and vertically-fractured wells, based on the integral of pressure drop function (**Eq. 2.9**). The objective was to smooth noisy data of well testing operations, in contrast to the well-known

pressure derivative that amplify variation between data points. They suggested the use of normalized pressure integral for the analysis of post-transient well-test data.

$$P_{Di} = \frac{1}{t_D} \int_0^{t_D} P_D(\tau) d\tau \dots\dots\dots (2.9)$$

Peres et al. (1989) presented the use of pressure integral to analyze slug test data. They demonstrated that by integrating the slug test pressure response over the producing time, equivalent pressure change data are generated and can be analyzed as constant surface rate.

Spivey et al. (1992) applied this definition to decline curve analysis for constant bottomhole pressures and variable-pressure/variable-rate flow rate systems in oil and gas wells. They presented a new type curves combining the dimensionless production rate and the dimensionless cumulative production on a single log-log scale. They concluded that a simultaneous matching of production and cumulative production is more sensitive to the choice of early and late-time stems than is matching production flow rate alone.

Palacio and Blasingame (1993) presented a theoretical expression for decline curve analysis from the material balance relation and the pseudosteady-state flow equation (**Eq. 2.10**). This should be used to perform decline analysis under variable rate/variable pressure drop condition employing the material balance time function. Although they presented solutions for liquid and gas, more emphasis was placed in the study of gas flow, solving the problem through the “totally liquid equivalent” concept.

$$P_D = 2\pi t_{ca_{DA}} + \frac{1}{2} \ln \left(\frac{4A}{e^{\gamma} C_A r_{wa}^2} \right) \dots\dots\dots (2.10)$$

For compressible fluids, **Eq. 2.10** can be expressed as follows:

$$\frac{q_g}{P_{pi} - P_{pwf}} b_{a,pss} = \frac{1}{1 + \left(\frac{m_a}{b_{a,pss}} \right) t_{ca}} \dots\dots\dots (2.11)$$

Where:

$$m_a = \frac{1}{Gc_{t_i}} \dots\dots\dots (2.12)$$

$$b_{a,pss} = \frac{141.2\mu_{g_i}B_{g_i}}{k_g h} \left[\frac{1}{2} \ln \left(\frac{4A}{e^{\gamma} C_A r_{wa}^2} \right) \right] \dots\dots\dots (2.13)$$

$$P_p = \left(\frac{\mu_g Z}{P} \right)_i \int_0^P \frac{P}{\mu_g(P)Z(P)} dp \dots\dots\dots (2.14)$$

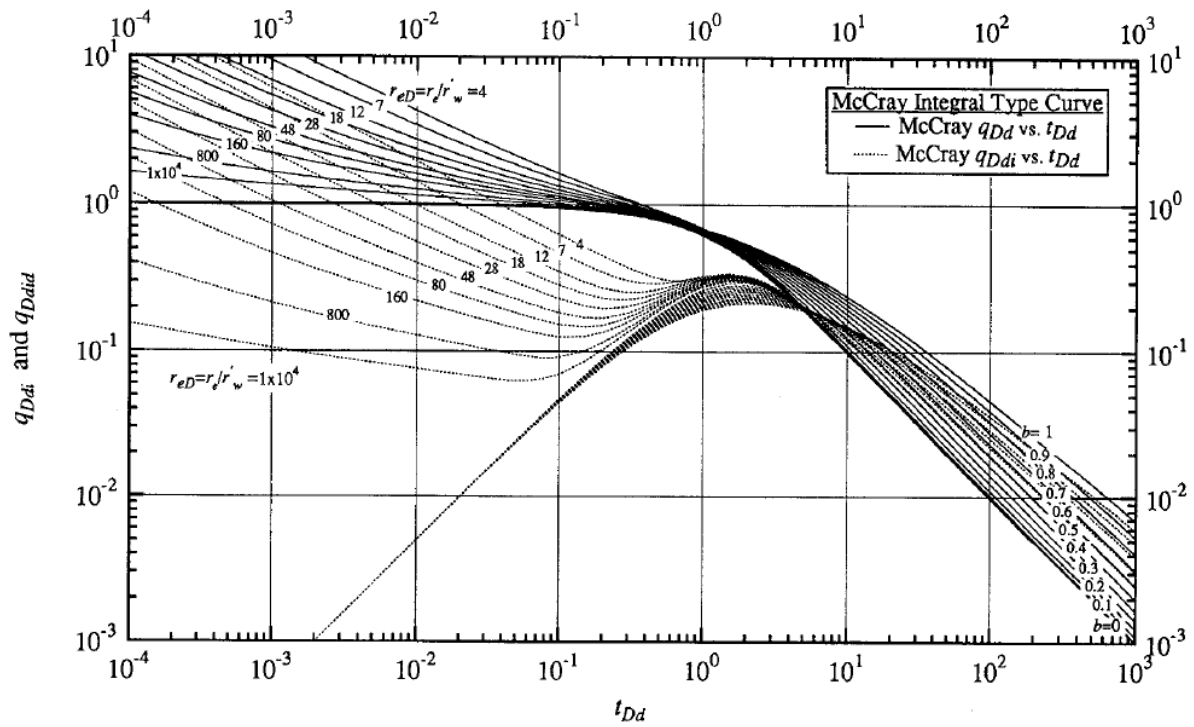


Figure 2.3 – Fetkovich-McGray type curves (After Palacio and Blasingame 1993)

Eq. 2.11 can be reduced to the following expression, similar to **Fetkovich (1980)** harmonic decline curve format:

$$q_{Dd} = \frac{1}{1+t_{ca,Dd}} \dots\dots\dots (2.15)$$

Where:

$$q_{Dd} = \frac{q_g}{P_{p_i} - P_{p_{wf}}} b_{a,pss} \dots\dots\dots (2.16)$$

$$t_{ca,Dd} = \left(\frac{m_a}{b_{a,pss}} \right) t_{ca} \dots\dots\dots (2.17)$$

This method allowed estimating the Original Gas-in-place (OGIP), permeability and wellbore skin. **Doublet et al. (1994)** describe this method for oil wells, obtaining similar output parameters.

Agarwal et al. (1999) presented decline type curves to estimate transient and pseudosteady-state parameters for homogeneous radial flow and hydraulically fractured wells. They evaluated the equivalency between qD and $1/PD$, proposed by Palacio and Blasingame, analyzing the constant rate solution for diffusivity equation. They focused their research in gas wells, applying the pseudo-pressure concept. Permeability and wellbore skin can be determined after obtaining an estimation of OGIP, which can be determined by iterative procedure using.

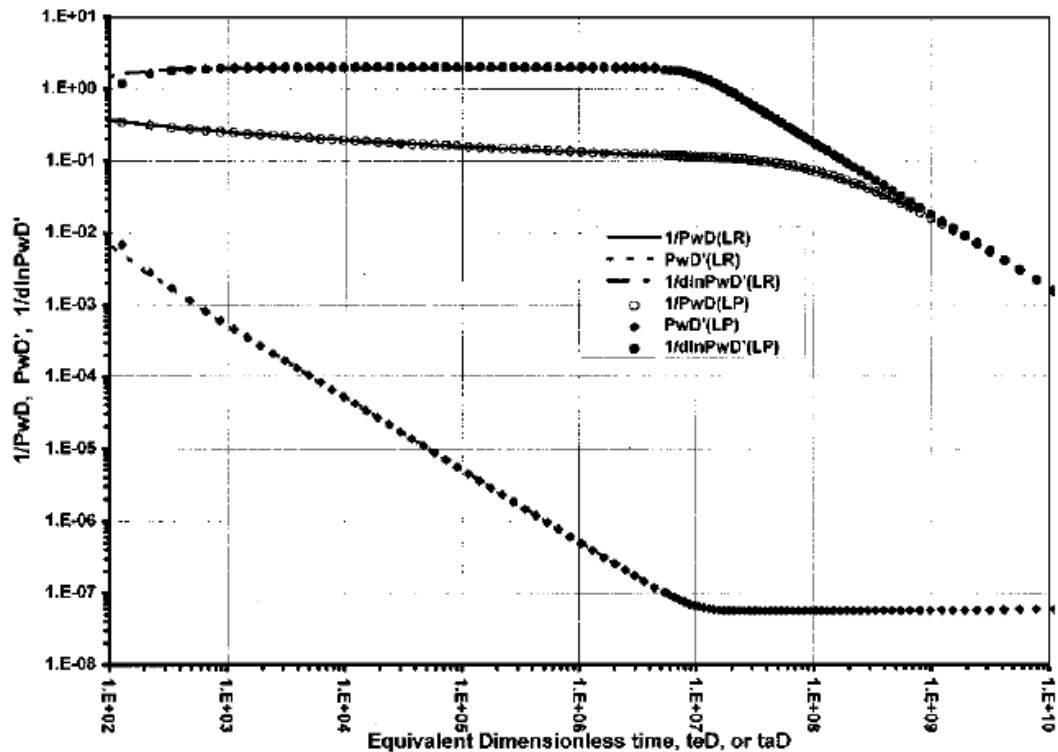


Figure 2.4 – Converting constant rate and constant BHP to equivalent rate liquid data, radial case (After Agarwal et al. 1999)

The authors employed the reciprocal of pressure $\left(1/p_D\right)$, reciprocal of log time derivative $\left(1/(dP_D/d\ln t_D)\right)$ and the pressure derivative $\left(dP_D/dt_D\right)$. These last curves can be used as diagnostic plot in the same Log-Log plot to determine the transient flow period $\left(1/(dP_D/d\ln t_D) = 2\right)$ and the beginning of pseudosteady-state flow regime $\left(1/(dP_D/d\ln t_D) = \text{Negative slope}\right)$ as can be seen in **Fig. 2.4**.

All previous methods were developed considering a single well system in the center of a closed system. **Marhaendrajana and Blasingame (2000)** developed a multi-well solution for a well performance in a rectangular bounded multi-well reservoir system (**Fig. 2.5**).

$$P_D([x_{wD,k} + \varepsilon], [y_{wD,k} + \varepsilon], t_{DA}) = \sum_{j=1}^{n_{well}} \int_0^{t_{DA}} q_{D,j}(\tau) \left(\frac{dP_{D,cr}(t_{DA}-\tau)}{d\tau} \right)_{k,j} d\tau + q_{Dk}(t_{DA})s_k \dots\dots\dots (2.18)$$

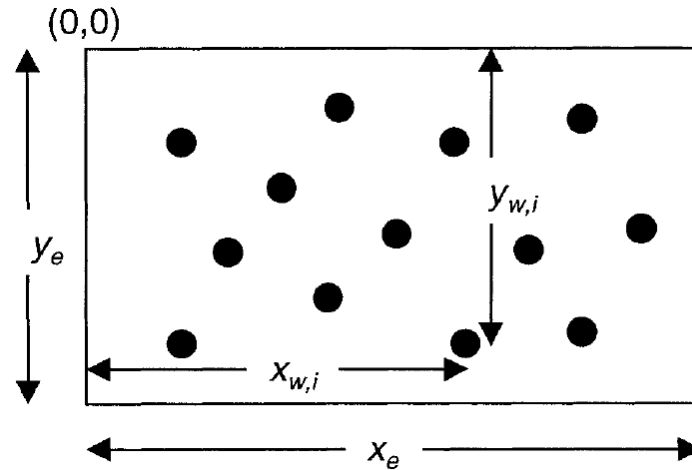


Figure 2.5 – Bounded rectangular reservoir with multiple wells located at arbitrary positions within the reservoir (After Marhaendrajana and Blasingame 2000)

The authors demonstrated that **Eq. 2.18** for boundary dominated flow can be written as **Eq. 2.19**, where $t_{c\ tot}$ is the “total material balance time”, and $b_{pss,mw}$ corresponds to a multi-well system:

$$\frac{q_k(t)}{P_i - P_{wf,k}(t)} = \frac{1}{\frac{1}{Nc_t} t_{c\ tot} + b_{pss,mw}} \dots\dots\dots (2.19)$$

Where:

$$t_{c\ tot} = \frac{1}{q_k(t)} \int_0^t \sum_{i=1}^{n_{well}} q_i(\tau) d\tau = \frac{N_{p,tot}}{q_k(t)} \dots\dots\dots (2.20)$$

$$b_{pss,mw} = 141.2 \frac{B\mu}{kh} \left[\ln \left(\frac{4(A/\beta_D)}{e^{\gamma} C_A r_{wa}^2} \right) \right] \dots\dots\dots (2.21)$$

It is well known that the volume drained by each well is directly proportional to the well's production, for a reservoir which is producing under pseudosteady-state conditions (**Dake 1998, pp. 144**). In a single-well system, Dietz shape factor (C_A) is dependent on the drainage shape and the well position with respect to the boundary (**Dake 1998 pp. 145**). Nevertheless, in a multi-well system Dietz shape factor depends also on the state of the other wells (number, position and rate/pressure). The apparent drainage area of the well in multi-well system depends on the ratio of the producing rate to the total field producing rate, called "Interaction Coefficient" (β_D). Under this concept, **Eq. 2.19** can be rewritten as:

$$q_{Dd} = \frac{1}{t_{Dd} + 1} \dots\dots\dots (2.22)$$

Where:

$$q_{Dd} = \frac{141.2B\mu}{kh} \frac{q_k(t)}{(P_i - P_{wf,k}(t))} \left[\ln(r_{eD}/\sqrt{\beta_D}) - \frac{1}{2} \right] \dots\dots\dots (2.23)$$

$$t_{Dd} = \frac{0.00633kt_{c\ tot}}{\phi\mu c_t A} \frac{2\pi}{\ln(r_{eD}/\sqrt{\beta_D}) - \frac{1}{2}} \dots\dots\dots (2.24)$$

Mattar and Anderson (2005) presented the "Dynamic Material Balance" (DMB), an extension of the "Flowing Material Balance" technique (**Mattar and McNeil 1998**) for variable flow rate. It considers a well producing located at the center of a circular reservoir producing at constant rate in pseudosteady-state flow regime (**Eq. 2.25**).

$$P_D = \frac{2t_D}{r_{eD}^2} + \ln(r_{eD}) - \frac{3}{4} \dots\dots\dots (2.25)$$

They expressed **Eq. 2.18** in the dimensional form for a single gas phase considering wellbore skin, based on the material (**Eq. 2.19**) balance time concept for gas wells (**Eq. 2.20**), and the flow normalized pseudo-pressure definition (**Eq. 2.22**) to take into account the variable flow rate behavior as:

$$\frac{\psi_i - \psi_{wf}}{q_g} = \frac{2P_i}{(\mu_i c_{gi}) Z_{iG}} t_a + b_{pss} \dots\dots\dots (2.26)$$

Where:

$$t_a = \frac{(\mu_i c_{gi}) Z_{iG}}{q_g} (\psi_i - \bar{\psi}) \dots\dots\dots (2.27)$$

$$b_{pss} = \frac{1.417 \times 10^6 T}{kh} \left[\ln \left(\frac{r_e}{r_{wa}} \right) - \frac{3}{4} \right] \dots\dots\dots (2.28)$$

$$\frac{\psi_i - \psi_{wf}}{q_g} \dots\dots\dots (2.29)$$

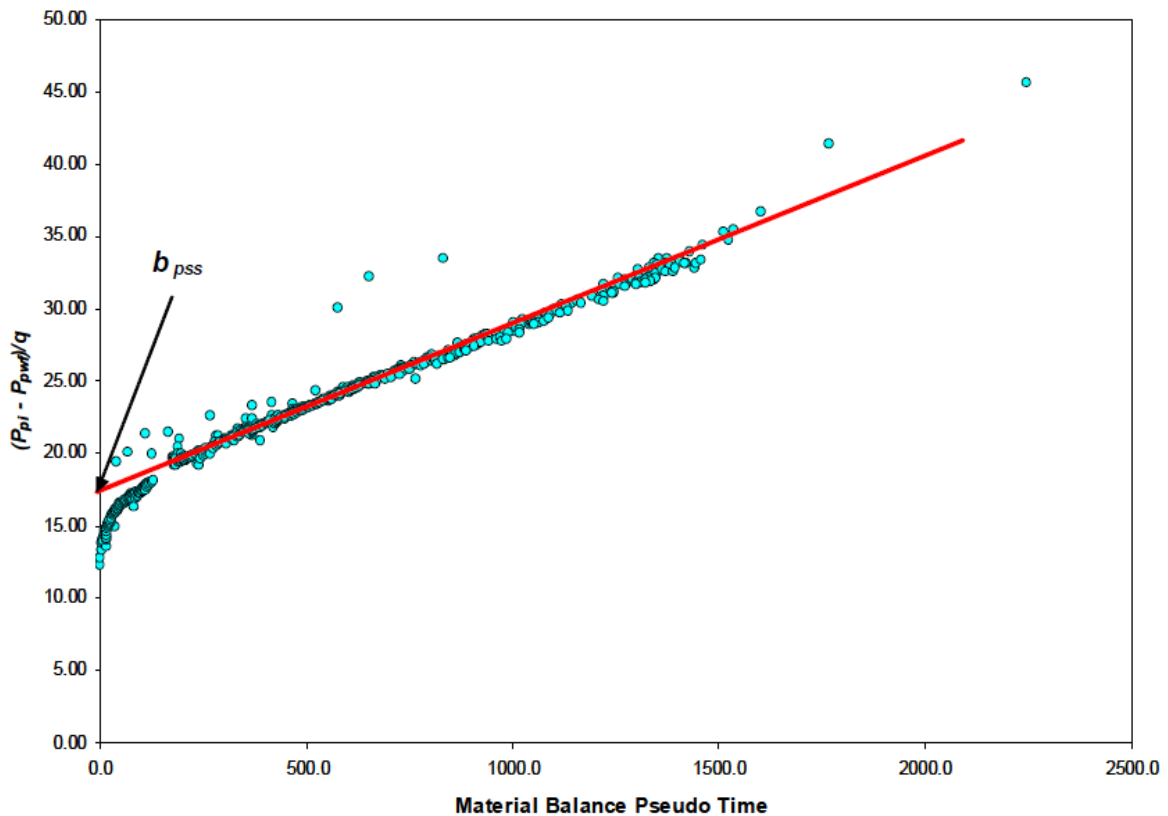


Figure 2.6 – Inverse productivity index plot (After Mattar and Anderson 2005)

A plot of $\frac{\psi_i - \psi_{wf}}{q_g}$ vs t_a will result in a straight line with slope $a = \frac{2P_i}{(\mu_i C_{gi})Z_i G}$. As can be seen, the OGIP is needed to calculate the adjusted pseudo-time and vice-versa (**Fig. 2.6**). Therefore it can be solved through an iterative procedure.

Eq. 2.26 also can be expressed as (**Ahmed 2005**):

$$\frac{q_g}{\psi_i - \psi_{wf}} = - \left(\frac{1}{Gb_{pss}} \right) Q_N + \frac{1}{b_{pss}} \dots\dots\dots (2.30)$$

Where:

$$Q_N = \frac{2q_g P_i t_a}{(\mu_i C_{gi})Z_i (\psi_i - \psi_{wf})} \dots\dots\dots (2.31)$$

In this case, a plot of $\frac{q_g}{(\psi_i - \psi_{wf})}$ vs. Q_N will result in a negative slope straight line, useful in for the iteration process, providing directly the value of the OGIP for the next iteration (similar to Agarwal-Garner method). This plot is also referred as rate cumulative plot.

Ismadi et al. (2011) combined the conventional material balance and the dynamic material balance methods, comparing them against pressure transient analysis. They used synthetic and real data to verify the methods obtaining consistent results. Other authors such as **Al-Reshedam et al. (2012)** and **Fernandez-Berrios (2012)**, presented applications of different APDA methods in hydraulically fractured oil wells and low permeability gas wells, respectively.

A comprehensive comparison of traditional (Arps and Fetkovich) and modern methods (Blasingame, NPI, Agarwal and DMB) were made by **Mattar and Anderson (2003)**. The authors highlighted the strengths and limitations of each method and presented three real field cases. Results confirmed the advantages of modern production data analysis techniques, with similar accuracy, over the traditional techniques. **Anderson and Mattar (2004)** presented a compilation of practical diagnostic procedures that can be applied to production data when making an interpretation.

Concerning gas-condensate reservoirs, **Heidari and Gerami (2011)** presented a robust analytical technique for analyzing gas-condensate reservoirs production decline data. They derived a two-phase material balance pseudo-time (**Eq. 2.34**) based on relative permeability (**Eq. 2.33**). The data availability and the complex calculation procedure make this methodology somewhat limited.

$$\frac{\psi_{tp_i} - \psi_{tp_{wf}}}{q_g} = b_{pss} + \frac{(1-S_{wi})\psi_{i_{tp}}}{GB_{gi}} t_{ca_{tp}} \dots\dots\dots (2.32)$$

Where:

$$\psi_{tp} = \int_{P_d}^P \left(\frac{k_{rg}}{\mu_g B_g} + \frac{k_{ro}}{\mu_o B_o} R_s \right) dp \dots\dots\dots (2.33)$$

$$t_{ca_{tp}} = \frac{1}{q_g(t)} \int_0^{t_a} q_g(\tau) d\tau = \frac{GB_{gi}}{(1-S_{wi})\psi_{tp_i}} \frac{(\psi_{tp_i} - \overline{\psi_{tp}})}{q_g} \dots\dots\dots (2.34)$$

Sadeghi et al. (2011) presented a single-phase production model to analyze production data of a gas-condensate reservoir. The authors evaluated the use of two-phase compressibility factor (Z_{tp}) for the estimation of average reservoir pressure (**Eq. 2.35**), required for the material balance pseudo-time. Results demonstrate that reasonable reserves estimations of gas condensate reservoirs can be obtained with a single phase technique. They validated their approach generating data, using a compositional simulator, over a wide range of gas condensate parameters.

$$\frac{\bar{P}}{Z_{tp}} = \frac{P_i}{Z_{tp_i}} \left(1 - \frac{G_p^*}{G^*} \right) \dots\dots\dots (2.35)$$

Where:

$$Z_{tp} = \frac{n_l}{n_t} Z_l + \frac{n_v}{n_t} Z_v \dots\dots\dots (2.36)$$

$$G_p^* = G_p + GE \times N_p \dots\dots\dots (2.37)$$

$$G^* = G + GE \times N \dots\dots\dots (2.38)$$

Arablo et al. (2014) proposed a simple analytical methodology to improve the estimation of OGIP and average reservoir pressures. They defined pseudo-pressure and material balance pseudo-time functions suitable for gas-condensate systems as a function of two-phase compressibility factor (Z_{tp}).

$$\frac{P_{pi}^* - P_{wf}^*}{q_g} = b_{pss}^* + \frac{1}{G c_{gi}^*} t_{ca}^* \dots\dots\dots (2.39)$$

Where:

$$P_p^* = \left(\frac{\mu_g Z_{tp}}{P} \right)_i \int_0^P \frac{P}{\mu_g Z_{tp}} dp \dots\dots\dots (2.40)$$

$$t_{ca}^* = \frac{\mu_{gi} c_{gi}^*}{q_g(t)} \int_0^t \frac{q_g(t)}{\mu_g c_g^*} dt \dots\dots\dots (2.41)$$

$$c_g^* = \frac{1}{p} - \frac{1}{Z_{tp}} \frac{\partial Z_{tp}}{\partial p} \dots\dots\dots (2.42)$$

They established three distinct regions on a Cartesian plot (**Fig. 2.7**) of normalized pseudo-pressure vs. modified material balance pseudo-time for gas-condensate. They recommended using the third region data points to determine OGIP, where both bottomhole pressures and average reservoir pressures are below the dew point pressure.

$$\frac{\bar{P}}{Z_{tp}} = \frac{P_i}{Z_{tp_i}} \left(1 - \frac{n_p}{n_i} \right) \dots\dots\dots (2.43)$$

Where:

$$n_i = (\rho_{gsc} + \rho_{osc} R_{vi}) G \dots\dots\dots (2.44)$$

$$n_p = \int_0^t \left(q_g \rho_{gsc} + \frac{q_g}{R} \rho_{osc} \right) dt \dots\dots\dots (2.45)$$

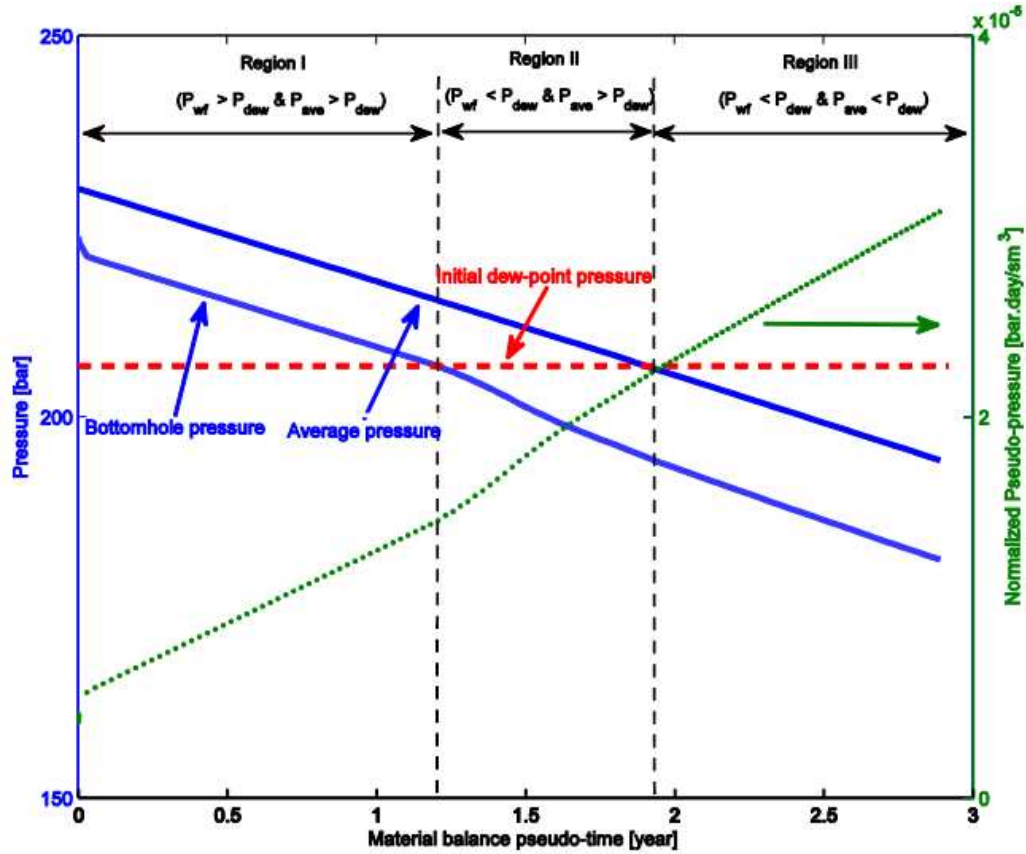


Figure 2.7 – Typical Cartesian plot of dry-gas normalized pseudo-pressure vs. dry gas material balance pseudo-time for a constant rate gas condensate well during boundary-dominated flow regime (After Arablo et al. 2007)

2.3. Production Data Analysis in NFR

Gerami et al. (2007) studied the use of pseudo-time and normalized material balance pseudo-time (Eq. 2.8), for naturally fractured reservoirs (NFR). They presented a model where storativity ratio (ω) is pressure dependent and varies through time (Eq. 2.46). However, the error in the calculation of flowing bottomhole pressures apparently is smaller if extrapolation is based on initial data points, close to initial reservoir pressure (Fig. 2.8).

$$t_{ca}^* = \frac{\mu_i c_{ti}}{q_g(t)} \int_0^{t_a} \frac{q_g(t)}{\mu c_t^*} dt_a \dots\dots\dots (2.46)$$

Where:

$$c_t^* = c_g + c_e [1 - c_g (P_i - \bar{P})] \dots\dots\dots (2.47)$$

$$c_e = \frac{\phi_2(\bar{c}_g + c_2)}{\phi_2(1 - S_{wi})(\bar{c}_g + c_1) + \phi_2(\bar{c}_g + c_2)} \dots\dots\dots (2.48)$$

$$\omega = \frac{\phi_2(\bar{c}_g + c_2)}{\phi_2(1 - S_{wi})(\bar{c}_g + c_1) + \phi_2(\bar{c}_g + c_2)} \dots\dots\dots (2.49)$$

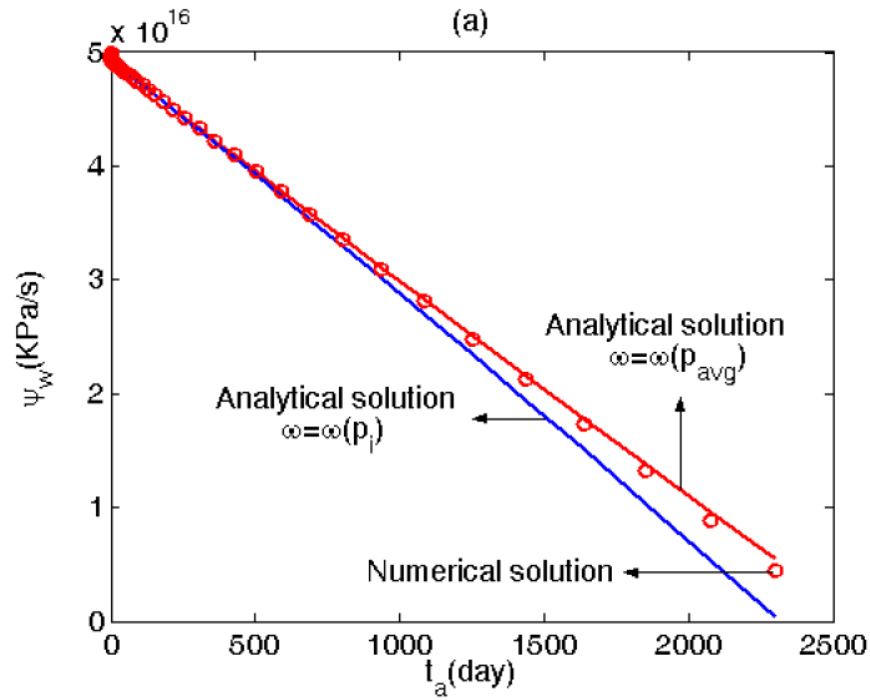


Figure 2.8 – Effect of a constant storativity ratio on behavior of the solution in NFR (After Gerami et al. 2007)

HoseinZareenejad et al. (2012) presented an application of current APDA methods in naturally fractured reservoirs. They analyzed three field cases using Fetkovich, Agarwal-Gardner and Blasingame type curves. They concluded that Agarwal-Gardner and Blasingame type curves techniques provide acceptable values of permeability compared pressure transient analysis despite high relative errors. On the other hand, wellbore skin presented very low negative values (i.e. skin: -10), which are out of range. The relevance of current APDA methods in NFR has not been fully evaluated yet.

It is important to point out that most APDA methods focused their analysis on the pseudo-steady state (PPS) flow regime and single phase flow. **Anderson and Mattar (2004)** resumed the main assumption required for the application the APDA methods:

- Chosen model provides an adequate description of the real reservoir / well system.
- Formation and well properties (permeability and skin) affecting flow are constant through time.
- Measured rates and pressures are representative of flow in the reservoir at sandface condition (no systematic measurement errors exist)
- Absence of external influence that changes well productivity (recompletions, plug backs, etc.)

In contrast to PTA, which provides more accurate values of permeability and skin, PDA methods are focused in long time production data, therefore their accuracy is related to reservoir size and shape (**Khamal 2009**).

3. PRESSURE TRANSIENT ANALYSIS IN NFR

This chapter presents a brief literature review of different models solutions proposed to characterize naturally fractured reservoirs through pressure transient analysis derived from the dual porosity model. Additionally it is presented the long-time approximation solutions divided in pseudosteady-state and transient interporosity flow models.

Naturally fractured reservoirs (NFR) are heterogeneous systems characterized by the presence of distinct types of porous media: matrix, fractures and vugs. Because of their different fluid-storage and conductivity characteristics, different mathematical models have been proposed to describe their complex interaction using production data such as: dual porosity model (**Warren and Root 1963**), dual porosity/dual permeability model (**Bourdet 1985**), triple porosity model (**Abdassah and Ershaghi 1986**) and multi-porosity model (**Kuhlman 2015**).

Daily production usually present a poorer data quality and may not well reflect the details required for an interpretation compared with pressure transient analysis, making triple-porosity or multi-porosity models difficult to use in practice. Nevertheless, dual porosity model proposed has demonstrated to match a surprising number of field cases and is still the more accepted and used in the petroleum industry. This model considers the presence of two porous media: matrix and fracture systems. Conceptually, there are two main assumptions that describe the fluid flow from the matrix to the fracture system: pseudosteady-state interporosity flow and transient interporosity flow.

3.1. Pseudosteady-state Interporosity flow Model

Warren and Root (1963), presented the dual porosity model following the two porous media formulation of **Barenblat et al. (1960)**. They idealized the heterogeneous reservoir as a set of spaced cubic blocks (**Fig. 3.1**), where blocks represents the matrix and the spacing between them, the fractures. They simplified their model by considering a pseudosteady-state (or restricted) interporosity flow model, which means that fluid transfer between matrix and

fracture systems occurs instantaneously. The fluid flow in the fracture is unsteady while in the matrix is pseudosteady. The interaction between these systems is characterized by two additional parameters: storativity ratio (ω) and interporosity flow coefficient (λ).

$$\omega = \frac{(\phi c_t)_f}{(\phi c_t)_f + (\phi c_t)_m} \dots\dots\dots (3.1)$$

$$\lambda = \alpha \frac{k_m}{k_f} r_w^2 \dots\dots\dots (3.2)$$

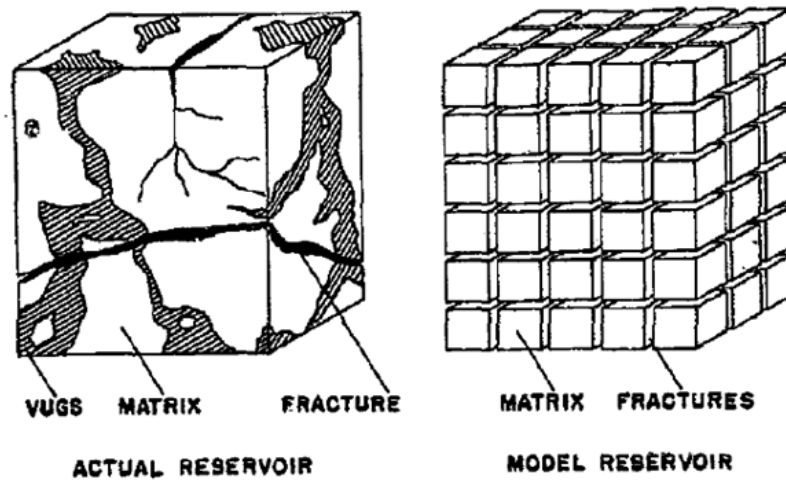


Figure 3.1 – Idealization of the heterogeneous porous medium (After Warren and Root)

The authors proposed the long-time approximate solution described by **Eq. 3.3**. They stated that as $\omega \rightarrow 1$ or $\lambda \rightarrow 0$, their solution approaches to the asymptotic solution given by **Van Everdingen and Hurst (1949)**. For finite reservoirs, the asymptote for the dimensionless drawdown (P_D), is a linear function of dimensionless time (t_D) with a slope of $\frac{1}{2}(R^2-1)$ and an intercept approximately equal to $[\ln(r_{eD}) - 3/4 + 2(1-\omega)^2/(\lambda r_{eD}^2)]$. Consequently, it was possible to evaluate r_{eD} , λ and ω from the asymptote and the difference curve. They recommended that data should be obtained before the effect of the reservoir boundary is felt at the well. Extreme caution should be used in the analysis of data secured during the later stages of build-up in a finite reservoir.

$$P_{wDf} = \frac{2}{r_{eD}^2 - 1} \left\{ \frac{1}{4} + t_{Df+m} + \frac{(1-\omega)^2}{\lambda} \left[1 - \exp \left(-\frac{\lambda t_{Df+m}}{\omega(1-\omega)} \right) \right] \right\} - \frac{3r_{eD}^4 - 4r_{eD}^4 \ln(r_{eD}) - 2r_{eD}^2 - 1}{4r_{eD}^4 (r_{eD}^2 - 1)^2} \dots (3.3)$$

Odeh (1965), presented a model quite similar to **Warren and Root**, however he concluded that a heterogeneous systems cannot be distinguished from homogeneous systems because the transition zone occurs rapidly due to large values of interporosity flow coefficient (λ).

Mavor and Cinco Ley (1979), based on the pseudosteady-state interporosity flow, studied the constant flow rate and constant pressure case for infinite and finite reservoirs. They described two limiting forms of **Warren and Root** model:

- First case: A non-communicating matrix with fluid storativity due to the fracture system ($k_m = 0, \lambda = 0$), represented by the $\omega = 10^{-3}$ curve in **Fig. 3.2**.
- Second case: A communicating matrix with fluid storativity due to total system represented by the $\omega = 10^{-3}$ curve.

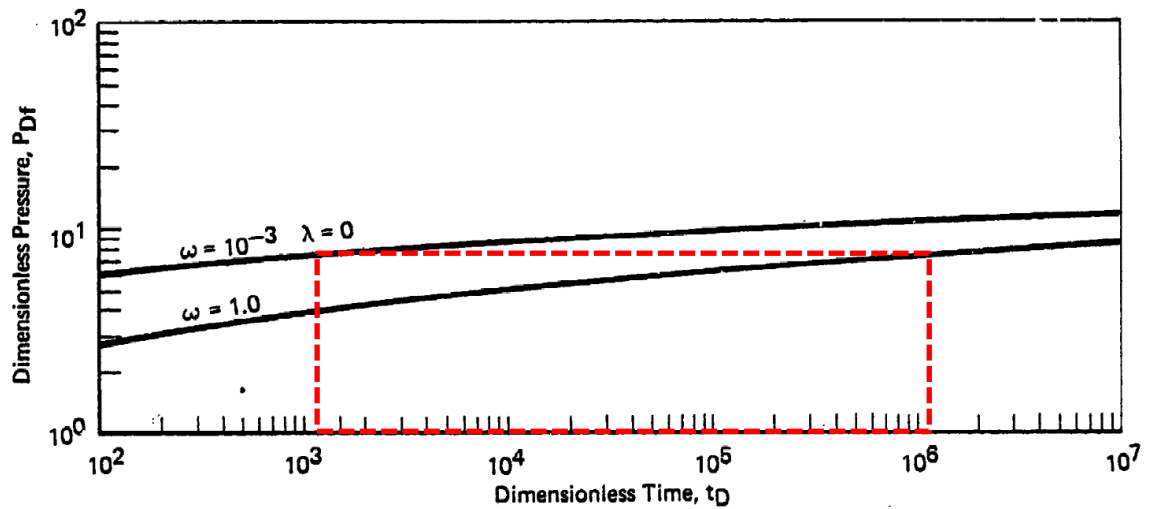


Figure 3.2 – Limiting forms of naturally fractured reservoir pressure behavior (After Mavor and Cinco Ley)

In **Fig. 3.2**, both curves are identical except that the time scale for the first case is 1000 times less than the second. This shift occurs since both cases are homogeneous reservoir solutions but the effective storativity is different. This means, that for extremely low matrix

permeability (fractures storativity behavior), boundary effects can occur a factor of $1/\omega$ sooner than would be expected from the size of the system (total reservoir storativity). This would eliminate the two slope behavior observed in pressure transient analysis.

For closed reservoirs with no-flow boundaries, the authors proposed the following long-time approximate solutions for the fracture system depletion (**Eq. 3.4**) and for the total system depletion (**Eq. 3.5**). This means that in a naturally fractured reservoir, the fractured system and total system may presents a boundary dominated flow.

$$\text{Fracture system:} \quad \frac{t_{DA}}{\omega} > 0.1 \text{ and for } t_D \leq \frac{\omega(1-\omega)}{11\lambda}$$

$$P_{wDf} = \frac{2\pi t_{DA}}{\omega} + \frac{1}{2} \ln \left(\frac{2.2458 A}{C_A r_w^2} \right) \dots\dots\dots (3.4)$$

$$\text{Total system:} \quad t_{DA} > 0.1 \text{ and } t_D \geq \frac{44.4(1-\omega)}{\lambda}$$

$$P_{wDf} = 2\pi t_{DA} + \frac{1}{2} \ln \left(\frac{2.2458 A}{C_A r_w^2} \right) \dots\dots\dots (3.5)$$

Da Prat (1981) presented a detailed analysis **Warren and Root** solution (**Eq. 3.3**) considering recommendations made by Mavor and Cinco Ley. He confirmed the fracture system solution; nevertheless he stated that total system behavior approximation includes an additional term (**Eq. 3.7**). Essentially, for short period of time only fracture volume will influence the wellbore pressure history, otherwise after enough time, bottomhole pressure behavior will be in contact with the total system volume (fractures + matrix).

$$\blacksquare \text{ Fracture system:} \quad 0.1 \leq t_D \leq \frac{\omega(1-\omega)}{\lambda}$$

$$P_{wDf} = \frac{2\pi t_{DA}}{\omega} + \frac{1}{2} \ln \left(\frac{2.2458 A}{C_A r_w^2} \right) \dots\dots\dots (3.6)$$

$$\blacksquare \text{ Total system:} \quad t_D \geq \frac{\omega(1-\omega)}{\lambda}$$

$$P_{wD_f} = 2\pi t_{AD} + \frac{1}{2} \ln \left(\frac{2.2458 A}{C_A r_w^2} \right) + \frac{2(1-\omega)^2}{\lambda r_{eD}^2} \dots\dots\dots (3.7)$$

Blasingame and Lee (1986) presented a methodology to determine reservoir properties in homogeneous, hydraulic fractured and naturally fractured reservoir through the use of decline curve analysis. Based on **Da Prat**'s dimensionless solutions of fracture depletion for constant pressure (**Eq. 3.10**), they transformed it to a constant flow rate (**Eq. 3.11**) using a relation for constant flow rate and constant pressure in Laplace domain.

$$q_{Df} = \frac{(r_{eD}^2 - 1)}{2} e^{\left(-\frac{\lambda}{(1-\omega)} t_{Df}\right)} \dots\dots\dots (3.10)$$

$$P_{wD_f} = \frac{2t_{Df}}{(r_{eD}^2 - 1)(1-\omega)} + \frac{2}{(r_{eD}^2 - 1)\lambda} \dots\dots\dots (3.11)$$

Igbokoyi and Tiab (2006) analyzed different matrix block flow models for closed boundary reservoir to determine the average reservoir pressure and drainage area. For pseudosteady-state interporosity flow, they obtained the same solution cited by Warren and Root and described by **Da Prat (Eq. 3.7)**, for a similar dimensionless time interval $t_{Df} \geq \frac{5\omega(1-\omega)}{\lambda}$.

3.2. Transient Interporosity flow Model

In contrast to Warren and Root model, **Kazemi (1969)** presented a numerical model to consider a transient (or unsteady) interporosity flow of fluids from the matrix to the fractures. He idealized the reservoir as consisting of a set of uniformly spaced horizontal matrix layers with a set of fractures between them (Slabs) (**Fig. 3.3a**). The results were similar to Warren and Root, but with a smooth transition zone.

An analytical description of Warren and Root (blocks) model and Kazemi model (slabs) was made by **De Swaan (1976)**. The matrix block solutions, for early and long-time, was approximated by a spherical block solution (**Fig. 3.3b**). The interaction between matrix and

fractures is characterized by four additional variables representing the diffusivities of porous media.

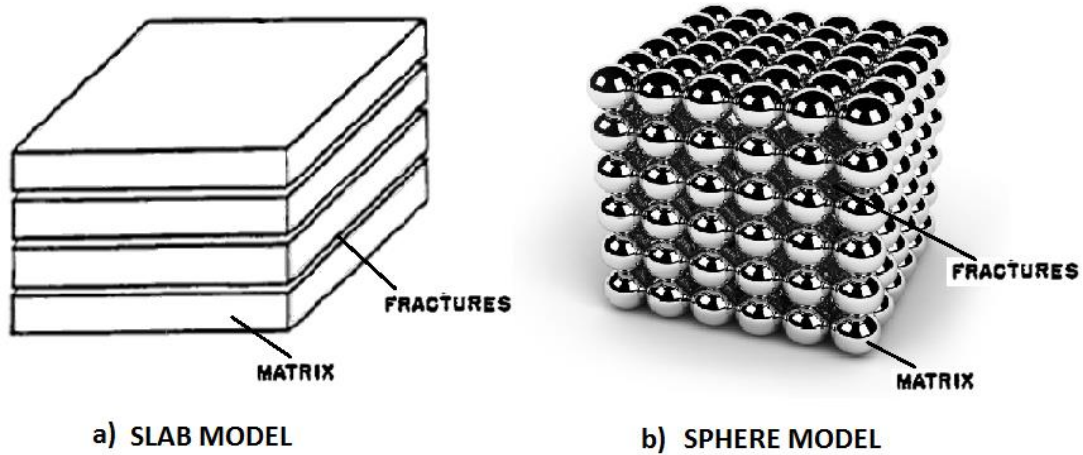


Figure 3.3 – Idealization of a heterogeneous porous medium – Kazemi (Slabs) and De Swaan (Spheres)

Some years later, **Najurieta (1980)** presented an approximate solution for De Swaan model, for the slab and block cases. Pressure solution can be described by five basic parameters: fracture and matrix porosity, fracture (k_f) and matrix (k_m) permeability and fracture spacing (h_m). He also defines interporosity flow functions based on the new variables:

For spheres:

$$f(u) = \frac{1}{\eta_f} + \frac{4}{u h_f h_m} \frac{k_m}{k_f} \left[\frac{h_m}{2} \sqrt{\frac{u}{\eta_m}} \coth \left(\frac{h_m}{2} \sqrt{\frac{u}{\eta_m}} \right) - 1 \right] \dots\dots\dots (3.12)$$

For slabs:

$$f(u) = \frac{1}{\eta_f} + \frac{2}{h_f \sqrt{u \eta_m}} \frac{k_m}{k_f} \tanh \left(\frac{h_m}{2} \sqrt{\frac{u}{\eta_m}} \right) \dots\dots\dots (3.13)$$

Bourdet and Gringarten (1980), following the theory developed by **De Swaan**, remarked that the pressure solution for transient flow in fissures is the same as for pseudosteady-state flow presented by **Mavor and Cinco Ley**. Additionally, they established interporosity flow function definitions based on the parameters “lumped variables” (ω and λ) defined Warren and Root:

For Slabs:

$$f(u) = \omega + \sqrt{\frac{\lambda(1-\omega)}{3u}} \tanh \sqrt{\frac{3(1-\omega)u}{\lambda}} \dots\dots\dots (3.14)$$

Where:

$$\lambda = 12 \frac{r_w^2}{h_m^2} \frac{k_m}{k_f} \quad (n = 1) \dots\dots\dots (3.15)$$

For Spheres:

$$f(u) = \omega + \frac{1}{5} \frac{\lambda}{u} \left[\sqrt{\frac{15(1-\omega)u}{\lambda}} \coth \sqrt{\frac{15(1-\omega)u}{\lambda}} - 1 \right] \dots\dots\dots (3.16)$$

Where:

$$\lambda = 15 \frac{r_w^2}{r_m^2} \frac{k_m}{k_f} \quad (n = 3) \dots\dots\dots (3.17)$$

Cinco Ley and Samaniego (1982), presented a transient interporosity flow model including wellbore storage and skin effect, based on the work of **De Swaan and Najurieta**. They considered the slab and spheres matrix geometries and proposed short-time, intermediate-time and long-time approximate solutions for infinite reservoirs. It is demonstrated that the behavior of NFR can be correlated by using a three dimensionless parameters: fracture storage parameter (ω), dimensionless matrix hydraulic diffusivity (η_{maD}) and the dimensionless fracture area (A_{fD}). They found that regardless to the matrix geometry the transition period might exhibit a straight line whose slope is equal to half the slope of the classical parallel semi-log straight lines.

Serra et al. (1983) presented an additional model for transient interporosity flow, assuming slab matrix geometry. They considered an infinite reservoir behavior and slightly compressible fluid of constant viscosity. Three possible flow regimes were identified, where the first correspond to the early time and third correspond to the late time behavior reported by **Warren and Root, De Swaan** and others. During the second flow regime pressure response is influenced by both matrix and fracture systems. Although these flow regimes were previously noted, they presented methods to identify them and obtain certain parameters such as: fracture flow capacity, matrix permeability, skin factor and dimensionless fracture coefficient.

Moench (1984) introduced the fracture skin concept. The effect of fracture skin is to delay flow contributions from the matrix to the fracture system. Fracture skin provides a theoretical justification for the pseudosteady-state interporosity flow approximation used in the **Warren and Root** model. His mathematical development assumed a transient interporosity flow and found that **Warren and Root** model would be a special case when fracture skin is sufficiently low.

Onur et al (1993) presented new type curves (derivative and integral-derivative) to aid the analysis of well-test data and estimate key parameters characteristics of NFR. They considered the pseudosteady-state interporosity flow of Warren and Root and transient interporosity flow of Kazemi and De Swaan for slab, spherical and cylindrical matrix block geometries. The type curves also could be used to identify the model represented by field data and then the appropriate type curve was used to obtain a complete analysis.

As can be seen in the review, most attention has been focused in pressure transient analysis which considers an infinite-acting reservoir case. In contrast, advanced production data analysis methods usually assume a closed boundary reservoir with no-flow boundaries. In **Igbokoyi and Tiab's (2006)** work, the transient interporosity flow for bounded reservoirs was also evaluated. They considered three different matrix geometries: slab, spherical and cubic blocks. They obtained the same solution in all cases for long-time, valid for $t_{Df} < \frac{(1-\omega)^2}{100\lambda}$.

$$P_{wDf} = 2\pi t_{AD} + \frac{1}{2} \ln \left(\frac{2.2458 A}{C_A r_w^2} \right) + s \dots\dots\dots (3.18)$$

Even though, the more probable flow regime between matrix and fractures is transient; in late time pseudosteady-state flow should be achieved (**Lee et al. 2003**). **Mavor and Cinco** **Ley** agreed that pseudosteady-state interporosity flow was a reasonable idealization, and the fracture skin concept proposed by **Moench**, added theoretical justification. For the sake of completeness, we considered important to evaluate both considerations.

4. DEVELOPMENT OF ADVANCED PRODUCTION DATA ANALYSIS FOR NFR

In this chapter, a dual porosity model was applied to derive advanced production data analysis methods. We first determined the approximated solutions of diffusivity equation for a closed boundary dual porosity reservoir, and constant flow rate. For the sake of completeness a pseudosteady-state and transient interporosity flows between fracture and matrix were evaluated. Based on the selected long-time approximations two selected advanced production methods were derived: Dynamic Material Balance and Blasingame type curve.

In this work, we considered a compressible fluid for the development of the equations for practical purposes. As we known, compressible fluids properties are pressure dependent, therefore to linearize the equations we used the material balance pseudo-time definition (**Eq. 4.1**) and normalized pseudo-pressure (**Eq. 4.2**).

$$t_{ca} = \frac{(\mu_g c_t)_i}{q_g} \int_0^t \frac{q_g}{\bar{\mu}_g \bar{c}_t} dt = \frac{G c_{ti}}{q_g} (P_{pi} - \bar{P}_p) \dots\dots\dots (4.1)$$

$$P_p = \left(\frac{\mu Z}{P} \right)_i \int_{P_{wf}}^P \frac{P}{\mu Z} dp \dots\dots\dots (4.2)$$

On the other hand, for slightly compressible fluids constants and units are the same, except for the following variations:

- Use pressure instead of normalized pseudo-pressure.
- The material balance pseudo-time is calculated as described by **Eq. 2.7**, because oil viscosity and oil formation fluid factor are considered constant through time.
- The units of oil formation volume factor is expressed as (bbl/STB), rather than (bbl/Mscf) for gas.

4.1. Definition of Dimensionless Variables

The following dimensionless variables are defined for compressible fluids based on conventional field units.

Fracture dimensionless pressure:

$$P_{Df} = \frac{k_f h}{142,2 q_g \mu_g B_g} (P_{p_i} - P_{p_{wf}}) \dots\dots\dots (4.3)$$

Dimensionless flow rate:

$$q_D = \frac{142,2 \mu_g B_g}{k_f h} \frac{q_g}{(P_{p_i} - P_{p_{wf}})} \dots\dots\dots (4.4)$$

Total system dimensionless time:

$$t_{Df} = \frac{6.33 \times 10^{-3} k_f}{(\phi c_{t_i})_{f+m} \mu_{g_i} r_w^2} t \dots\dots\dots (4.5)$$

Total system dimensionless time based on the drainage area:

$$t_{DAf} = \frac{6.33 \times 10^{-3} k_f}{(\phi c_{t_i})_{f+m} \mu_{g_i} A} t \dots\dots\dots (4.6)$$

Dimensionless drainage radius:

$$r_{eD} = \frac{r_e}{r_{wa}} \dots\dots\dots (4.7)$$

4.2. Long-Time Approximations for Dual Porosity Model

First we need to determine the long-time approximations of diffusivity equation in a dual porosity system, for each interporosity flow, pseudosteady-state and transient. We assume a closed circular reservoir with no-flow outer boundary and constant rate.

4.2.1 Pseudosteady-state Interporosity Flow

The literature review covered, different authors agreed with the asymptotic long-time approximations for fracture system and total system. The boundary-dominated flow for

fracture system is described by **Eq. 3.6**. For total system there were two approximations (**Eq. 3.7** and **Eq. 3.11**), which were compared with the Laplace domain solution, in time domain using Gaver-Stehfest algorithm (**Fig. 4.1**).

The behavior of the two systems is better described by **Eq. 3.6** for the fracture system and by **Eq. 3.7** for total system. The derivation of this approximated solutions were described by **Da Prat**, and is presented in **Appendix A**. These equations can be rewritten, assuming a circular area, as:

$$\text{For fracture system: } 0.1 \leq t_{Df} \leq \frac{\omega(1-\omega)}{\lambda}$$

$$P_{Df} = \frac{2t_{Df}}{\omega r_{eD}^2} + \ln(r_{eD}) - \frac{3}{4} + s \dots\dots\dots (4.8)$$

$$\text{For total system: } t_{Df} \geq \frac{\omega(1-\omega)}{\lambda}$$

$$P_{Df} = \frac{2t_{Df}}{r_{eD}^2} + \ln(r_{eD}) - \frac{3}{4} + \frac{2(1-\omega)^2}{\lambda r_{eD}^2} + s \dots\dots\dots (4.9)$$

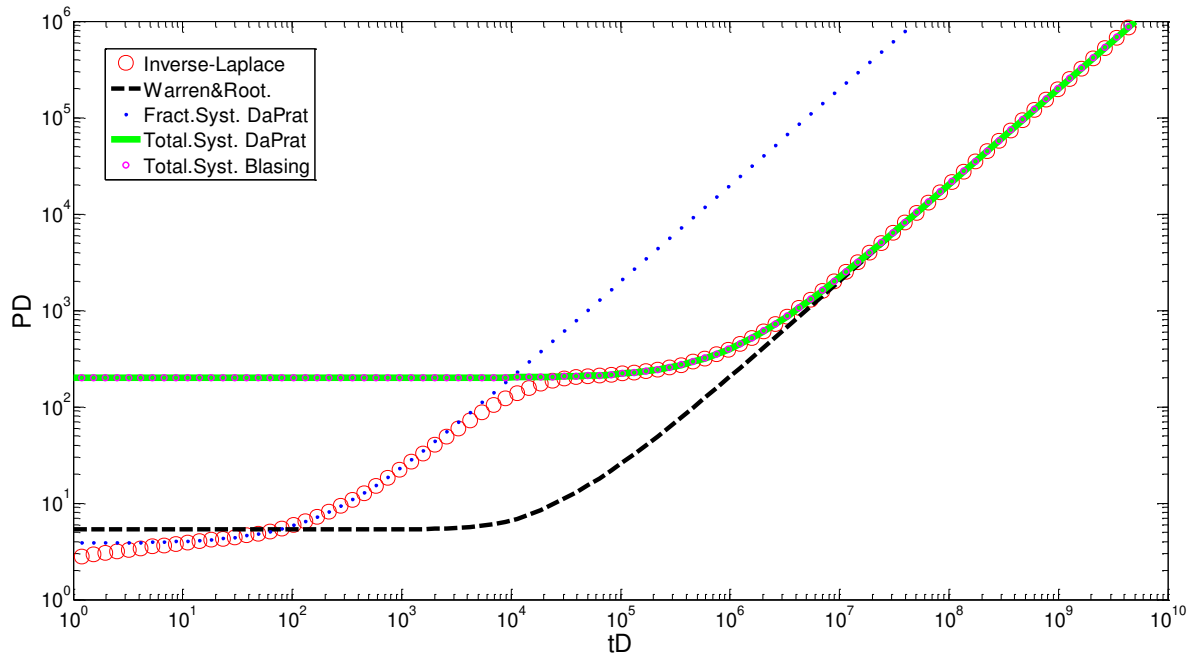


Figure 4.1 – Comparison of approximate solutions for a dual porosity finite reservoir and PPS interporosity flow, produced at constant rate. $r_{eD} = 100$; $\omega = 0.01$; $\lambda = 1 \times 10^{-6}$.

4.2.2 Transient Interporosity Flow

In spite of the approximation published by **Igbokoyi and Tiab (2006)** for transient interporosity flow, we considered important to confirm those solutions. The development was based on the lumped variables (ω and λ) and the two best-known flow geometries: slabs and spheres. A detailed development is presented in **Appendix B**.

In Laplace domain the solution of radial-flow diffusivity equation in closed boundary reservoir, for constant flow rate considering $CD = 0$ and $skin = 0$, at wellbore is:

$$\overline{P_{wDf}} = \frac{k_0(\sqrt{uf(u)})I_1(\sqrt{uf(u)} r_{eD}) + k_1(\sqrt{uf(u)} r_{eD})I_0(\sqrt{uf(u)})}{u\sqrt{uf(u)}[k_1(\sqrt{uf(u)})I_1(\sqrt{uf(u)} r_{eD}) - k_0(\sqrt{uf(u)} r_{eD})I_0(\sqrt{uf(u)})]} \dots\dots\dots (4.10)$$

First the Bessel functions were evaluated for long-time (small arguments $u \rightarrow 0$), obtaining the following result:

$$\overline{P_{wDf}} = \frac{1}{u}k_2(\sqrt{uf(u)} r_{eD}) - \frac{1}{u}k_0(\sqrt{uf(u)} r_{eD}) - \frac{1}{2}\frac{\ln(uf(u))}{u} + \frac{1}{u}\ln(2) - \frac{1}{u}\gamma \dots\dots\dots (4.11)$$

Next, the interporosity flow function, or transfer function, was evaluated for the long-time for slab and sphere geometry models separately:

SLAB MODEL:

$$f(u) = \omega + \sqrt{\frac{1}{3}\frac{\lambda(1-\omega)}{u}} \tanh \sqrt{\frac{3(1-\omega)u}{\lambda}} \dots\dots\dots (4.12)$$

According to **Raghavan and Ozkan (1994)**, $f(u \rightarrow 0) = 1$, then inverting to time domain following **Blasingame (1993)** procedure, we obtain:

$$P_{wDf} = \frac{2 t_{Df}}{r_{eD}^2} \exp\left(\frac{-r_{eD}^2}{4t_{Df}}\right) - \frac{1}{2} Ei\left(\frac{r_{eD}^2}{4t_{Df}}\right) + \frac{1}{2} \ln\left(\frac{4t_{Df}}{e^\gamma}\right) \dots\dots\dots (4.13)$$

To avoid using the exponential functions as a base of APDA development in NFR, **Eq. 4.12** can be simplified one more time. The exponential function in the first term tends toward unity for long-time and applying the logarithmic approximation to the second term, we obtain:

$$P_{wDf} = \frac{2 t_{Df}}{r_{eD}^2} + \ln(r_{eD}) - 0.5634 \dots\dots\dots (4.14)$$

SPHERICAL MODEL:

$$f(u) = \omega + \frac{1}{5} \frac{\lambda}{u} \left[\sqrt{\frac{15(1-\omega)u}{\lambda}} \coth \sqrt{\frac{15(1-\omega)u}{\lambda}} - 1 \right] \dots\dots\dots (4.15)$$

Applying the following approximation to **Eq. 4.14**: $\coth(x) \approx \frac{1}{x} + \frac{x}{3}$ (Najurieta 1980), $f(u \rightarrow 0) = 1$. Consequently, we would obtain the same solution for the slab model:

$$P_{wDf} = \frac{2 t_{Df}}{r_{eD}^2} + \ln(r_{eD}) - 0.5634 \dots\dots\dots (4.16)$$

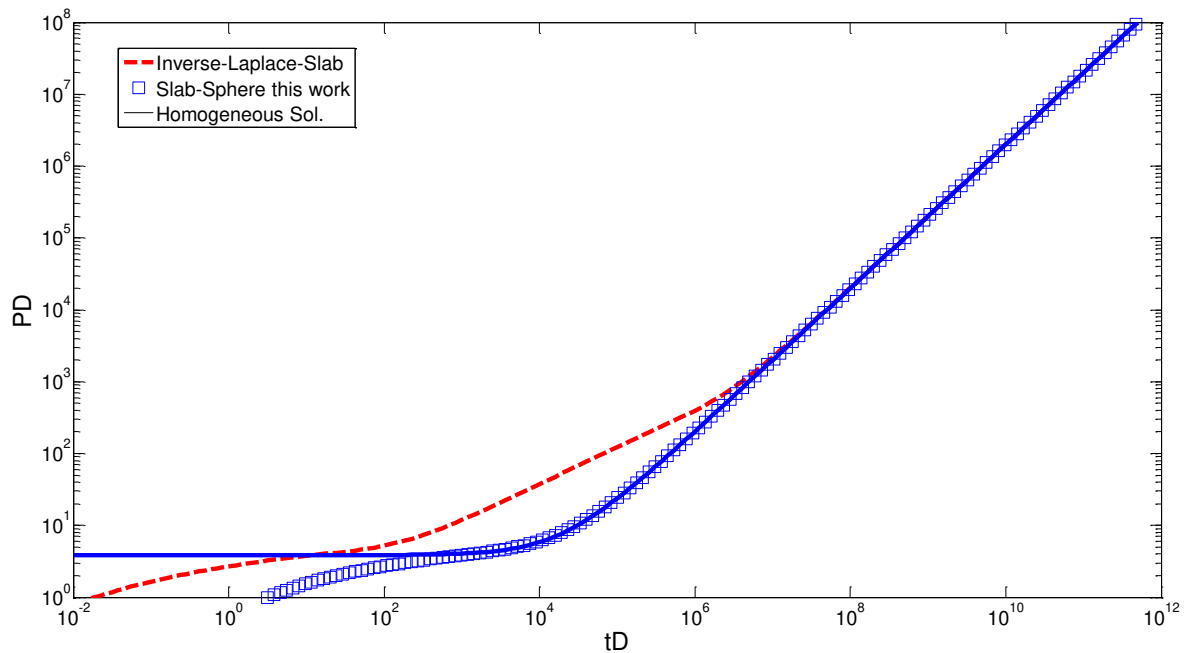


Figure 4.2 – Comparison of approximate solutions for a dual porosity finite reservoir and transient interporosity flow, produced at constant rate. $r_{eD} = 100$; $\omega = 0.01$; $\lambda = 1 \times 10^{-6}$.

This solution is close to the most well-known solution for homogeneous reservoirs (**Eq. 4.16**). The difference between both constant values can be observed in **Fig. 4.2**.

$$P_{wDf} = \frac{2t_{Df}}{r_{eD}^2} + \ln(r_{eD}) - \frac{3}{4} \dots\dots\dots (4.17)$$

As can be seen in **Fig. 4.2**, long-time approximate solution for slab and spheres models are essentially the homogeneous solution. Therefore in naturally fractured reservoirs with transient interporosity flow behavior, current APDA methods developed for homogeneous systems can be applied.

4.3. Material Balance Time in Naturally Fractured Reservoirs

Before deriving the APDA methods for NFR, it was important to evaluate the behavior of the material balance time concept (**Eq. 2.7**) in dimensionless units. This relation in dimensionless variables is given by **Eq. 4.18**.

$$t_{cD} = \frac{N_{pDf}}{q_{Df}} = \frac{\int_0^{t_D} q_D(t_D) dt_D}{q_{Df}} \dots\dots\dots (4.18)$$

The solution for constant pressure (q_{Df}) can be obtained from the solution for constant flow rate (**Eq. 4.10**) by applying the constant wellbore pressure/constant flow rate relation in Laplace domain proposed by **Van Everdingen and Hurst (1965)**:

$$\overline{q_{Df}} = \frac{1}{u^2 \overline{P_{wDf}}} \dots\dots\dots (4.19)$$

Substituting **Eq. 4.10** into **Eq. 4.19**:

$$\overline{q_{Df}} = \frac{[k_1(\sqrt{uf(u)}) I_1(\sqrt{uf(u)} r_{eD}) - k_1(\sqrt{uf(u)} r_{eD}) I_1(\sqrt{uf(u)})]}{\sqrt{uf(u)} [k_0(\sqrt{uf(u)}) I_1(\sqrt{uf(u)} r_{eD}) + k_1(\sqrt{uf(u)} r_{eD}) I_0(\sqrt{uf(u)})]} \dots\dots\dots (4.20)$$

The dimensionless cumulative production (N_{pD}) can be determined applying the integral Laplace property described by **Eq. 4.21 (Spiegel 1965)**:

$$\overline{N_{pDf}} = \frac{\overline{q_{Df}}}{u} \dots\dots\dots (4.21)$$

In contrast to homogeneous systems, a Log-Log plot of q_{Df} vs t_{Df} and $1/P_{wDf}$ vs t_{Df} , presents great difference between the solutions (**Fig. 4.3**). Nevertheless, the use of the material balance time (t_{cD}) instead of dimensionless time (t_{Df}) for constant pressure solution corrects the late time of the plot. This confirms the equivalency with respect to the constant rate solution considering the total volume of the system. As a consequence, APDA for NFR methods could also be applied to variable BHP and variable flow rate.

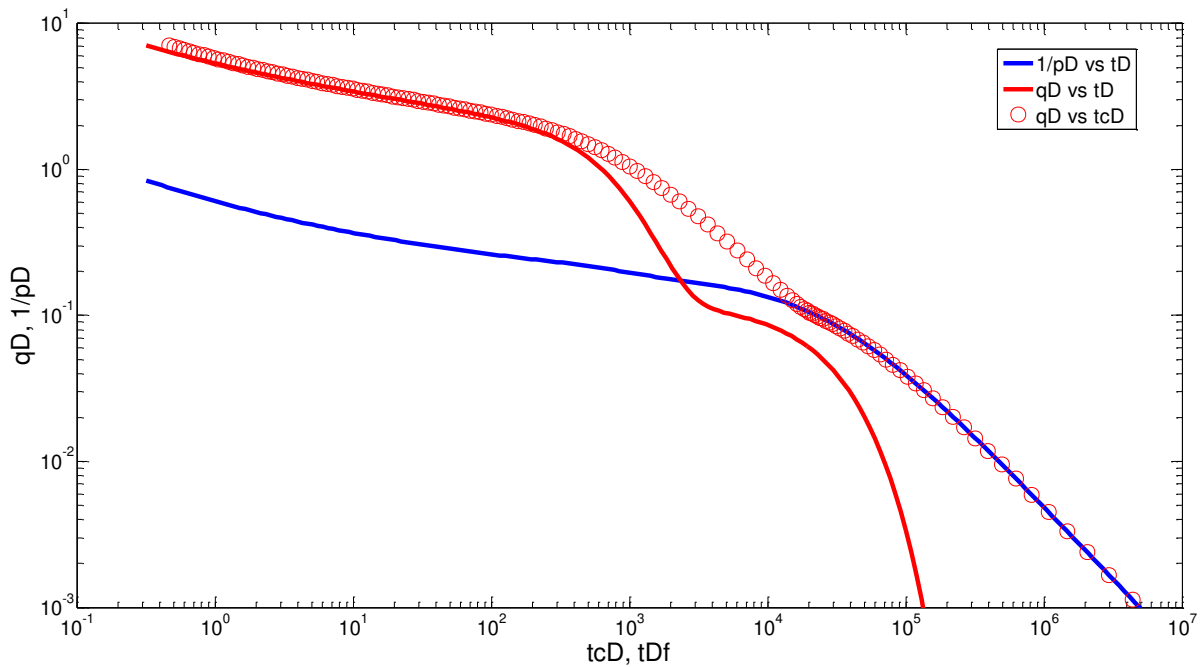


Figure 4.3 – Comparison of diffusivity solutions for dual porosity system between constant flow rate ($1/P_{wDf}$) and constant flowing pressure (q_{Df}). $r_{eD} = 100$; $\omega = 0.1$; $\lambda = 1 \times 10^{-4}$.

4.4. Derivation of Production Data Analysis Methods for NFR

As presented in literature review, the main APDA techniques were developed based on similar assumptions and share a comparable accuracy. For this reason, two APDA methods were selected to derive the dual porosity model: dynamic material balance (a type curveless method), and Blasingame type curves. It is important to remember that the development presented here is based corresponds to NFR with pseudosteady-state interporosity flow.

Dynamic Material Balance (DBM) was chosen for being a straight-forward method and for offering better resolution Cartesian plot scale compared to type-curve log-log methods in estimating fluid in place (**Mattar and Anderson 2003**). On the other hand, the Blasingame type curve method has been the focus of attention in recent years and it smooths noisy data by using the rate integral function.

4.4.1 Dynamic Material Balance method for NFR

For pseudosteady-state interporosity flow, **Eq. 4.8** and **Eq. 4.9** can be expressed in the dimensional units following the same procedure made by **Mattar and Anderson (2005)**. We considered a single gas phase compressible fluid flow and a volumetric circular reservoir.

Given the definition of total initial compressibility (**Eq. 4.22**), total compressibility of each system can be approximated to gas compressibility due to the difference between gas and liquid compressibility (**Eq. 4.23**). This assumption leads to a constant storativity ratio (ω) through time.

$$c_{t_i} = c_{t_{if}} + c_{t_{im}} \dots\dots\dots (4.22)$$

$$c_{t_i} \approx c_{g_{if}} + c_{g_{im}} \cong 2c_{g_i} \dots\dots\dots (4.23)$$

With these considerations, applying the dimensionless definitions (**Eq. 4.3** to **Eq. 4.7**) to **Eq. 4.8** and **Eq.4.9**, the fracture and total system pressure drop are described as:

For fractures system:

$$P_{p_i} - P_{p_{wf}} = \frac{1}{c_{g_i} \omega G} t_{ca} + \frac{142.2 q_{g_i} \mu_{g_i} B_{g_i}}{k_f h} \left[\ln \left(\frac{r_e}{r_{wa}} \right) - \frac{3}{4} \right] \dots\dots\dots (4.24)$$

For total system:

$$P_{p_i} - P_{p_{wf}} = \frac{1}{c_{g_i} G} t_{ca} + \frac{142.2 q_{g_i} \mu_{g_i} B_{g_i}}{k_f h} \left[\ln \left(\frac{r_e}{r_{wa}} \right) - \frac{3}{4} + \frac{2(1-\omega)^2 r_{wa}^2}{\lambda r_e^2} \right] \dots\dots\dots (4.25)$$

Where:

$$G = \frac{(\phi_f + \phi_m) \pi r_e^2 h}{B_{gi}} \dots\dots\dots (4.26)$$

$$\phi_m = (1 - \phi_f) \phi_{gr} \dots\dots\dots (4.27)$$

Simplified **Eq. 4.24** and **Eq. 4.25** by defining the inverse productivity constant of the fracture system (b_{pss}) and total system (\tilde{b}_{pss}), rearranging terms and expressing them as a straight line we obtain **Eq. 28** and **29**. A detailed development is presented in **Appendix C**.

For fracture system:

$$\frac{P_{pi} - P_{pwf}}{q_g} = m_f t_{ca} + b_{pss} \dots\dots\dots (4.28)$$

For total system:

$$\frac{P_{pi} - P_{pwf}}{q_g} = m_{f+m} t_{ca} + \tilde{b}_{pss} \dots\dots\dots (4.29)$$

Where:

$$m_f = \frac{1}{\omega G c_{ti}} \dots\dots\dots (4.30)$$

$$m_{f+m} = \frac{1}{G c_{ti}} \dots\dots\dots (4.31)$$

$$b_{pss} = \frac{142.2 q_{gi} \mu_{gi} B_{gi}}{k_f h} \left[\ln \left(\frac{r_e}{r_{wa}} \right) - \frac{3}{4} \right] \dots\dots\dots (4.32)$$

$$\tilde{b}_{pss} = \frac{142.2 q_{gi} \mu_{gi} B_{gi}}{k_f h} \left[\ln \left(\frac{r_e}{r_{wa}} \right) - \frac{3}{4} + \frac{2(1-\omega)^2 r_{wa}^2}{\lambda r_e^2} \right] \dots\dots\dots (4.33)$$

A Cartesian plot of $\left(\frac{P_{pi} - P_{pwf}}{q_g} \right)$ vs. t_{ca} is known as Inverse Productivity Plot (**Fig. 4.4**).

In this plot, fluid produced at a boundary-dominated flow constitutes a straight line tendency. Contrary to single porosity model, in this case there are two straight line behaviors, defined by **Eq. 4.28** and **Eq. 4.29**.

Mathematically gas volume stored in fracture and total systems could be determined separately from each slope. However, this depends of the nature of the fluid, production data frequency, and characteristics of the fractured system the fracture OGIP (ωG) could not be

determined (orange dashed line) (Eq. 4.28). Preferential conditions would be low mobility fluids (k/μ), high production data frequency (i.e. $\Delta t = 1$ hr.) and very low matrix permeability. The total system Original Gas-in-place (OGIP) is determined from the second slope (green dashed line) (Eq. 4.29).

The correct material balance pseudo-time (t_{ca}) and averages normalized pseudo-pressures ($\overline{P_p}$) can be obtained using Eq. 4.1 through an iterative process:

- First an initial value of OGIP is assumed
- The average reservoir pressures are calculated using the material balance relationship:
$$\frac{P}{Z} = \frac{P_i}{Z_i} \left(1 - \frac{Gp}{G} \right).$$
- Next, the material balance pseudo-time is calculated and plotted against the normalized pseudo-pressure (Fig. 4.4).
- Then a new value of OGIP is determined graphically from the second slope, which represent the total system fluid volume.
- Finally, the new OGIP is compared with the initial guess of step “a”. If they are different the new OGIP is used in step “b”. The process is repeated until obtain convergence of OGIP, therefore the correct t_{ca} values.

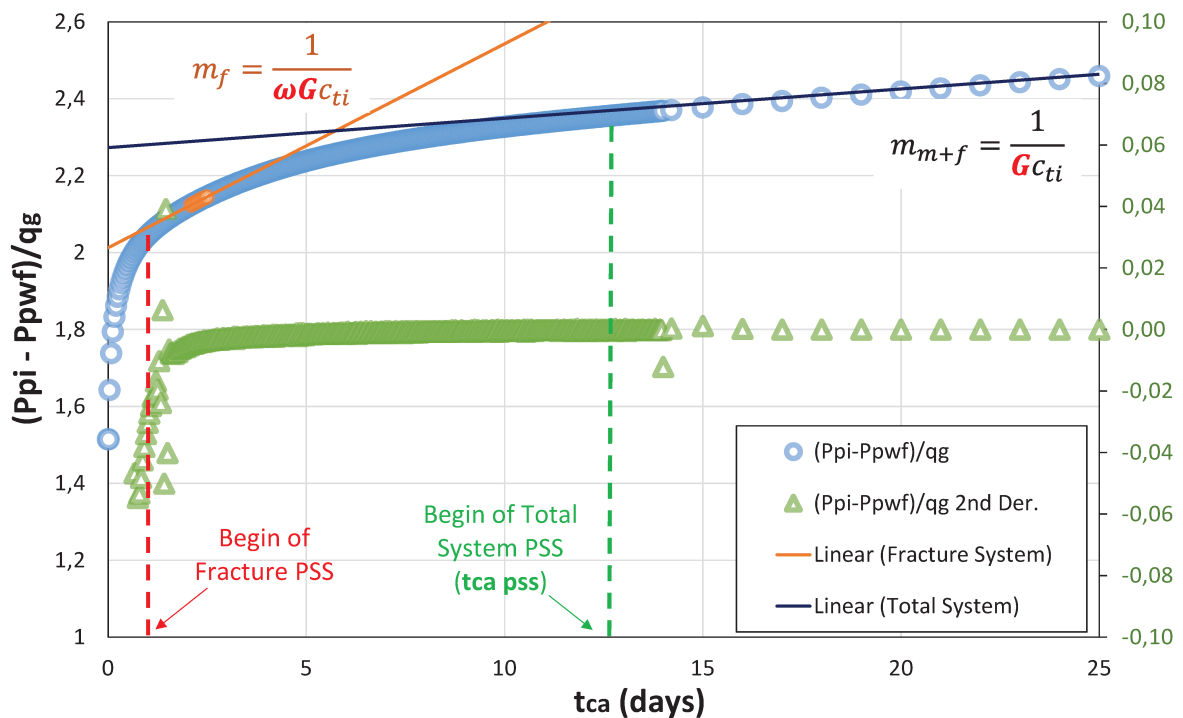


Figure 4.4 – Inverse productivity plot for Dual Porosity System.

Another result of the iterative process would also be the average reservoir pressure, given the relation between OGIP and average P/Z, which are necessary for fluid properties calculations. If the first slope, corresponding to the fluid volume in fractures, is identified in the Cartesian plot, an estimation of the storativity ratio (ω) can be made.

Once the OGIP is determined, the fracture permeability can be calculated if we know the time at which the pressure drop reaches the total system volume (**Fig. 4.4**), also called pseudosteady-state total system time ($t_{ca\,pss}$). This parameter can be determined graphically using the second derivative of the normalized pseudo-pressure $d^2(\frac{P_{pi}-P_{w\,f}}{q_g})/dt_{ca}^2$, when this becomes zero (**Fig. 4.4**).

$$k_f = \frac{t_{DA}[(\phi c_t)_f + (\phi c_t)_m] \mu_{g_i} A}{0,00633 \, t_{ca\,pss}} \dots\dots\dots (4.34)$$

Wellbore skin can be determined through **Eq. 4.35**, also with an iterative process, if ω and λ are available data (i.e. from a previous well testing). It is important to remark that wellbore skin is strongly dependent on these values, especially for damaged formations, otherwise some error is incorporated. The additional term ε becomes considerable for negative values of wellbore skin (stimulated wells):

$$S = \ln\left(\frac{r_w}{r_{wa}}\right) \dots\dots\dots (4.35)$$

Where:

$$r_{wa} = \frac{r_e}{e^{\left(\frac{\tilde{b}_{pss} k_f h}{141.2 \, B g_i \mu_{g_i}} + \frac{3}{4} - \frac{2(1-\omega)^2 r_{wa}^2}{\lambda r_e^2}\right)}} = \frac{r_e}{e^{\left(\frac{\tilde{b}_{pss} k_f h}{141.2 \, B g_i \mu_{g_i}} + \frac{3}{4} - \varepsilon\right)}} \dots\dots\dots (4.36)$$

$$\varepsilon = \frac{2(1-\omega)^2 r_{wa}^2}{\lambda r_e^2} = \frac{2(1-\omega)^2}{\lambda r_e^2} \dots\dots\dots (4.37)$$

Another useful configuration of this method, to determine OGIP, should be obtained if we rearrange and simplify terms in **Eq. 4.28** and **Eq. 4.29**, leaving them in its simplest form (similar to **Agarwal-Garner** method):

For fracture system:

$$\frac{q_g}{P_{p_i} - P_{p_{wf}}} = - \frac{1}{\omega G b_{pss}} \frac{\omega G (P_{p_i} - \bar{P}_p)}{(P_{p_i} - P_{p_{wf}})} + \frac{1}{b_{pss}} \dots \dots \dots (4.38)$$

For total system:

$$\frac{q_g}{P_{p_i} - P_{p_{wf}}} = - \frac{1}{G \tilde{b}_{pss}} \frac{G (P_{p_i} - \bar{P}_p)}{(P_{p_i} - P_{p_{wf}})} + \frac{1}{\tilde{b}_{pss}} \dots \dots \dots (4.39)$$

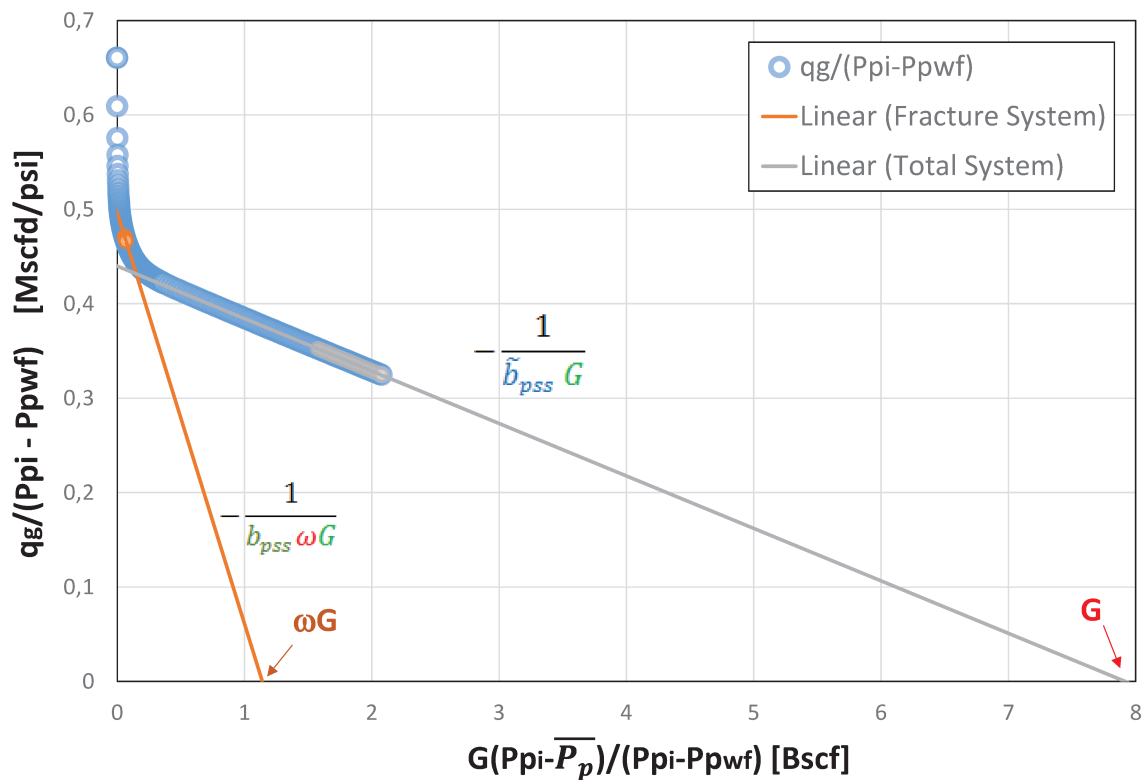


Figure 4.5 – Material balance plot for dual porosity system.

4.4.2 Blasingame Type Curve method for NFR

Aiming to obtain the storativity ratio (ω) and the interporosity (λ) flow coefficient from the available production data, we derived the Blasingame type curve method for NFR. The use of type curves basically consist in matching theoretical solutions of a determined system

with an analogous production data response to determined reservoir. For convenience type curves are usually presented in terms of dimensionless variables (defined at the beginning of this chapter) and production data in dimensional real variables.

As was presented for DMB method, we have two approximate solutions to describe the behavior of fractures and total system respectively. Nevertheless, for the type curve method we employed only approximate solutions for the total system volume (**Eq. 4.9**). The type curves are generated with the exact solution in Laplace space which accounts for all flow regimes and systems, therefore the fracture system behavior will match automatically.

Type Curve Development:

The type curves are constructed following the same procedure of **Palacio and Blasingame**, for dual porosity system. The dimensionless decline rate (q_{Ddf}) and the dimensionless decline time (t_{Ddf}) are defined as:

$$q_{Ddf} = q_{Df} \left[\ln(r_{eD}) - \frac{1}{2} \right] \dots\dots\dots (4.40)$$

This corresponds in dimensional variables to:

$$q_{Ddf} = \frac{142,2\mu_{gi}B_{gi}}{k_f h} \frac{q_g}{(p_{pi} - p_{wff})} \left[\ln(r_{eD}) - \frac{1}{2} \right] \dots\dots\dots (4.41)$$

and

$$t_{Ddf} = \frac{1}{\frac{1}{2}(r_{eD}^2 - 1) \left(\ln(r_{eD}) - \frac{1}{2} \right)} t_{DAf} \dots\dots\dots (4.42)$$

In dimensional time is:

$$t_{Ddf} = \frac{1}{\frac{1}{2}(r_{eD}^2 - 1) \left(\ln(r_{eD}) - \frac{1}{2} \right)} \frac{6.33 \times 10^{-3} k_f}{(\phi c_{ti})_{f+m} \mu_{gi} A} t \dots\dots\dots (4.43)$$

The dimensionless decline rate integral (q_{Ddi}), was defined as (**McCray 1990**) to smooth noisy production data (**McCray 1990**) and the dimensionless decline rate integral derivative (q_{Ddid}), to identify typical behavior of a fractured system:

$$q_{Ddid} = \frac{N_{pDd}}{t_{Ddf}} = \frac{1}{t_{Ddf}} \int_0^{t_{Dd}} q_{Ddf}(t_{Ddf}) dt_{Ddf} \dots \dots \dots (4.44)$$

$$q_{Ddid} = -\frac{dq_{Ddid}}{d \ln(t_{Ddf})} = -t_{Dd} \frac{dq_{Ddi}}{dt_{Ddf}} = q_{Ddid} - q_{Ddf} \dots \dots \dots (4.45)$$

The Blasingame type curve for a dual porosity system is presented in **Fig. 4.6**. This figure shows the sensibility of storativity ratio (ω), where unity corresponds to the case of a homogeneous reservoir. As can be seen, the dimensionless decline rate integral derivative (q_{Ddid}) is the variable that visually assists in identifying determined characteristics of the system.

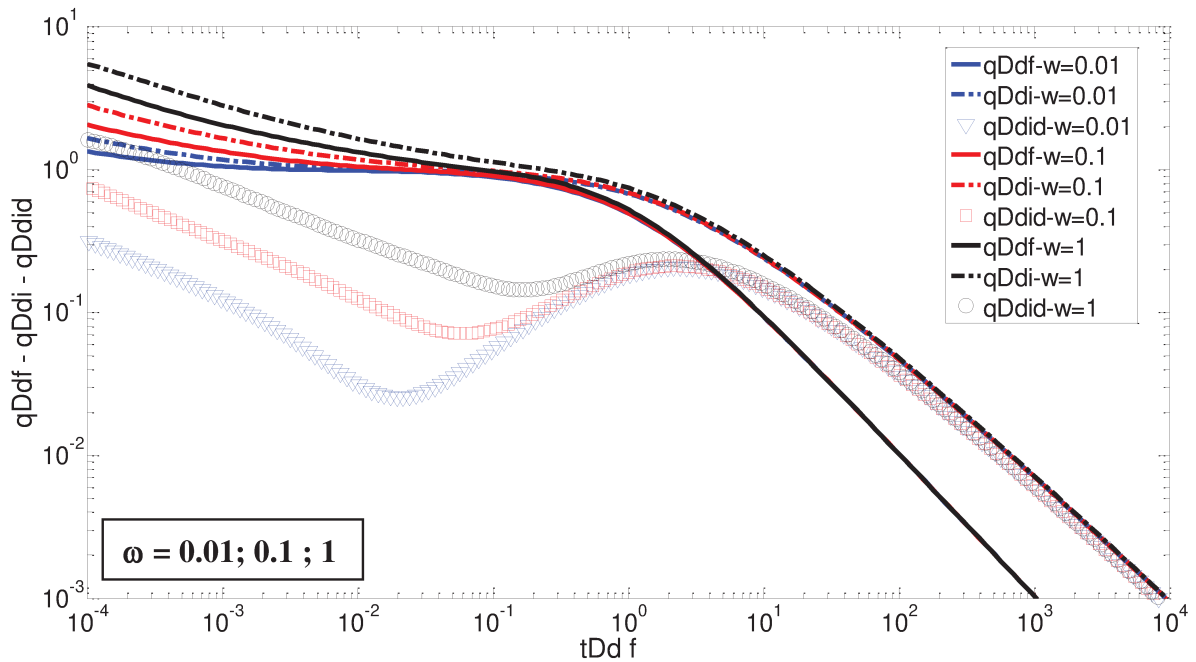


Figure 4.6 – Decline type curves for dual porosity systems. $r_{eD} = 100$; $\lambda = 1 \times 10^{-4}$.

The derivation of dimensional variables is the same as described for the dynamic material balance method, until **Eq. 4.29**. This last equation can be rearranged as **Eq. 4.46** and reduced to the **Arps (1945)** harmonic decline curve format (**Eq. 4.47**) by defining additional dimensionless variables: dimensionless decline rate (q_{Ddf}) and dimensionless decline time (t_{caDd}). It is understood that Blasingame type curve requires the same procedure, as described for DMB, to determine the material balance pseudo-time (t_{ca}) for the total fluid volume.

For total system:

$$\frac{q_g}{P_{p_i} - P_{p_{wf}}} \tilde{b}_{pss} = \frac{1}{1 + \frac{m_{f+m} t_{ca}}{\tilde{b}_{pss}}} \dots\dots\dots (4.46)$$

$$q_{Dd_{f+m}} = \frac{1}{1 + t_{caDd}} \dots\dots\dots (4.47)$$

Where:

$$q_{Dd_{f+m}} = \frac{q_g}{P_{p_i} - P_{p_{wf}}} \tilde{b}_{pss} \dots\dots\dots (4.48)$$

$$t_{caDd} = \frac{m_{f+m}}{\tilde{b}_{pss}} t_{ca} \dots\dots\dots (4.49)$$

Finally, a scaled Log-Log plot of $\frac{q_g}{P_{p_i} - P_{p_{wf}}}$ vs. t_{ca} would overlay the q_{Dd_f} vs. t_{Dd_f} trend for a harmonic decline on **Fetkovich** type curve. To improve the match, similar to **Eq. 4.44** and **Eq. 4.45**, the normalized pseudo-pressure rate $\frac{q_g}{P_{p_i} - P_{p_{wf}}}$ can be integrated (**Eq. 4.50**) and then derived (**Eq. 4.51**).

$$\left(\frac{q_g}{P_{p_i} - P_{p_{wf}}} \right)_i = \frac{1}{t_{ca}} \int_0^{t_{ca}} \left(\frac{q_g}{P_{p_i} - P_{p_{wf}}} \right) dt_{ca} \dots\dots\dots (4.50)$$

$$\left(\frac{q_g}{P_{p_i} - P_{p_{wf}}} \right)_{id} = -t_{ca} \frac{d}{dt_{ca}} \left[\left(\frac{q_g}{P_{p_i} - P_{p_{wf}}} \right)_i \right] \dots\dots\dots (4.51)$$

The matching process is easier with the use of three variables, especially for noisy production data. Once the match is achieved with production data variables, the type curve plot and the Log-Log plot provides the following information: q_{Dd_f} , $\left[\frac{q_g}{(P_{p_i} - P_{p_{wf}})} \right]$, t_{Dd_f} , t_{ca} , r_{eD} , ω and λ . A detailed matching process is described in **Appendix D**.

The fracture permeability can be calculated from **Eq. 4.41**:

$$k_f = \frac{142,2 \mu g_i B g_i}{h} \frac{\left[\frac{q_g}{(P_{p_i} - P_{p_{wf}})} \right]_{MP}}{(q_{Dd_f})_{MP}} \left(\ln(r_{eD}) - \frac{1}{2} + \frac{2(1-\omega)^2 r_{wa}^2}{\lambda r_e^2} \right) \dots\dots\dots (4.52)$$

Wellbore skin is calculated from **Eq. 4.53** once the dimensionless external radius (r_{eD}) is obtained from the matching process:

$$S = \ln \left(\frac{r_w}{r_{wa}} \right) \dots\dots\dots (4.53)$$

Where:

$$r_{wa} = \frac{r_e}{r_{eD}} \dots\dots\dots (4.54)$$

The OGIP is obtained from **Eq. 4.55**:

$$G = \frac{1}{c_{ti}} \frac{t_{ca}}{t_{Ddf}} \frac{\left[\frac{q_g}{(P_{pi} - P_{wfp})} \right]_{MP}}{(q_{Ddf})_{MP}} \dots\dots\dots (4.55)$$

As it was pointed out at the end of section 4.2, naturally fractured reservoirs with transient interporosity flow demonstrated that the long-time approximate solution is the same as for homogeneous reservoirs. Therefore, current APDA methods can be applied for their analysis and are better described by the original authors.

4.5. Considerations for Gas-Condensate Reservoirs

For gas-condensate reservoirs, the normalized pseudo-pressure (**Eq. 2.42**) was corrected using the two phase compressibility factor (Z_{tp}), to avoid under estimation of the OGIP. This approach first proposed by **Sadeghi et al. (2011)**, for the two-phase region (below dew point pressure). The Z_{tp} can be obtained from Equation of State (EOS) or estimated using correlations (**Raya et al.**).

5. VALIDATION OF THE METHODS

In this chapter, the advanced production data analysis methods based on the dual porosity model are validated using synthetic data and real field data. The synthetic data was generated by a commercial simulator (IMEX-CMG). Two cases are presented: a constant gas flow rate well and a variable oil flow rate well. The real field case study corresponds to a gas-condensate naturally fractured reservoir producing from Devonian sandstones.

5.1. Reservoir Simulation Model

This section aims to confirm the accuracy of the modified methods compared with the information of a known dual porosity reservoir model. The evaluated parameters are the Original Gas-in-Place (OGIP), averages reservoir pressures, and reservoir parameters (fracture permeability, wellbore skin, storativity ratio and interporosity flow coefficient. In this section two cases (single phase flow) were evaluated: a constant gas flow rate and a variable oil flow rate.

5.1.1 Constant Gas Flow Rate Well

The gas simulation model was built using a radial grid, with 50 radial divisions and an external radius of 3000 ft. As commented in Chapter 2, the developments of the equations for APDA were done considering a single phase compressible fluid. This case also evaluated the assumption of constant storativity ratio (ω) as a function of pressure.

The reservoir and fluid properties are summarized in **Table 5.1** and the general production data in **Table 5.2** (data frequency: 1 hr.). **Fig. 5.1** presents the production history plot for constant gas flow rate.

Table 5.1 – Reservoir and fluid properties for the simulated example: Gas reservoir

Initial Conditions		
Initial Reservoir Pressure, P_i	6000	(psia)
Reservoir Temperature, T_r	250	(°F)
Original Gas-in-Place, OGIP	100.89	(Bscf)
Fluid Properties		
Specific Gravity of Gas, SG_g	0.6	
Formation Volume Factor, B_g	0.0036	(scf/cf)
Gas Viscosity, μ_g	0.026	(cp)
Gas Compressibility, c_g	1.37E-4	(1/psi)
Water compressibility, c_w	3E-6	(1/psi)
Well Information		
Vertical well depth	14700	(ft)
Wellbore radius, r_w	0,25	(ft)
Wellbore skin, s	0	
Formation Properties		
Formation Thickness, h	200	(ft)
Fracture Permeability, k_f	10	(md)
Fracture Porosity, ϕ_f	0.08	(fraction)
Matrix Porosity, ϕ_m	0.005	(fraction)
Fracture Compressibility, c_f	3.5×10^{-6}	(1/psi)
Matrix Compressibility, c_m	5.5×10^{-6}	(1/psi)
Water Saturation, S_w	0.2	(fraction)
Storativity Ratio, ω	0.1	(fraction)
Interporosity flow coefficient, λ	6×10^{-8}	(fraction)

Table 5.2 – General production information

Production Parameters		
Gas flow rate, q_g (CONST.)	15	MMscfd
Production time, t_p	12	(months)
Cumulative Gas Produced, G_p	5.475	(Bscf)
Average Reservoir Pressure, P_r	5558.62	(psi)

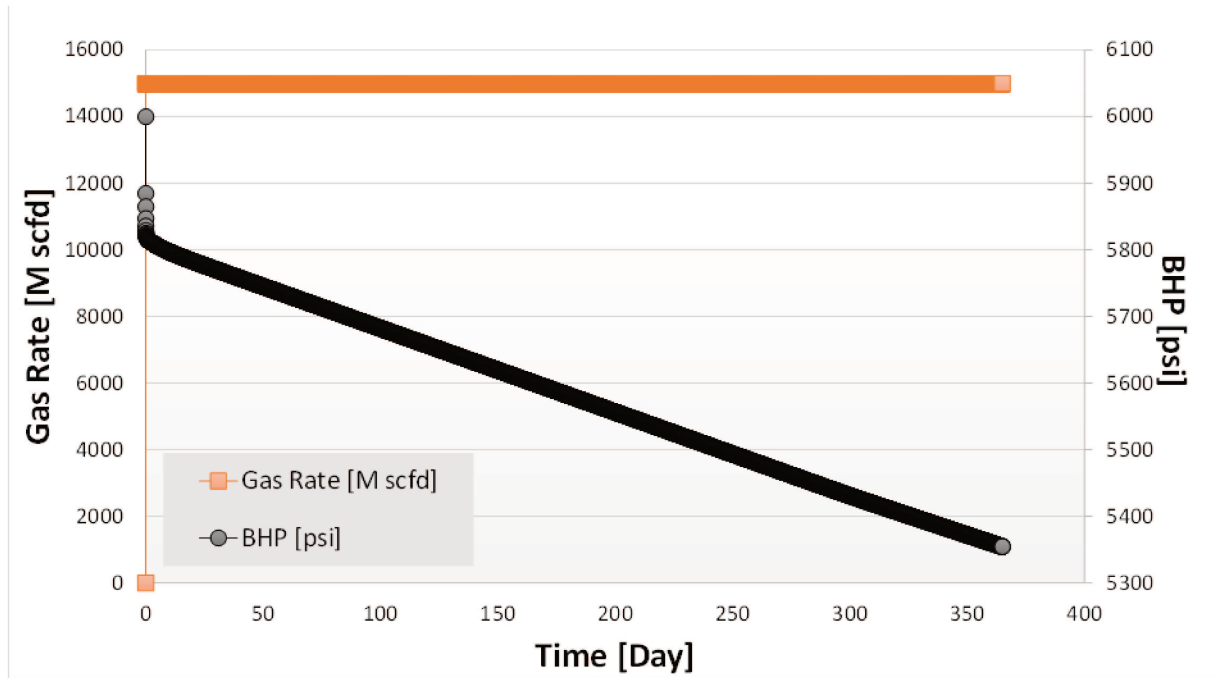


Figure 5.1 – Production history plot. Constant gas flow rate.

The production data was first analyzed with DMB method, we first calculate the normalized pseudo-pressure $\left(\frac{(P_{pi}-P_{pwf})}{q_g}\right)$ and estimate the material balance pseudo-time through the iterative procedure described in Chapter 4. After few iterations using inverse productivity plot (**Fig. 5.2**) we determined an OGIP of 115.48 Bscf.

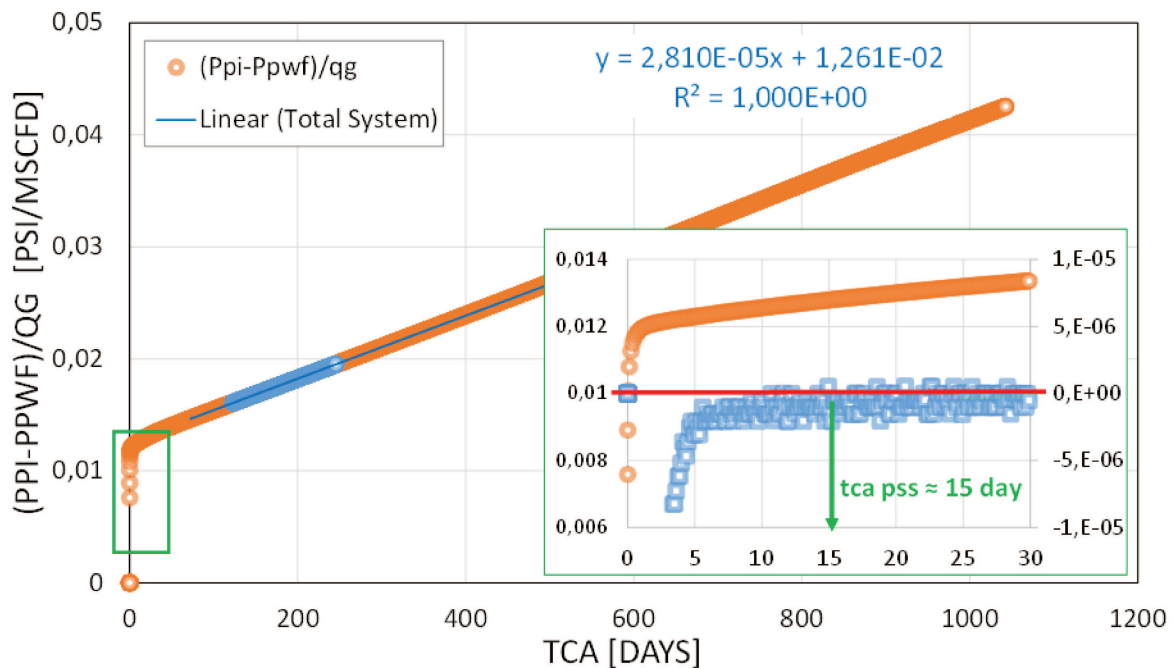


Figure 5.2 – Inverse productivity plot for dual porosity system. Constant gas flow rate.

The second derivative of normalized pseudo-pressure helps to estimate the time at which total system reaches the boundaries of the reservoir ($t_{ca-pss} \approx 17$ days) required for the calculation of the fracture permeability. The wellbore skin (considering ω and λ known variables from previous well testing). Fracture system was not detected by the second derivative apparently due to the high mobility of the gas.

On the other hand, the type curve method allows determining additional parameters. Once (t_{ca}) was determined iteratively in DMB method procedure, these values were used for the type curve method match. Next we calculate the normalized rate, the normalized rate integral and the integral derivative and plotted in a Log-Log scale. The type curves are constructed for the dual porosity system parameters ($\omega = 0.1$; $\lambda = 6E-8$, and $r_{eD} = 12000$). Finally, after a match is achieved as presented in **Fig. 5.3**, we obtain the match variables presented in **Table 5.3**.

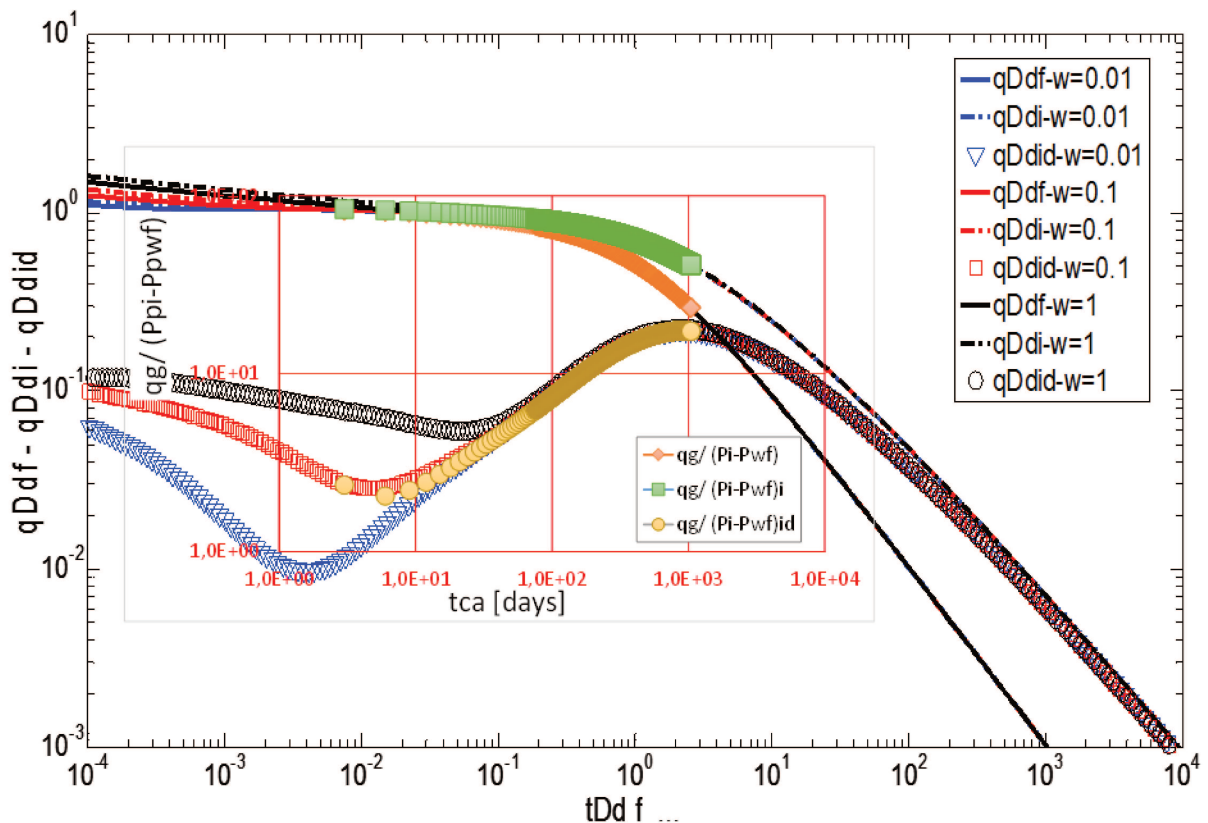


Figure 5.3 – Blasingame type curves for dual porosity system. Constant gas flow rate. $r_{eD} = 12000$ and $\lambda = 6E-8$.

Table 5.3 – Match point for dual porosity system type curve: Constant gas flow rate

Type Curve Plotting Functions	Value	Data Plotting Functions	Value
$t_{Dd f}$	1E-1	r_{eD}	12000
$q_{Dd f}$	5E-2	ω	0.1
t_{ca}	4E+1	λ	6E-8
$q_g/(P_{pi}-P_{pwf})$	4E+0		

A summary of the results of DMB and the type curve methods are presented in **Table 5.4**, with the respective error compared to the simulator values. These results were obtained after 365 days of production, with a cumulative production of 5.474 Bscf which represents a recovery factor of 5.43 %, and an average pressure drop of 7.36%.

Table 5.4 – Results of DMB and type curve methods: Constant gas flow rate.

	Simulator	DMB	% error	Type Curve	% error
OGIP [Bscf]	100.89	106.76	0.81	103.69	2.77
r_e [ft]	3000	3011.00	0.37	2967.47	1.08
P. avg. [psia]	5558.58	5522.99	0.64	-	-
K_f [md]	10	8.51	14.9	8.48	15.2
s	0	4.46	-	0	-
ω	0.1	-	-	0.1	0
λ	6E-8	-	-	6E-8	0

The behavior of the correct total compressibility and approximated total compressibility as a function of pressure is presented in the left side of **Fig.5.4**. In addition, the variation of storativity ratio is plotted in the right side of the figure. It can be observed, that the change in the storativity ratio (ω) as a function of pressure is a minimum, therefore the assumption of a constant storativity ratio is be valid at this point.

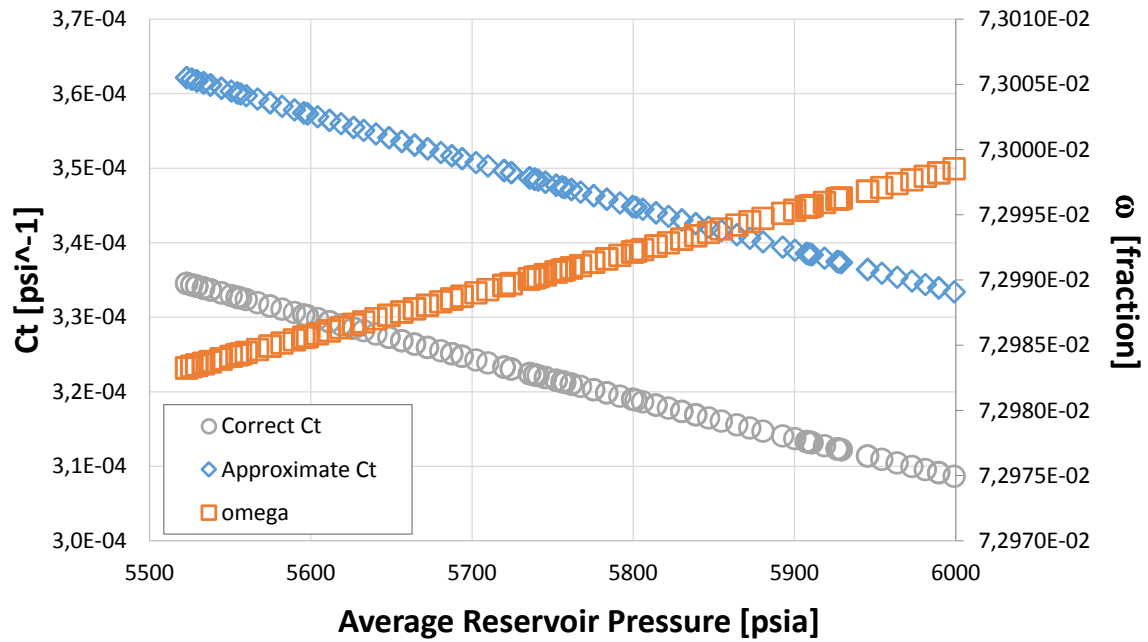


Figure 5.4 – Total compressibility and storativity ratio vs. pressure.

5.1.2 Variable Oil Flow Rate Well

The oil simulation model was built using a radial grid, with 30 radial divisions and an external radius of 1500 ft. For this case study, the storativity ratio (ω) was considered constant through time, because rock and fluid compressibility are assumed to be constant.

The reservoir and fluid properties are summarized in **Table 4.5**. The general production information is presented in **Table 5.6** and the variable oil flow rate schedule in **Table 5.7** and plotted in **Fig. 5.5** (data frequency: 1 day). As in the previous Case1, we first calculate the normalized pseudo-pressure $\left(\frac{(p_{pi} - p_{wf})}{q_g}\right)$ to analyze the data with the DMB method.

The inverse productivity plot (**Fig. 5.6**) provides directly, without iterations for liquids, the value of Original Oil-in-Place (OOIP): 7.99 MMSTB. According to the behavior of the second derivative of the normalized pseudo-pressure, the time at which total system reaches the reservoir boundaries (t_{c-pss}) is 3 days. For a daily data points, the fracture system boundary dominated flow is rarely observed. A higher data frequency would be helpful (i.e. 1 hr).

Table 5.5 – Reservoir and fluid properties for the simulated example: Oil reservoir

Initial Conditions		
Initial Reservoir Pressure, P_i	5000	(psia)
Reservoir Temperature, T_r	115	(°F)
Original Oil-in-Place, OOIP	7.74	(MMSTB)
Fluid Properties		
Oil Viscosity, μ_o	1.9	(cp)
Formation Volume Factor, B_o	1.12	(bbl/STB)
Well Information		
Wellbore radius, r_w	0,25	(ft)
Drainage radius, r_e	1500	(ft)
Wellbore skin, s	2	
Formation Properties		
Formation Thickness, h	100	(ft)
Fracture Porosity, ϕ_f	0.08	(fraction)
Matrix Porosity, ϕ_m	0.005	(fraction)
Fracture Compressibility, c_f	3×10^{-6}	(1/psi)
Matrix Compressibility, c_m	5.5×10^{-6}	(1/psi)
Fracture Permeability, k_f	50	(md)
Storativity Ratio, ω	0.1	(fraction)
Interporosity flow coefficient, λ	5×10^{-8}	(fraction)

Table 5.6 – General Production Information

Production Parameters		
Oil flow rate, q_o (VARIABLE)	-	Table 4.7
Production time, t_p	12	(months)
Cumulative Oil Produced, N_p	121.25	(MSTB)
Average Reservoir Pressure, P_r	4105.25	(psi)

Table 5.7 – Variable Oil Flow Rate Schedule.

Cumulative Time (days)	Oil Rate (BPD)	Cumulative Time (days)	Oil Rate (BPD)
0	0	77	0
15	300	140	300
30	0	191	450
45	300	250	400
56	400	323	300
76	500	365	250

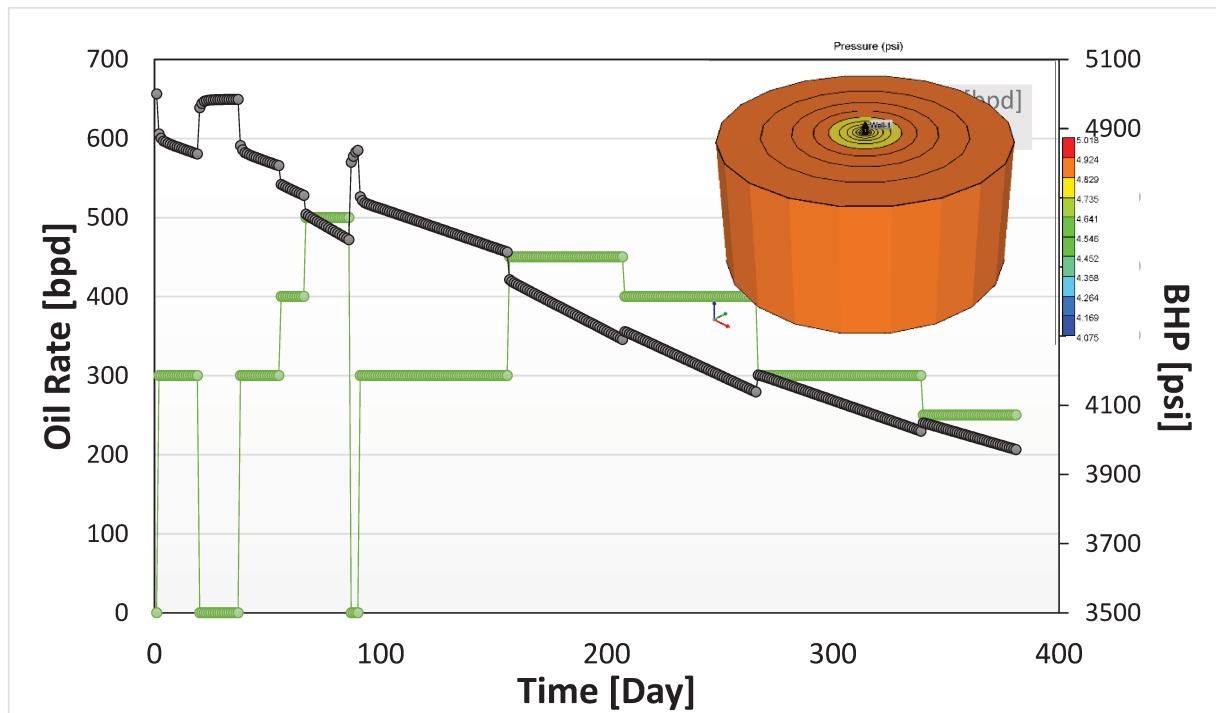


Figure 5.5 – Production history plot. Variable oil flow rate.

For the type curve method (**Fig. 5.7**), the same procedure as gas simulated case study is applied. First the normalized rate, normalized rate integral and its normalized rate integral derivative are calculated, and then the types curves are generated for $\omega = 0.1$ and $\lambda = 5E-8$. This time we performed a sensitivity of the external dimensionless radius (r_{eD}) for 6000, 10000 and 20000, because the wellbore skin is different of zero ($r_{eD} \neq 6000$). The matched parameters are presented in **Table 5.8** and a comparison of results in **Table 5.9**.

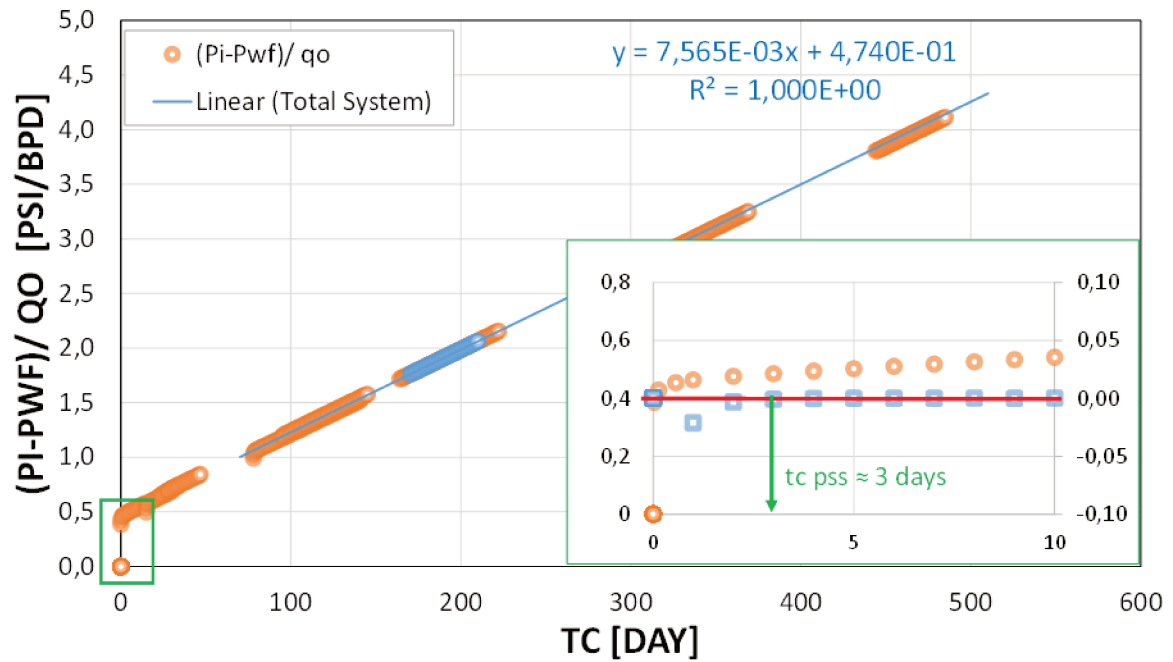


Figure 5.6 – Inverse productivity plot for dual porosity system. Variable oil flow rate.

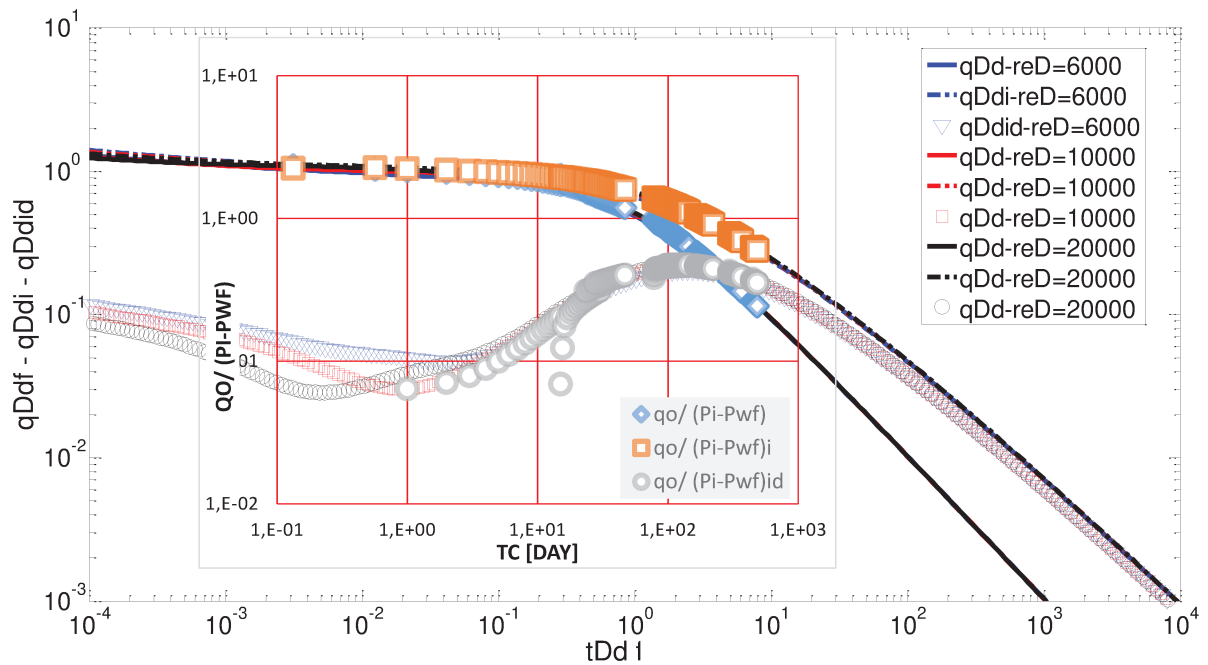


Figure 5.7 – Blasingame type curves for dual porosity system. Variable oil rate case. $\omega = 0.1$ and $\lambda = 5E-8$

As can be seen, by applying the material balance time concept, the variable production converge to an equivalent constant production flow rate for DMB method (**Fig. 5.6**) and type curve method (**Fig. 5.7**). It is important to point out, that if conventional APDA based on single porosity were applied, fracture permeability doubles ($k_f = 71$ md) in Blasingame method, and wellbore skin is negative for DMB method ($s = -0.91$).

Table 5.8 – Match point for dual porosity system type curve: Variable oil flow rate.

Type Curve Plotting Functions	Value	Data Plotting Functions	Value
t_{Ddf}	1E-1	r_{eD}	10000
q_{Ddf}	2E-1	ω	0.1
t_{ca}	6E+0	λ	5E-8
$q_g/(P_{pi}-P_{pwf})$	4E-1		

Table 5.9 – Results of DMB and type curve methods: Variable oil flow rate.

	N. Simulator	DMB	% error	Type Curve	% error
OOIP [MMSTB]	7.74	7.99	3.22	7.25	6.33
r_e [ft]	1500	1536.9	2.46	1464.32	2.38
P. avg. [psia]	4105.25	4082.74	0.54	3989.58	2.81
K_f [md]	50	44.43	11.14	55.35	10.7
s	2	0.266	-	0.54	-
ω	0.1	-	-	0.1	0
λ	5E-8	-	-	5E-8	0

These results were obtained after 365 days of production, a cumulative production of 121.25 MSTB, which represent a recovery factor of 1.52 %, and an average pressure drop of 17.89%. Nevertheless, according to **Fig. 5.6** and **Fig. 5.7**, with less time of production history, around 3.5 months, same results could be obtained.

5.2. Field Case Study: Devonian Gas-Condensate Field

The field case study was based on production data from a gas-condensate reservoir (Devonian sandstone) from Bolivia. First we presented some background information of the

field, then the production data was analyzed with modified APDA methods and finally the results were presented and compared with reserves report of the field.

Background Information about the Field

The field presents an anticline structure and is located in Sub-Andean region of Bolivia. The reservoir under analysis was classified as naturally fractured sandstone after numerous petrophysic studies. According to the classification made by Nelson (1985), this corresponds to a Type II (fluid storage is concentrated in matrix and the fractured network provides permeability to the system).

The field has eight producing wells, located along the structural map (**Fig. 5.8**) and the longitudinal cross-section (**Fig. 5.9**). The field started production in 2003, with four wells (X-1, X-2, X-3 and X-4). The production data selected for the analysis corresponds to the well X-3, and the period of analysis from 2003 to 2007, when well 5 starts producing.

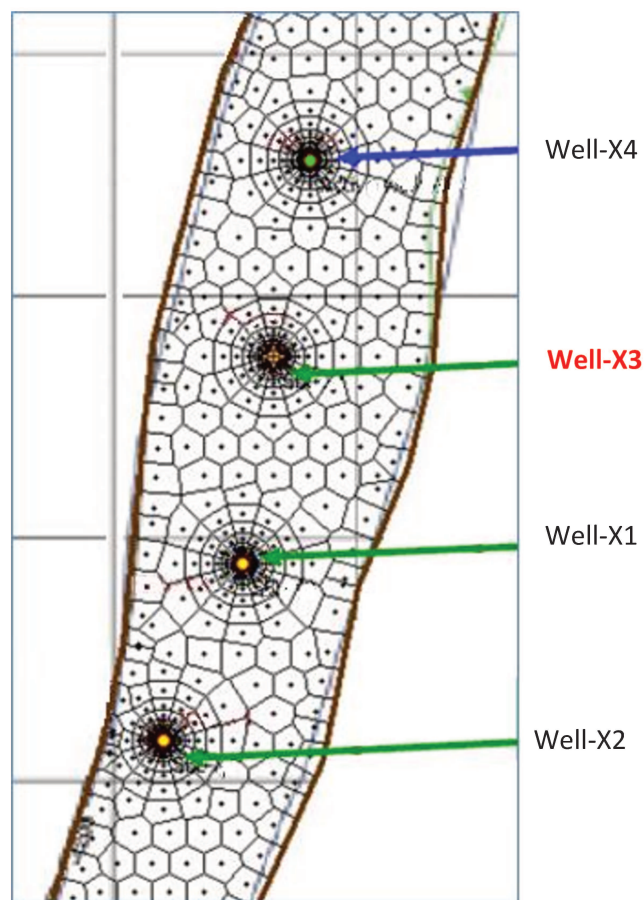


Figure 5.8 – Structural map. Field case study.

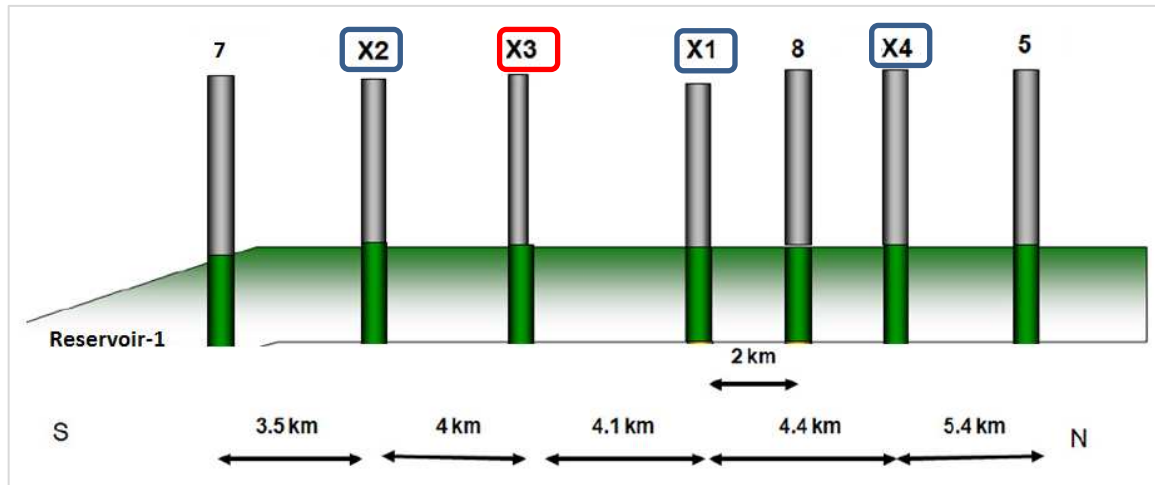


Figure 5.9 – Longitudinal section of the reservoir. Field case study.

Data Preparation and Diagnostics

Data preparation is really important before performing the analysis to avoid misinterpretations. Authors such as **Mattar and Anderson (2003)**, **Ilk et al. (2007)** and **Ilk et al. (2010)** presented methodologies to perform this step, which can be summarized as follows:

- a) Asses data viability
 - Production history data for data quality correlation
 - Reservoir and fluid data (P_i , Porosity, Net Pay, Saturations, PVT data)
 - Well records (history of interventions)
 - Measured flowing bottomhole pressures (calculate if necessary)
- b) Check data quality and Correlation
 - Fluid rate and BHP vs time: check for data correlation
 - BHP vs fluid rate: determine flow regimes
 - Clean/edit data for clarity
- c) Preliminary Diagnosis
 - Identify the expected reservoir type (Volumetric, water drive, etc.)
 - Identifying flow regimes (Diagnostic plots: Normalized PI/Blasingame)
 - Data filtering for clarity (wellbore dynamics, spikes, production noise)
 - Data review/editing (well cleanup, recompletions)
- d) Refine model parameters and summary history match.

A. DATA VIABILITY

- Production history data:

Production flow rate was measured at surface separators, with a frequency of 5 data points/month approximately (**Fig. 5.10**). The period of time for the analysis was from January 2003 to October 2006. This is because after this date, wells from the second phase of the projects start production. Well X-3 was selected for the analysis due to data availability.

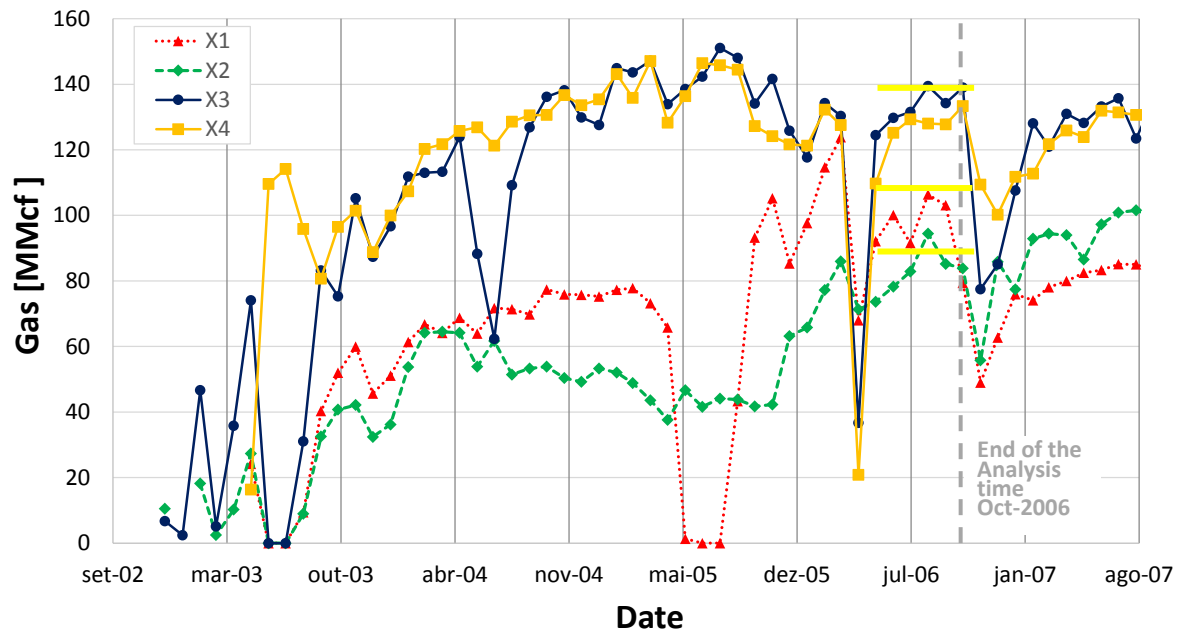


Figure 5.10 – Gas production flow rate of all four wells.

- Reservoir and fluid data:

The main reservoir and fluid data is summarized in **Table 5.10**. It is important to point out that OGIP was certified after seven years of production with conventional material balance method.

- Well Records:

The well operation history did not register any workover for this well. It just registered several well shut-ins and change in choke size.

- Bottomhole Pressures:

Accuracy of bottomhole pressure is crucial for the APDA techniques, therefore measured data is preferable. For Well X3, measured data is available with a data frequency of 1 min. As flow rate must be coupled with available bottomhole pressure, then it is desirable to have at least daily

production flow rate in order to avoid pressure data loss. However due the low frequency of production flow rate data, most of bottomhole pressure data was lost (**Fig. 5.11**).

Table 5.10 – Reservoir and fluid properties for the real field case study

Initial Conditions		
Initial Reservoir Pressure, P_i	7315	(psia)
Reservoir Temperature, T_r	230	(°F)
Original Gas-in-Place, G	8244	(Bscf)
Fluid Properties		
Specific Gravity of Gas, SG_g	0.68	
Condensate density, API	53.5	°
Condensate-Gas Ratio, CGR	25.7	STB/MMscf
Formation Volume Factor, B_g	0.0036	(scf/cf)
Gas Viscosity, μ_g	0.026	(cp)
Gas Compressibility, c_g	1.37E-4	(1/psi)
Water compressibility, c_w	3E-6	(1/psi)
Well Information		
Vertical well depth	11259.7	(ft)
Wellbore radius, r_w	0,271	(ft)
Wellbore skin, s	2.7	
Formation Properties		
Formation Thickness, h	298.55	(ft)
Fracture Porosity, ϕ_f	0.0244	(fraction)
Matrix Porosity, ϕ_m	0.0033	(fraction)
Fracture Permeability, k_f	113	(md)
Storativity Ratio, ω	0.048	(fraction)
Interporosity flow coefficient, λ	6×10^{-8}	(fraction)

In absence of measured pressure data, it must be calculated using a careful selection of flow correlations. **Cox et al. (2006)** presented a complete study about this topic.

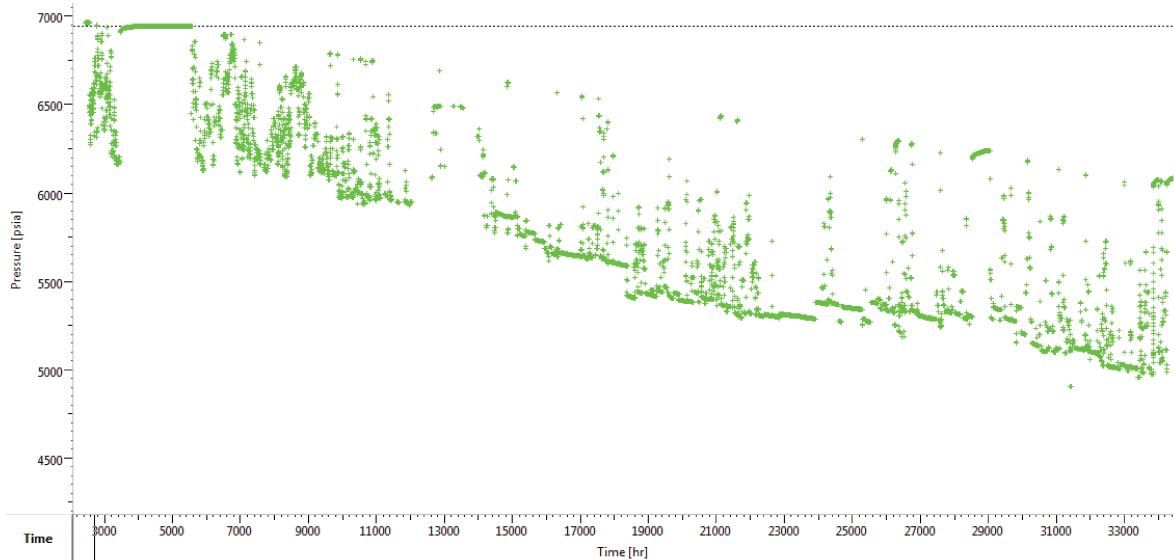


Figure 5.11 – Bottomhole Pressure History. Well X-3.

B. DATA QUALITY AND CORRELATION

In this section we apply two best-known diagnostic plots used in APDA:

- The production history plot: This plot (**Fig. 5.12**) helps to visualize data changes in time, helping identify uncorrelated data, which means changes in pressure drop, must correspond to changes in flow rate. In the case of Well-X3, apparently shows a good correlation between flow rates and bottomhole pressures.

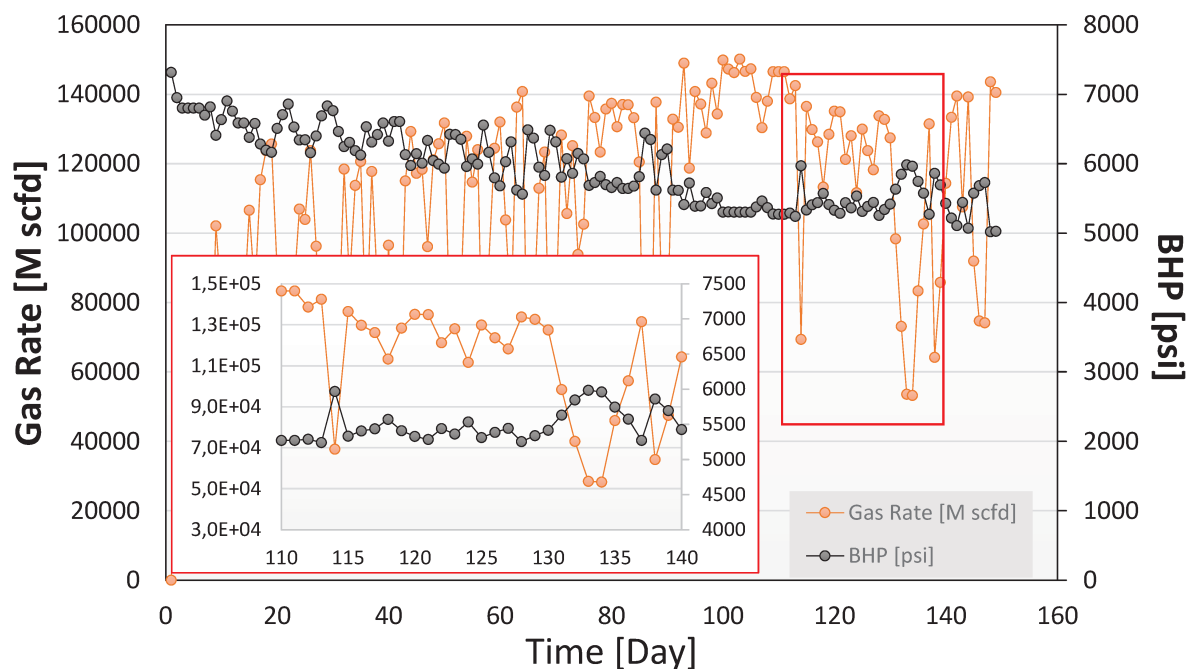


Figure 5.12 – Diagnostic plot: Gas flow rate and BHP vs. time. Well X-3.

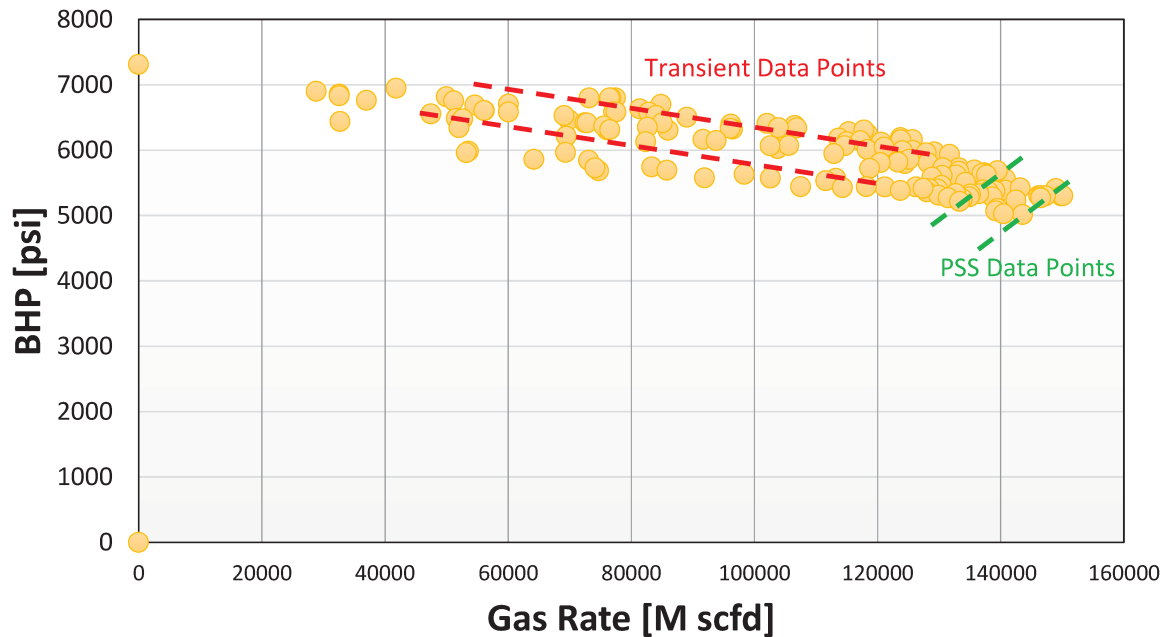


Figure 5.13 – Diagnostic plot: Pressure-rate plot. Well X-3.

- The Pressure-Rate correlation plot: This plot (**Fig. 5.13**), formalized as a diagnostic plot by **Kabir and Izgec (2006)**, helps to identify flow regimes. Production data of Well-X3 presents a general noisy transient flow trend, identified by a negative slope straight line. The pseudosteady-state flow trend, represented by a positive slope straight line, is not clearly located in the plot. However an estimation of the existence of this last flow regime could be done identify these data points with the Inverse productivity plot (**Figure 5.14**). The correlation between pressure and rate helps may be used to delete part of noisy uncorrelated data. For our analysis all production data was used.

C. PREMILINARY DIAGNOSIS

Once production and pressure data are correlated and the presence of pseudosteady-state flow is confirmed, the analysis can be performed. In this case, we are dealing with a gas-condensate reservoir, according to the literature review this kind of reservoirs can be analyzed as single-phase flow or multi-phase flow. This time the study was analyzed considering a single-phase flow, as presented by **Sadeghi et al.**

2011, therefore the correction for retrograde condensation focused on two variables: the normalized pseudo-pressure and the total gas production.

Next, after few iterations, we estimated the total system OGIP (2462.8 Bscf) through the DMB method (**Fig. 5.14** and **Fig. 5.15**). As a consequence of production data dispersion, it was very difficult to determine the OGIP using just **Fig. 5.14**. Therefore, the material balance plot (**Fig. 5.15** – See **Eq. 4.39**) was used to confirm this result providing a clear straight line trend.

The fracture OGIP and fracture permeability could not be clearly estimated with this method, due to the absence of transient flow regime data. The zoom view of **Fig. 5.14**, shows that the first points correspond to material balance pseudo-time with no clear begin of total system pseudosteady-state.

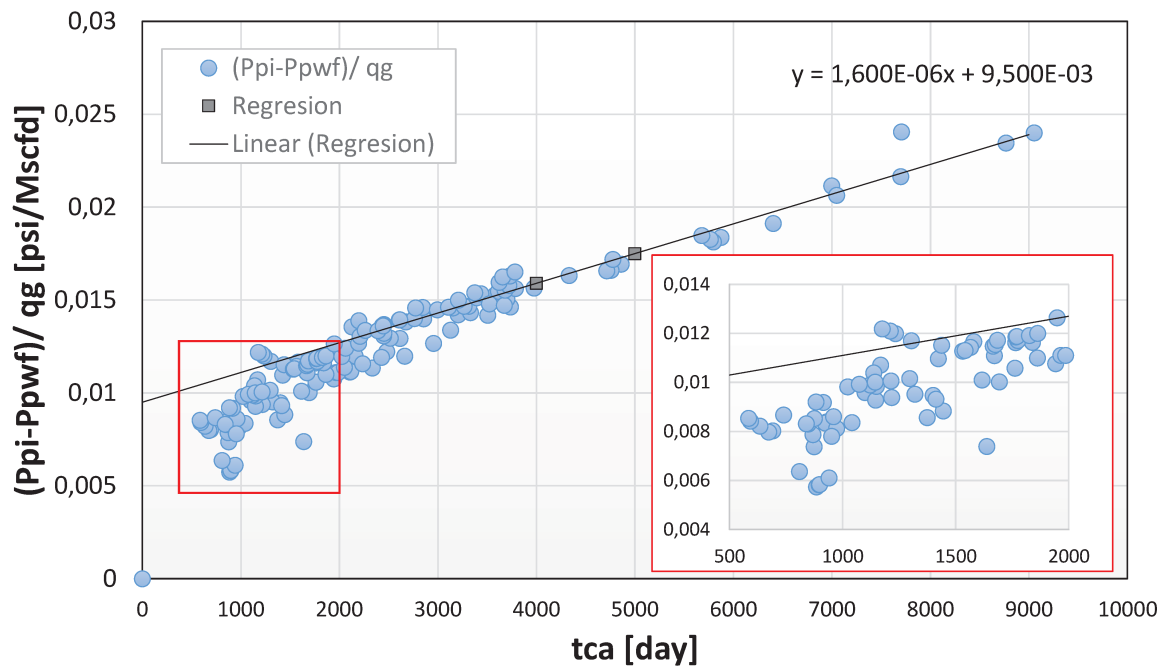


Figure 5.14 –Inverse productivity plot for dual porosity system. Well X-3.

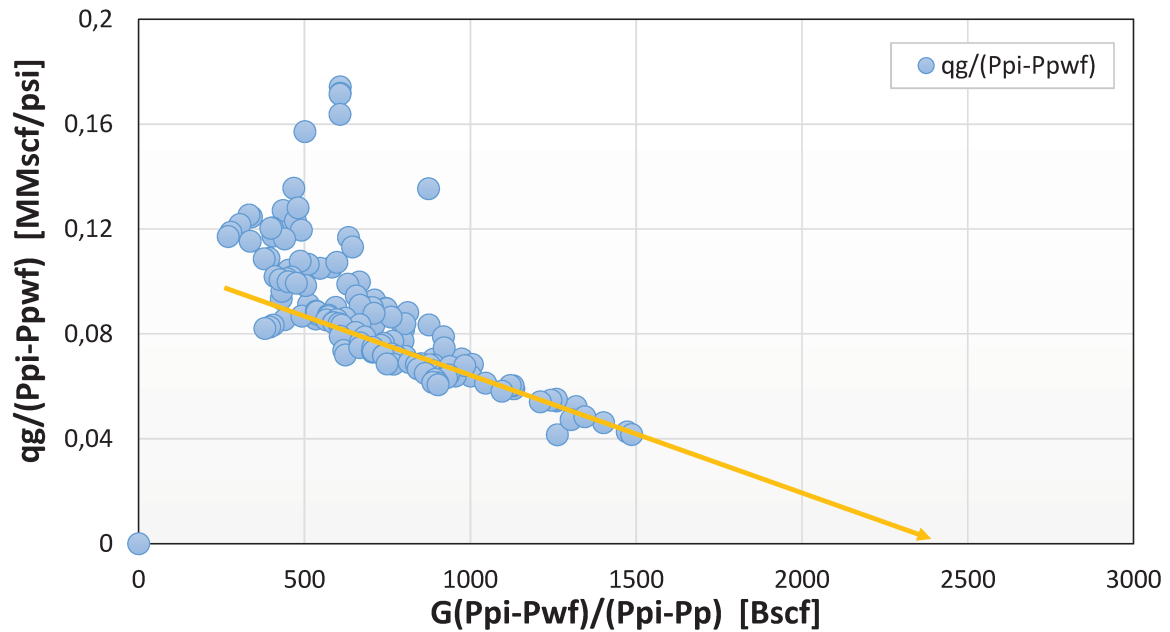


Figure 5.15 –Material balance plot for dual porosity system. Well X-3.

Once the OGIP was determined, the material balance pseudo-time (t_{ca}) was implicitly available to be used in the type curve method. The type curves were generated for different values of ω and λ . However, the low data frequency observed in **Fig. 5.16**, makes difficult to obtain a complete match of production data to obtain the variables: r_{eD} , ω and λ . As commented before, these variables have a strong influence on the estimation of permeability and skin. Consequently, the OGIP is the only value that can be calculated because only the last part of the data (right-hand points) matches the pseudosteady-state region of the plot (high values of t_{ca}).

Just for comparison we presented type curves for $\omega = 0.05$ and $\lambda = 6 \times 10^{-8}$, obtained from a previous well testing of the well, along with the homogeneous case of $\omega = 0.1$, and $r_{eD} = 100000$. It can be observed the impact of low data frequency over APDA methods. The match values is presented in **Table 5.11**, the OGIP obtained 2955.3 Bscf.

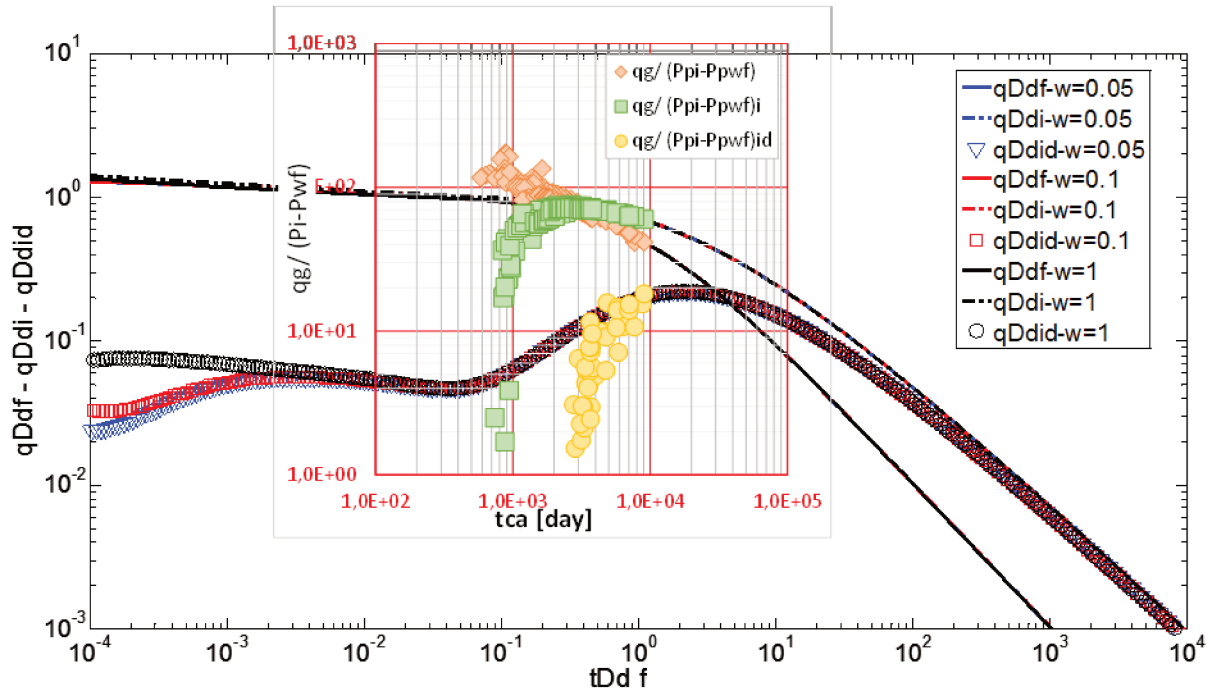


Figure 5.16 – Blasingame type curves for dual porosity system. Well X-3. $r_{eD} = 1E5$ and $\lambda = 6E-8$.

Table 5.11 – Match point for dual porosity system type curve. Well X-3.

Type Curve Plotting Functions	Value	Data Plotting Functions	Value
$t_{Dd f}$	1E-1	r_{eD}	-
$q_{Dd f}$	6E-1	ω	-
t_{ca}	9E+2	λ	-
$q_g / (P_{pi} - P_{pwf})$	5E+1		

The OGIP estimated from both methods corresponds to the drained area, of the well under analysis (Well-X3), when it was producing at PSS condition. In the field case study there are four wells producing for 3.7 years. The average flow gas rate of each well at the moment of the analysis are presented in table 5.12, they correspond to the highlighted part in yellow (July 2006) according to **Fig. 5.10**.

Table 5.12 – Determination of the total Original Gas-in-Place: DMB method.

Wells	Gas Flow Rate [MMscf]	% of Total Gas flow Rate	OGIP [Bscf]
Well 1	100	22.37	
Well 2	82	18.34	
Well 3	135	30.20	2463
Well 4	130	29.08	
Total	447	100.00	8155

Following the theory explained by **Marhaendrajana and Blasingame**, the fluid flow rates is proportional to the drainage radius of each well, consequently it is related to the OGIP corresponding to each well. This relation means that, the production percentage of a well over the total field production is equivalent to the OGIP percentage of the well over the total OGIP. **Table 5.12** presents the steps to obtain the total OGIP. Finally, in **Table 4.13** we present the results from both methods.

Table 5.13 – Results of DMB and type curve methods. Real field case study.

	CMB	DMB	% error	Type Curve	% error
Well OGIP [Bscf]	-	2462.8	-	2955.3	-
r_e [ft]	-	8480.1	-	9289.53	-
Total OGIP [Bscf]	8244	8155	1.09	9785	18.69
K_f [md]	45	-	-	-	-
s	2	-	-	-	-

These results were obtained with 147 Bscf of production data, after 3.7 years of production, which represents a recovery factor of 5.89 %, and an average pressure drop of 12.81%.

5.3. Discussion of the Results

Comments of case 1: Constant gas flow rate with no wellbore skin and pseudo-steady state interporosity flow.

Dynamic material balance and Blasingame type curve method for compressible fluids in naturally fractured reservoirs demonstrated a comparable low relative error in the estimation of OGIP ($< 3\%$), consequently the average reservoir pressure were very accurate.

The fracture permeability estimated with DMB had a good proximity with the simulated model. Wellbore skin is very sensitive to the correct estimation of total system pseudosteady-state material balance pseudo-time ($t_{ca\ pss} \approx 17$). The second derivative of normalized pseudo-pressure proved to provide good approximation to the reference value (skin = 0). It was necessary to have previous knowledge, usually from well testing, of storativity ratio (ω) and interporosity flow coefficient (λ) for the calculation of wellbore skin.

The type curve method, despite its long process, provides accurate values of fracture permeability and wellbore skin. In addition, storativity ratio and interporosity flow coefficient could also be determined directly with this method.

As can be seen in **Fig. 5.4**, that single flow of compressible fluid presents does not present considerable variations of storativity ratio (ω) as a function of pressure, as was pointed out by **Gerami et al. (2007)**. Furthermore, the behavior between the correct total compressibility, which includes fluid saturations, and the approximated total compressibility are very similar. In this case, the approximated total compressibility is given by the assumption that gas compressibility rules in total compressibility of both systems.

Comments of case 2: Variable oil flow rate with wellbore skin and pseudosteady-state interporosity flow.

Dynamic material balance and Blasingame type curve method showed very accurate estimates of OOIP ($< 6.5\%$), and the average reservoir pressure ($< 3\%$) in NFR with a slightly compressible fluid. In this case, the well shut-ins and changes in production flow rate did not affect the match process following the boundary-dominated behavior.

The fracture permeability calculated was in the same order of the reference value ($\pm 10\%$). The wellbore skin calculated described a damaged well ($s = 0.54$ and 0.27), with little variation with respect to the simulated model ($s = 2$). The application of current APDA methods for homogeneous systems, lead to error in the estimation of these variables.

Comments of case 3: Real field data with wellbore skin, low flow rate data frequency and pseudosteady-state interporosity flow.

This example is typical from many hydrocarbon reservoirs. Many wells have access to a high data frequency (i.e. 1 sec) bottomhole flowing pressures, however daily flow rate measurements is not very common. As has been described before, for a correct analysis these data must have a similar accuracy and frequency, so better interpretation can be made.

In absence of daily data, reservoir parameters could not be determined. Nevertheless, low frequency data allows the estimation of OGIP and average reservoir pressures. In this case, the DMB showed small error compared with the type curve method. This would be due to the scale of the plots, a Cartesian plot has better resolution than a Log-Log plot.

This new approach describes the details and modifications of APDA methods to analyze daily production data of carbonates reservoirs. It would represent an important improvement in the state-of-the art of APDA, because there are publications where homogeneous methods are used for the interpretation. Advanced production data analysis and pressure transient analysis techniques should complement with each other.

The principal limitation of this approach would be the presence of large wellbore storage or strong phase segregation even though they are often present in buildups. This effect could mask the dual porosity behavior, especially for high values of interporosity flow coefficient. The methods were derived considering a closed reservoir with no-flow boundary. It is not applicable to reservoirs with external influence of pressure such as active water influx, water or gas injection, etc. Finally, in gas wells it is common to have a rate dependent skin, which was not considered in our approach.

It is important to point out that APDA techniques can estimate the Hydrocarbon-in-place with similar precision of conventional material balance but in less time. The hydrocarbon-in-place determined by conventional material balance is considered very accurate after approximately 10% of gas reserves have been produced (**Holstein 2007**) or average reservoir pressure decline of at least 10% of the original reservoir pressure (**Cosentino 2001**). According to the results it is possible to determine de OOIP with average reservoir pressure drop between 3 to 7% with APDA techniques.

6. SUMMARY AND CONCLUSIONS

6.1. Summary

This work has extended the applicability of current production data analysis techniques for naturally fractured reservoirs. We provided the derivation of two semi-analytical methods based on the dual porosity model: type curveless method (dynamic material balance) and a type curve method (Blasingame TC).

Long-time approximated solutions of diffusivity equation in dual porosity systems were developed for both interporosity flow models (pseudosteady-state and transient). These dimensionless solutions were compared with the exact solution in Laplace domain by using the Gaver-Stehfest numerical algorithm. It was confirmed the applicability of approximated homogeneous solutions in reservoirs with transient interporosity flow between matrix and fractures. A different solution must be used for the case reservoirs with pseudosteady-state interporosity flow.

Dynamic material balance and Blasingame type curve method were developed from the long-time approximate solutions. For DMB, fracture permeability (k_f) could be estimated by using the second derivative of the normalized flow rate. Wellbore skin is strongly dependent of storativity ratio (ω) and interporosity flow coefficient (λ), and can be estimated if they available from previous pressure transient analysis. The type curve method provides additional parameters compared with DMB, such as ω and λ estimated directly from the daily production data.

These methods were validated using numerical simulation dual porosity model and real field case data. The synthetic data was generated for two cases: constant oil flow rate and variable gas flow rate. The field case data belongs to a gas-condensate reservoir from Devonian sandstone. The type curveless and the type curve method provide considerable accurate estimations of hydrocarbon-in-place and reservoir parameters for heterogeneous

systems. The methods were developed considering the application of the material balance pseudo-time, therefore they are applicable to variable flow rate/variable pressure cases.

6.2. Conclusions

The following conclusions are derived from this work:

- Advanced production data analysis techniques were successfully derived based on dual porosity model, aiming to analyze production data of naturally fractured reservoirs. The methods were developed considering pseudosteady-state and transient interporosity flow and validated using numerical simulation.
- Naturally Fractured Reservoirs with pseudosteady-state interporosity flow could present two boundary-dominated flow long-time behavior, one for fracture system and the other for total system.
- Fractured reservoirs with transient interporosity flow exhibit a homogeneous long-time behavior, therefore can be analyzed using current advanced production analysis techniques developed for homogenous reservoirs.
- The dynamic material balance and type curve methods can provide accurate estimations of Hydrocarbon-in-place for naturally fractured reservoirs.
- In fractured reservoirs with pseudosteady-state interporosity flow, the DMB requires the previous knowledge of storativity ratio (ω) and the interporosity flow coefficient (λ), for the estimations of wellbore skin (s).
- In fractured reservoirs with pseudosteady-state interporosity flow, a type curve method can provide additional parameters such as storativity ratio (ω) and the interporosity flow coefficient (λ) directly from daily production data.
- The estimation of dual porosity reservoir parameters requires at least daily production data for dynamic material balance and type curve methods. Lower data frequency lead to the loss of output results, providing just hydrocarbon-in-place.
- Advanced production data analysis can determine the hydrocarbon-in-place in less time that required by conventional material balance techniques.

6.3. Recommendations for Future Work

Possible extensions of this semi-analytical approach could be given by the inclusion of multi-phase flow model in dual porosity system, comparison between dual porosity model and dual permeability model, and evaluation of the non-Darcy flow in naturally fractured gas reservoirs. On the other hand, future work could be developed considering new solutions models for different well geometry configurations such as horizontal wells or slanted wells.

REFERENCES

- Abdassah D. and Ershagui I. 1986. Triple-Porosity System for Representing Naturally Fractured Reservoirs. SPE Formation Evaluation. April: 113-127.
- Abramowitz M., Stegun I. 1964. Handbook of Mathematical Functions. 10th Printing, Table 29.3. pp. 1028. National Bureau of Standards. Washington.
- Agarwal R. G., Gardner D. C., Kleinstiber S. W., Fussel Del D. 1999. Analyzing Well Production Data using Combined-Type-Curve and Decline-Curve Analysis Concepts. Res Eng & Eval. Vol. 2 (5): 478-486.
- Ahmed T., McKinney P. D. 2005. Advanced Reservoir Engineering. 1st Edition. Chap. 3. pp. 182-184, 261-262, GPP - Elsevier.
- Al-Reshedam F. S., Gawish A., and Dmour H. N. 2009. Evaluation the methodologies of Analyzing Production and Pressure Data of Hydraulic Fractured Wells in Low Permeability Gas Reservoirs. Oil and Gas Business. www.ogbus.ru/eng
- Anderson D., Mattar L. 2004. Practical Diagnostics Using Production Data and Flowing Pressures. SPE ATCE. Houston, Texas. September 26-29. SPE 89939.
- Arabloo M., Heidari M., Gerami S. 2014. A New Approach for Analysis of Production Data from Constant Production Rate Wells in Gas Condensate Reservoirs. Journal of Natural Gas Science and Engineering. Vol. 21: 725-731.
- Arps J. J. 1945. Analysis of Decline Curves. Trans. AIME. 160, 228-247.
- Barenblatt G. I. and Zheltov Y. 1960. Fundamental Equations of Filtration of Homogeneous Liquids in Fissured Rocks. Soviet Physics, Doklady. Vol. 5: 5-522.
- Blasingame T. A., and Lee W. J. 1986. Variable-Rate Reservoir Limits Testing. Permian Basin Oil & Gas Recovery Conference of the SPE. Midlan, TX, March 13-14, SPE 15028.
- Blasingame T. A., Johnston J. L. and Lee W. J. 1989. Type-Curve Analysis Using the Pressure Integral Method. SPE California Regional Meeting. Bakersfield, California. April 5-7, SPE 18799.
- Blasingame T. A. 1993. Semi-Analytical Solutions for a Bounded Circular Reservoir-No Flow and Constant Pressure Outer Boundary Conditions: Unfractured Well Case. Production Operation Symposium. Oklahoma City, Oklahoma. March 21-23. SPE 25479.

Bourdet D. and Gringarten A. C. 1980. Determination of Fissure Volume and Block Size in Fractured Reservoirs by Type-Curve Analysis. 55th ATC of SPE. Dallas, TX, September 21-24, SPE 9293.

Bourdet D. 1985. Pressure Behavior of Layered Reservoirs with Crossflow. Bakersfield, California, March 27-29, SPE 13628.

Carslaw H. S., Jaeger J. C. 1959. Conduction of Heat in Solids. 2nd Edition, Table V. pp. 495. Oxford and the Clarendon Press. Great Britain.

Clarkson C. R. 2009. Case Study: Production Data and Pressure Transient Analysis of Horse Canyon CBM wells. J of Can Pet Technol. Vol. 48 (10): 27-38.

Coax S.A., Sutton R. P., and Blasingame T. A. 2006. Errors Introduced by Multiphase Flow Correlations on Production Analysis. SPE Annual Technical Conference and Exhibition. San Antonio, Texas. September 24-27. SPE 102488.

Cosentino L. 2001. Integrated Reservoir Studies. 1st Edition. Appendix. pp. 303. Institut Français du Pétrole Publications, Editions Technip. Paris, France.

Da Prat G. 1981. Well Test Analysis for Naturally-Fractured Reservoirs. PhD Thesis. Stanford University. Stanford, California (July).

Da Prat G. 1990. Well Test Analysis for Fractured Reservoir Evaluation. 1st Edition, Chap. 3. pp. 70-71. Elsevier Science Publishers, Netherlands.

Dake L. 1998. Fundamentals of Reservoir Engineering. 17th Edition, Chap. 1. pp. 144, 145. Elsevier. The Netherlands.

Doublet L. E., Pande P. K., McCollum T. J. and Blasingame T. A. 1994. Decline Curve Analysis using type curves-Analysis of Oil Well Production Data Using Material Balance Time: Application to Field Cases. Petroleum Conference and Exhibition. Veracruz, Mexico. October 10-13. SPE 28688.

Fernandez M., and Berrios V. 2012. Integrated Dynamic Flow Analysis to Characterize an Unconventional Reservoir in Argentina: The Loma La Lata Case. SPE Annual Technical Conference Exhibition. San Antonio, Texas. October 8-10. SPE 156163.

Fetkovich M. J. 1973. Decline Curve Analysis Using Type Curves. Society of Petroleum Engineers of AIME. 48th Annual Fall Meeting of SPE AIME. Nevada, USA. September 30 – October 3th. SPE 4629.

Fetkovich M. J. 1980. Decline Curve Analysis Using Type Curves. J of Pet Technol. June. pp 1065-1077.

Gerami S., Pooladi-Davish M. 2007. Decline Curve Analysis for Naturally Fractured Gas Reservoirs: A Study on the Applicability of “Pseudo-time” and “Material Balance Pseudo-

time”. International Petroleum Technology Conference. Dubai. December 4-6. IPTC-11278-PP.

Heidari M., Gerami S. 2011. A New Model for Modern Production-Decline Analysis of Gas/Condensate Reservoirs. J of Can Pet Technol. July/August: 10-23.

HoseinZareenejad M., Nasriani A., and Nasriani H. R. 2012. Application of Decline Analysis in Fractured Reservoirs, Field Case Studies. J of Chem and Pet Eng. University of Tehran. Vol. 46 (1):53-62.

Holstein E. 2007. Reservoir Engineering and Petrophysics – Petroleum Engineering Handbook. 1st Edition. Chap. 10: 1017. SPE Vol V.

Igbokoyi A. O., Tiab D. 2006. Estimation of Average Reservoir Pressure and Drainage Area in Naturally Fractured Reservoirs – Tiab’s Direct Synthesis. First International Conference and Exhibition. Cancun, Mexico, August 31th-September 2nd. SPE 104060.

Ismadi D., Kabir C. S., Hasan A. R. 2011. The use of Combined Static and Dynamic Material-Balance Methods in Gas Reservoirs. SPE Asia Pacific Oil and Gas Conference and Exhibition. Jakarta, Indonesia. September 20-22. SPE 145798.

Kabir C. S. and Izgec B. 2006. Diagnosis of Reservoir Behavior from Measured Pressure/Rate Data. SPE Gas Technology Symposium. Calgary, Canada. October 5-8. SPE 84472.

Kuhlman K. L. 2015. Multiporosity Flow in Fractured Low-Permeability Rocks. Applied System Analysis & Research Dept. Sandia National Laboratories. Livermore, California. February.

Lee J., Rollins J. B., Spivey J. P. 2003. Pressure Transient Testing. 1st Edition. Chap. 7: 142. SPE Textbook Series Vol 9.

McCray T. L. 1990. Reservoir Analysis Using Production Decline Data and Adjusted Time. MS Thesis. Texas A&M University. College Station, Texas.

Mattar L., and McNeil R. 1998. The Flowing Gas Material Balance. J of Can Pet Technol. Vol. 37 (2): 52-55.

Mattar L. and D. Anderson. 2003. A Systematic and Comprehensive Methodology for Advanced Analysis of Production Data. SPE annual Technical Conference. Denver, Colorado. October 5-8. SPE 84472.

Mattar L. and D. Anderson. 2005. Dynamic Material Balance (Oil or Gas-in-place without shut-ins). 6th Canadian International Petroleum Conference. Calgary, Alberta, Canada. June 7-9. PAPER 2005-113.

Marhaendrajana T. 2000. Modeling and Analysis of Flow Behavior in Single and Multi-well Bounded Reservoirs. PhD Thesis. Texas A&M University. Texas (May 2000)

- Mavor M. J. and Cinco Ley H. 1979. Transient Pressure Behavior of Naturally Fractured Reservoirs. American Institute of Mining, Metallurgical and Petroleum Engineers. California. April 18-20. SPE 7977.
- Moench A. F. 1984. Double-Porosity Models for a Fissured Groundwater Reservoir with Fracture Skin. Water Resources Research. Vol 20 (7): 831-846. Paper number 4W0381.
- Nelson R. A. 2001. Geologic Analysis of Naturally Fractured Reservoirs. 2nd Edition, Chap. 2. pp. 101-103. Gulf Professional Publishing, Houston-TX.
- Odeh A. S. 1965. Unsteady-state Behavior of Naturally Fractured Reservoirs. Soc. Pet. Eng. J. March: 60-64.
- Onur M., Satman A. and Reynolds A. C. 1993. New Type Curves for Analyzing the Transition Time Data From Naturally Fractured Reservoirs. SPE Rocky Mountain Regional/Low Permeability Reservoir Symposium. Denver, CO. April 26-28, SPE 25873.
- Palacio J. C., Blasingame T. A. 1993. Decline-Curve Analysis using Type Curves – Analysis of Gas Well Production Data. Rocky Mountain Regional and Low Permeability Reservoir Symposium. Denver, CO. 26-28 April. SPE 25909.
- Peres A., Onur M., Reynolds A. C. 1989. A New General Pressure-Analysis Procedure for Slug Tests. SPE California Regional Meeting. Bakersfield, California. April 5-7. SPE 18801.
- Rayes D. G., Piper L. D., McCain Jr. W. D., Poston S. W. 1992. Two-Phase Compressibility Factors for Retrograde Gases. SPE Form Eval. - March. pp 87-118. SPE 20055.
- Reiss L. H. 1980. The Reservoir Engineering Aspects of Fractured Formations. 1st Edition. Chap. 3. pp. 19, 22. Gulf Professional Publishing, Paris.
- Raghavan R., Ozkan E. 1994. A method for computing unsteady flows in porous media. 1st Edition. Chap. V. pp. 105. Longman Scientific & Technical, Britain.
- Roberts G. E., Kaufman H. 1966. Table of Laplace Transforms. 1st Edition. Section 2, pp. 306. W. B. Saunders Company. Philadelphia and London.
- Sadeghi A., Gerami S., Masihi M. 2011. Investigation into the capability of a modern decline curve analysis for gas condensate reservoirs. Scientia Iranica. Vol. 18 (3): 491-501.
- Serra K., Reynolds A. C. and Raghavan R. 1983. New Pressure Transient Analysis Methods for Naturally Fractured Reservoirs. January 1st. SPE 10586.
- Spiegel, M. R. 1965. Laplace Transforms. 1st Edition. Chap. 1. pp. 4. Schaum's Outlines Series. United States of America.
- Spivey J. P., Gatens J. M., Semmelbeck, M. E. and Lee W. J. 1992. Integrated Type Curves for Advanced Decline Curves Analysis. SPE Mid-Continent Gas Symposium. Amarillo, Texas. April 13-14. SPE 24301.

Sun H. 2015. Advanced Production Decline Analysis and Application. 1st Edition. Chap. XI. pp. 105. Gulf Professional Publishing (Elsevier), USA.

Warren J. E., Root, P. J. 1963. The Behavior of Naturally Fractures Reservoirs. SPE Journal. September. Pp. 245-255.

Van Everdingen, A. F., Hurst W. 1949. The Application of the Laplace Transformation to Flow Problems in Reservoirs. Petroleum Transactions AIME. December, pp. 305-323.

APPENDIX A

APPROXIMATED SOLUTION OF DIFFUSIVITY EQUATION FOR DUAL POROSITY SYSTEM (PSEUDOSTEADY-STATE INTERPOROSITY FLOW) WITH NO-FLOW OUTER BOUNDARY.

The solution of diffusivity equation for dual porosity system in Laplace domain with no-flow outer boundary at the wellbore ($r_D = 1$) is given by (Da Prat 1981), for $CD = 0$ and $skin = 0$:

$$\overline{P_{wDf}} = \frac{k_0(\sqrt{uf(u)})I_1(\sqrt{uf(u)} r_{eD}) + k_1(\sqrt{uf(u)} r_{eD})I_0(\sqrt{uf(u)})}{u\sqrt{uf(u)}[k_1(\sqrt{uf(u)})I_1(\sqrt{uf(u)} r_{eD}) - k_1(\sqrt{uf(u)} r_{eD})I_1(\sqrt{uf(u)})]} \dots\dots\dots (A-1)$$

Warren and Root (1963) presented the following approximation for long time:

$$\begin{aligned} P_{wDf} = & \frac{2}{r_{eD}^2 - 1} \left\{ \frac{1}{4} + t_{Df} + \frac{(1-\omega)^2}{\lambda} \left[1 - \exp\left(-\frac{\lambda t_{Df}}{\omega(1-\omega)}\right) \right] \right\} - \\ & \frac{3r_{eD}^4 - 4r_{eD}^4 \ln(r_{eD}) - 2r_{eD}^2 - 1}{4r_{eD}^4(r_{eD}^2 - 1)^2} \dots\dots\dots (A-2) \end{aligned}$$

Considering that in most cases $r_{eD}^2 \gg 1$, then the term $r_{eD}^2 - 1$ can be replaced by r_{eD}^2 (**Da Prat**):

$$P_{wDf} = \frac{2t_{Df}}{r_{eD}^2} + \ln(r_{eD}) - \frac{3}{4} + \frac{2(1-\omega)^2}{\lambda r_{eD}^2} \left[1 - \exp\left(-\frac{\lambda t_{Df}}{\omega(1-\omega)}\right) \right] \dots\dots\dots (A-3)$$

Writing the equation as a function of t_{DA} instead of t_D :

$$\begin{aligned} t_{DA} &= \frac{t_D}{A} & A &= \pi r_e^2 & r_{eD} &= \frac{r_e}{r_w} \\ P_{wDf} &= 2\pi t_{DA} + \frac{1}{2} \ln\left(\frac{2.2458 A}{C_A r_w^2}\right) + \frac{2\pi(1-\omega)^2}{\lambda A} \left[1 - \exp\left(-\frac{\lambda A t_{DA}}{\omega(1-\omega)}\right) \right] \dots\dots\dots (A-4) \end{aligned}$$

Expanding the exponential term:

$$e^{-x} = 1 - x + \frac{x^2}{2!} - \frac{x^3}{3!} + \dots \quad x = \frac{\lambda A t_{DA}}{\omega(1-\omega)}$$

Then we have:

$$P_{wD_f} = 2\pi t_{DA} + \frac{1}{2} \ln \left(\frac{2.2458 A}{C_A r_w^2} \right) + \frac{2\pi(1-\omega)^2}{\lambda A} \left\{ 1 - \left[1 - \frac{\lambda A t_{DA}}{\omega(1-\omega)} + \left(\frac{\lambda A t_{DA}}{\omega(1-\omega)} \right)^2 - \dots \right] \right\} \dots \dots \dots (A-5)$$

$$P_{wD_f} = \frac{1}{2} \ln \left(\frac{2.2458 A}{C_A r_w^2} \right) + 2\pi \left(\frac{t_{DA}}{\omega} \right) - \frac{2\pi\lambda A}{2} \left(\frac{t_{DA}}{\omega} \right)^2 \dots \dots \dots (A-6)$$

Reducing **Eq. A-6** using the Big “O” notation:

$$P_{wD_f} = 2\pi t_{DA} + \frac{1}{2} \ln \left(\frac{2.2458 A}{C_A r_w^2} \right) + O \left[\lambda \left(\frac{t_{DA}}{\omega} \right)^2 \right] \dots \dots \dots (A-7)$$

Then, for $\lambda = 0$, the exponential term: $e^{-x} \cong 1$. Case of: $0.1 \leq t_D \leq \frac{\omega(1-\omega)}{\lambda}$

$$P_{wD_f} = \frac{2\pi t_{DA}}{\omega} + \frac{1}{2} \ln \left(\frac{2.2458 A}{C_A r_w^2} \right) \dots \dots \dots (A-8)$$

Then, for $\lambda \neq 0$, $t_{DA} \rightarrow \infty$ and the exponential term: $e^{-x} \cong 0$. Case of: $t_D \geq \frac{\omega(1-\omega)}{\lambda}$

$$P_{wD_f} = 2\pi t_{DA} + \frac{1}{2} \ln \left(\frac{2.2458 A}{C_A r_w^2} \right) + \frac{2(1-\omega)^2}{\lambda r_{eD}^2} \dots \dots \dots (A-9)$$

APPENDIX B

APPROXIMATED SOLUTION OF DIFFUSIVITY EQUATION FOR DUAL POROSITY SYSTEM (TRANSIENT INTERPOROSITY FLOW) WITH NO-FLOW OUTER BOUNDARY.

Transient interporosity flow considers different representation of fractured system: slabs, blocks, spheres, etc. In all situations the solution in Laplace domain of diffusivity equation for constant rate are the same (**Bourdet and Gringarten 1980**). For $CD = 0$, and $skin = 0$:

$$\overline{P_{wDf}} = \frac{k_0(\sqrt{uf(u)})I_1(\sqrt{uf(u)} r_{eD}) + k_1(\sqrt{uf(u)} r_{eD})I_0(\sqrt{uf(u)})}{u\sqrt{uf(u)}[k_1(\sqrt{uf(u)})I_1(\sqrt{uf(u)} r_{eD}) - k_1(\sqrt{uf(u)} r_{eD})I_1(\sqrt{uf(u)})]} \dots\dots\dots (B-1)$$

For long time ($t \rightarrow \infty$), it is necessary to apply approximation for small arguments of Bessel functions ($u \rightarrow 0$). From **Abramowitz and Stegun (1964)**, pp. 375, Eq. 9.6.7 and 9.6.12:

$$\begin{aligned} K_0(Z) &\approx -\left(\gamma + \ln \frac{Z}{2}\right) & I_0(Z) &\approx 1 \\ K_1(Z) &\approx \frac{1}{Z} & (Z)I_1(Z) &\approx 0 \end{aligned}$$

Substituting in **Eq. B-1** we obtain:

$$\begin{aligned} \overline{P_{wDf}} &= \frac{\left(-\ln \frac{(\sqrt{uf(u)})}{2} - \gamma\right) I_1(\sqrt{uf(u)} r_{eD}) + k_1(\sqrt{uf(u)} r_{eD})}{u\sqrt{uf(u)} \left[\frac{1}{\sqrt{uf(u)}} I_1(\sqrt{uf(u)} r_{eD})\right]} \\ \overline{P_{wDf}} &= \frac{\left(-\ln \frac{(\sqrt{uf(u)})}{2} - \gamma\right) I_1(\sqrt{uf(u)} r_{eD}) + k_1(\sqrt{uf(u)} r_{eD})}{u I_1(\sqrt{uf(u)} r_{eD})} \\ \overline{P_{wDf}} &= \frac{k_1(\sqrt{uf(u)} r_{eD})}{u I_1(\sqrt{uf(u)} r_{eD})} - \frac{\left(\ln \frac{(\sqrt{uf(u)})}{2} + \gamma\right) I_1(\sqrt{uf(u)} r_{eD})}{u I_1(\sqrt{uf(u)} r_{eD})} \\ \overline{P_{wDf}} &= \frac{k_1(\sqrt{uf(u)} r_{eD})}{u I_1(\sqrt{uf(u)} r_{eD})} - \frac{(\ln \sqrt{uf(u)} - \ln(2) + \gamma)}{u} \end{aligned}$$

$$\begin{aligned} \overline{P_{wDf}} &= \frac{k_1(\sqrt{uf(u)} r_{eD})}{u I_1(\sqrt{uf(u)} r_{eD})} - \frac{\left(\frac{1}{2} \ln(uf(u)) - \ln(2) + \gamma\right)}{u} \\ \overline{P_{wDf}} &= \frac{k_1(\sqrt{uf(u)} r_{eD})}{u I_1(\sqrt{uf(u)} r_{eD})} - \frac{1}{2} \frac{\ln(uf(u))}{u} + \frac{1}{u} \ln(2) - \frac{1}{u} \gamma \dots\dots\dots (B-2) \end{aligned}$$

Applying **Blasingame (1993)** procedure for the first term and a “I Bessel function” property, we obtain:

$$\begin{aligned} k_1(Z) &\cong \frac{Z}{2} [k_2(Z) - k_0(Z)] & I_1(Z) &\cong \frac{Z}{2} \left(1 + \frac{Z^2}{8}\right) \\ \overline{P_{wDf}} &= \frac{\frac{\sqrt{uf(u)} r_{eD}}{2} \left[k_2\left(\sqrt{uf(u)} r_{eD}\right) - k_0\left(\sqrt{uf(u)} r_{eD}\right) \right]}{u \frac{\sqrt{uf(u)} r_{eD}}{2}} - \frac{1}{2} \frac{\ln(uf(u))}{u} + \frac{1}{u} \ln(2) - \frac{1}{u} \gamma \\ \overline{P_{wDf}} &= \frac{1}{u} \left[k_2\left(\sqrt{uf(u)} r_{eD}\right) - k_0\left(\sqrt{uf(u)} r_{eD}\right) \right] - \frac{1}{2} \frac{\ln(uf(u))}{u} + \frac{1}{u} \ln(2) - \frac{1}{u} \gamma \\ \overline{P_{wDf}} &= \frac{1}{u} k_2\left(\sqrt{uf(u)} r_{eD}\right) - \frac{1}{u} k_0\left(\sqrt{uf(u)} r_{eD}\right) - \frac{1}{2} \frac{\ln(uf(u))}{u} + \frac{1}{u} \ln(2) - \frac{1}{u} \gamma \dots\dots (B-3) \end{aligned}$$

The next step is to evaluate the behavior of the transfer function matrix-fracture in Eq. B-3 for large values of time ($u \rightarrow 0$), for: Slab and Sphere models.

A. Transfer function for slab model:

$$f(u) = \omega + \sqrt{\frac{1}{3} \frac{\lambda(1-\omega)}{u}} \tanh \sqrt{\frac{3(1-\omega)u}{\lambda}} \dots\dots\dots (B-4)$$

The limit of Eq. B-4 can be evaluated by approximating the hyperbolic tangent for $u \rightarrow 0$: $\tanh(x) \approx x$:

$$\begin{aligned} \lim_{u \rightarrow 0} \left[\omega + \sqrt{\frac{1}{3} \frac{\lambda(1-\omega)}{u}} \left(\sqrt{\frac{3(1-\omega)u}{\lambda}} \right) \right] &= 1 \\ \lim_{u \rightarrow 0} [\omega + (1 - \omega)] &= 1 \dots\dots\dots (B-5) \end{aligned}$$

Therefore, for slab model $f(u \rightarrow 0) = 1$ (same as **Raghavan and Ozkan, 1994**), which means that Slab model at long time behaves as homogeneous. Substituting this result in **Eq. B-3** we obtain:

$$\overline{P_{wDf}} = \frac{1}{u} k_2(\sqrt{u} r_{eD}) - \frac{1}{u} k_0(\sqrt{u} r_{eD}) - \frac{1}{2} \frac{\ln(u)}{u} + \frac{1}{u} \ln(2) - \frac{1}{u} \gamma \dots\dots\dots (B-6)$$

The inverse of Laplace transform can be obtained following **Blasingame (1993)** procedure, applying standard tables published by **Carslaw and Jaeger (1959)**, **Abramowitz and Stegun (1964)** and **Roberts and Kaufman (1966)**:

$$P_{wDf} = \frac{2 t_{Df}}{r_{eD}^2} \exp\left(\frac{-r_{eD}^2}{4t_{Df}}\right) - \frac{1}{2} Ei\left(\frac{r_{eD}^2}{4t_{Df}}\right) + \frac{1}{2} \ln(t_{Df} + \gamma) + \ln(2) - \gamma$$

$$P_{wDf} = \frac{2 t_{Df}}{r_{eD}^2} \exp\left(\frac{-r_{eD}^2}{4t_{Df}}\right) - \frac{1}{2} Ei\left(\frac{r_{eD}^2}{4t_{Df}}\right) + \frac{1}{2} \left(\ln(t_{Df}) + \ln(4) - \ln(e^\gamma)\right)$$

$$P_{wDf} = \frac{2 t_{Df}}{r_{eD}^2} \exp\left(\frac{-r_{eD}^2}{4t_{Df}}\right) - \frac{1}{2} Ei\left(\frac{r_{eD}^2}{4t_{Df}}\right) + \frac{1}{2} \ln\left(\frac{4t_{Df}}{e^\gamma}\right) \dots\dots\dots (B-7)$$

Material Balance Term **Reservoir Shape Effects Term** **Infinite-Acting Term**

Eq. B-7 is similar to the solution proposed by Blasingame (1993), however with a logarithmic approximation for the infinite acting term. The first exponential term of **Eq. B-7** tends toward to unity for large values of t_{Df} ($t_{Df} \rightarrow \infty$), and applying the logarithmic approximation on the second term we obtain:

$$P_{wDf} = \frac{2 t_{Df}}{r_{eD}^2} + \frac{1}{2} \ln\left(\frac{e^\gamma r_{eD}^2}{4t_{Df}}\right) + \frac{1}{2} \ln\left(\frac{4t_{Df}}{e^\gamma}\right)$$

$$P_{wDf} = \frac{2 t_{Df}}{r_{eD}^2} + \frac{1}{2} \left[\frac{\gamma r_{eD}^2}{e^\gamma}\right]$$

$$P_{wDf} = \frac{2 t_{Df}}{r_{eD}^2} + \ln(r_{eD}) - 0.5634 \dots\dots\dots (B-8)$$

B. Transfer function for spherical model:

$$f(u) = \omega + \frac{1}{5} \frac{\lambda}{u} \left[\sqrt{\frac{15(1-\omega)u}{\lambda}} \coth \sqrt{\frac{15(1-\omega)u}{\lambda}} - 1 \right] \dots\dots\dots (B-9)$$

Eq. B-9 can be rewritten as:

$$f(u) = \omega + \frac{1}{5} \frac{\lambda}{u} [(D\sqrt{u}) \coth(D\sqrt{u}) - 1] \dots\dots\dots (B-10)$$

$$\text{Where: } D = \sqrt{\frac{15(1-\omega)}{\lambda}}$$

Following the same procedure for the slab case, the hyperbolic cotangent for $u \rightarrow 0$, can be approximated as: $\coth(x) \approx \frac{1}{x} + \frac{x}{3}$ or $(x)\coth(x) - 1 \approx \frac{x^2}{3}$, therefore:

$$\begin{aligned} \lim_{u \rightarrow 0} \left[\omega + \frac{1}{5} \frac{\lambda}{u} \left[\left(\sqrt{\frac{15(1-\omega)}{\lambda}} \sqrt{u} \right)^2 \right] \right] &= 1 \\ \lim_{u \rightarrow 0} \left[\omega + \frac{1}{5} \frac{\lambda}{u} \left(\frac{15(1-\omega)u}{\lambda} \right) \right] &= \omega + (1 - \omega) = 1 \dots\dots\dots (B-11) \end{aligned}$$

As can be seen, for long time the sphere model behaves like homogeneous $f(u) = 1$, consequently we would obtain the same answer that for the slab case:

$$P_{wD_f} = \frac{2 t_{D_f}}{r_{eD}^2} + \ln(r_{eD}) - 0.5634 \dots\dots\dots (B-12)$$

For a better understanding, solutions for slab (**Eq. B-8**) and spheres (**Eq. B-12**) models can be plotted in dimensionless coordinates and compared with the Laplace solution applying the Gaver-Stehfest algorithm. Both solutions approximate to the homogeneous reservoirs solution:

$$P_{wD_f} \approx \frac{2t_D}{r_{eD}^2} + \ln(r_{eD}) - \frac{3}{4} \dots\dots\dots (B-13)$$

APPENDIX C

DEVELOPMENT OF DYNAMIC MATERIAL BALANCE FOR NATURALLY FRACTURED RESERVOIRS

The dimensionless solution of diffusivity equation for NFR at constant rate for the case of matrix pseudosteady-state flow regime and close reservoir given by **Eq. A-8** and **Eq. A-9**, can be written for a circular reservoir as:

For fracture system: $0.1 \leq t_{Df} \leq \frac{\omega(1-\omega)}{\lambda}$

$$P_{wDf} = \frac{2t_D}{\omega r_{eD}^2} + \ln(r_{eD}) - \frac{3}{4} + s \dots\dots\dots (C-1)$$

For total system: $t_{Df} \geq \frac{\omega(1-\omega)}{\lambda}$

$$P_{wDf} = \frac{2t_D}{r_{eD}^2} + \ln(r_{eD}) - \frac{3}{4} + s + \frac{2(1-\omega)^2}{\lambda r_{eD}^2} \dots\dots\dots (C-2)$$

Where:

$$\omega = \frac{\phi_f c_f}{\phi_m c_m + \phi_f c_f} \dots\dots\dots (C-3)$$

$$\lambda = \alpha \frac{k_m}{k_f} r_w^2 \dots\dots\dots (C-4)$$

Using the dimensionless definition for dual porosity model, compressible fluid and effective wellbore radius definition, Eq. C-1 and C-2 could be written for oil reservoirs as follows:

For fracture system:

$$P_{pi} - P_{pwf} = \frac{141.2 q_g \beta_{gi} \mu_{gi}}{k_f h} \left[\frac{0.000527 k_f t}{[(\phi c_t)_f + (\phi c_t)_m] \omega \mu_{gi} r_e^2} + \ln\left(\frac{r_e}{r_{wa}}\right) - \frac{3}{4} \right] \dots\dots\dots (C-5)$$

For total system:

$$P_{p_i} - P_{p_{wf}} = \frac{141.2 q_g \beta_{g_i} \mu_{g_i}}{k_f h} \left[\frac{0.000527 k_f t}{[(\phi c_t)_f + (\phi c_t)_m] \mu_{g_i} r_e^2} + \ln \left(\frac{r_e}{r_{wa}} \right) - \frac{3}{4} + \frac{2(1-\omega)^2 r_{wa}^2}{\lambda r_e^2} \right] \dots\dots\dots (C-6)$$

Where:

$$P_p = \left(\frac{\mu Z}{P} \right)_i \int_{P_{wf}}^P \frac{P}{\mu Z} dp \dots\dots\dots (C-7)$$

$$r_{wa} = r_w e^{-s} \dots\dots\dots (C-8)$$

Using **Warren and Root (1963)** definition of matrix and fracture compressibilities, the fractures and the matrix can be approximated to the gas compressibility because it is greater compared with the other values (except abnormally pressured reservoirs):

$$c_{em} = c_g + \frac{c_p + S_w c_w + S_o c_o}{1 - S_w - S_o} \cong c_g \dots\dots\dots (C-9)$$

$$c_{ef} = c_g \dots\dots\dots (C-10)$$

Then a similar procedure made by **Mattar and Anderson (2005)** can be applied to **Eq. C-5** and **C-6**. They considered a volumetric gas reservoir and used definition of normalized material balance pseudo-time for variable rates:

For fracture system:

$$P_{p_i} - P_{p_{wf}} = \frac{1}{\omega G c_{t_i}} t_{ca} + \frac{141.2 q_g \beta_{g_i} \mu_{g_i}}{k_f h} \left[\ln \left(\frac{r_e}{r_{wa}} \right) - \frac{3}{4} \right] \dots\dots\dots (C-11)$$

For total system:

$$P_{p_i} - P_{p_{wf}} = \frac{1}{G c_{t_i}} t_{ca} + \frac{141.2 q_g \beta_{g_i} \mu_{g_i}}{k_f h} \left[\ln \left(\frac{r_e}{r_{wa}} \right) - \frac{3}{4} + \frac{2(1-\omega)^2 r_{wa}^2}{\lambda r_e^2} \right] \dots\dots (C-12)$$

Where:

$$t_{ca} = \frac{(\mu_g c_t)_i}{q_g} \int_0^t \frac{q_g}{\bar{\mu}_g \bar{c}_t} dt = \frac{G c_{t_i}}{q_g} (P_{p_i} - \bar{P}_p) \dots\dots\dots (C-13)$$

$$G = \frac{(\phi_f + \phi_m) Ah}{B_{g_i}} \dots\dots\dots (C-14)$$

$$C_{t_i} \cong 2C_{g_i} \dots\dots\dots (C-15)$$

Simplifying the **Eq. C-11** and **Eq. B-12** by defining b_{pss} and \tilde{b}_{pss} the equations are and dividing by q_g :

For fracture system:

$$\frac{P_{p_i} - P_{p_{wf}}}{q_g} = m_f t_{ca} + b_{pss} \dots\dots\dots (C-16)$$

For total system:

$$\frac{P_{p_i} - P_{p_{wf}}}{q_g} = m_{f+m} t_{ca} + \tilde{b}_{pss} \dots\dots\dots (C-17)$$

Where:

$$m_f = \frac{1}{\omega G C_{t_i}} \dots\dots\dots (C-18)$$

$$m_{f+m} = \frac{1}{G C_{t_i}} \dots\dots\dots (C-19)$$

$$b_{pss} = \frac{142.2 q_{g_i} \mu_{g_i} B_{g_i}}{k_f h} \left[\ln \left(\frac{r_e}{r_{wa}} \right) - \frac{3}{4} \right] \dots\dots\dots (C-20)$$

$$\tilde{b}_{pss} = \frac{142.2 q_{g_i} \mu_{g_i} B_{g_i}}{k_f h} \left[\ln \left(\frac{r_e}{r_{wa}} \right) - \frac{3}{4} + \frac{2(1-\omega)^2 r_{wa}^2}{\lambda r_e^2} \right] \dots\dots\dots (C-21)$$

Rearranging terms and expressing Eq. C-16 and Eq. C-17 as a straight line:

For fracture system:

$$\frac{q_g}{P_{p_i} - P_{p_{wf}}} = - \frac{1}{\omega G b_{pss}} \frac{q_g t_{ca}}{(P_{p_i} - P_{p_{wf}}) C_{t_i}} + \frac{1}{b_{pss}} \dots\dots\dots (C-22)$$

For total system:

$$\frac{q_g}{P_{p_i} - P_{p_{wf}}} = - \frac{1}{G \tilde{b}_{pss}} \frac{q_g t_{ca}}{(P_{p_i} - P_{p_{wf}}) C_{t_i}} + \frac{1}{\tilde{b}_{pss}} \dots\dots\dots (C-23)$$

Finally, substituting the material balance pseudo-time definition (**Eq. C-13**), the simplest of this method is (similar to **Clarkson 2009**):

For fracture system:

$$\frac{q_g}{P_{p_i} - P_{p_{wf}}} = - \frac{1}{\omega \tilde{G} b_{pss}} \frac{\omega G(P_{p_i} - \bar{P}_p)}{(P_{p_i} - P_{p_{wf}})} + \frac{1}{b_{pss}} \dots \dots \dots (4.24)$$

For total system:

$$\frac{q_g}{P_{p_i} - P_{p_{wf}}} = - \frac{1}{\tilde{G} \tilde{b}_{pss}} \frac{G(P_{p_i} - \bar{P}_p)}{(P_{p_i} - P_{p_{wf}})} + \frac{1}{\tilde{b}_{pss}} \dots \dots \dots (4.25)$$

APPENDIX D

DEVELOPMENT OF BLASINGAME TYPE CURVES FOR NATURALLY FRACTURED RESERVOIRS

Type Curve Development:

As defined by **Palacio and Blasingame 1993**, the dimensionless decline rate (q_{Ddf}) and the dimensionless decline time (t_{Ddf}) for dual porosity system are defined as:

$$q_{Ddf} = q_{Df} \left[\ln(r_{eD}) - \frac{1}{2} \right] \dots\dots\dots (D-1)$$

$$t_{Ddf} = \frac{1}{\frac{1}{2}(r_{eD}^2 - 1) \left(\ln(r_{eD}) - \frac{1}{2} \right)} t_{DAf} \dots\dots\dots (D-2)$$

Where:

$$q_{Df} = \frac{1}{P_{wDf}} = \frac{1}{\mathcal{L}^{-1}\{\overline{P_{wDf}}\}} \dots\dots\dots (D-3)$$

The dimensionless fractured pressure at the wellbore can be determined by **Eq. D-4**, using the algorithm of Gaver-Stehfest.

$$\overline{P_{wDf}} = \frac{k_0(\sqrt{uf(u)})I_1(\sqrt{uf(u)} r_{eD}) + k_1(\sqrt{uf(u)} r_{eD})I_0(\sqrt{uf(u)})}{u\sqrt{uf(u)} \left[k_1(\sqrt{uf(u)})I_1(\sqrt{uf(u)} r_{eD}) - k_1(\sqrt{uf(u)} r_{eD})I_1(\sqrt{uf(u)}) \right]} \dots\dots\dots (D-4)$$

The correct function $f(u)$ must be used, depending on the fluid transfer model between matrix and fracture (pseudosteady-state or transient):

For pseudosteady-state interporosity flow:

$$f(u) = \omega + \frac{1}{5} \frac{\lambda}{u} \left[\sqrt{\frac{15(1-\omega)u}{\lambda}} \coth \sqrt{\frac{15(1-\omega)u}{\lambda}} - 1 \right] \dots\dots\dots (D-5)$$

For transient interporosity flow (Slabs):

$$f(u) = \omega + \sqrt{\frac{1}{3} \frac{\lambda(1-\omega)}{u}} \tanh \sqrt{\frac{3(1-\omega)u}{\lambda}} \dots\dots\dots (D-6)$$

For transient interporosity flow (Spheres):

$$f(u) = \omega + \frac{1}{5} \frac{\lambda}{u} \left[\sqrt{\frac{15(1-\omega)u}{\lambda}} \coth \sqrt{\frac{15(1-\omega)u}{\lambda}} - 1 \right] \dots\dots\dots (D-7)$$

Finally, the matching procedure is improved by defining the dimensionless decline rate integral (q_{Ddi}) to smooth noisy production data (McCray 1990) and the dimensionless decline rate integral derivative (q_{Ddid}), to identify typical behavior of a fractured system:

$$q_{Ddid} = \frac{N_{pDd}}{t_{Ddf}} = \frac{1}{t_{Ddf}} \int_0^{t_{Dd}} q_{Ddf}(t_{Ddf}) dt_{Ddf} \dots\dots\dots (D-8)$$

$$q_{Ddid} = -\frac{dq_{Ddi}}{d \ln(t_{Ddf})} = -t_{Dd} \frac{dq_{Ddi}}{dt_{Ddf}} = q_{Ddi} - q_{Ddf} \dots\dots\dots (D-9)$$

Examples of Blasingame type curve for dual porosity system is presented in **Fig. D.1**, **D.2** and **D.3**.

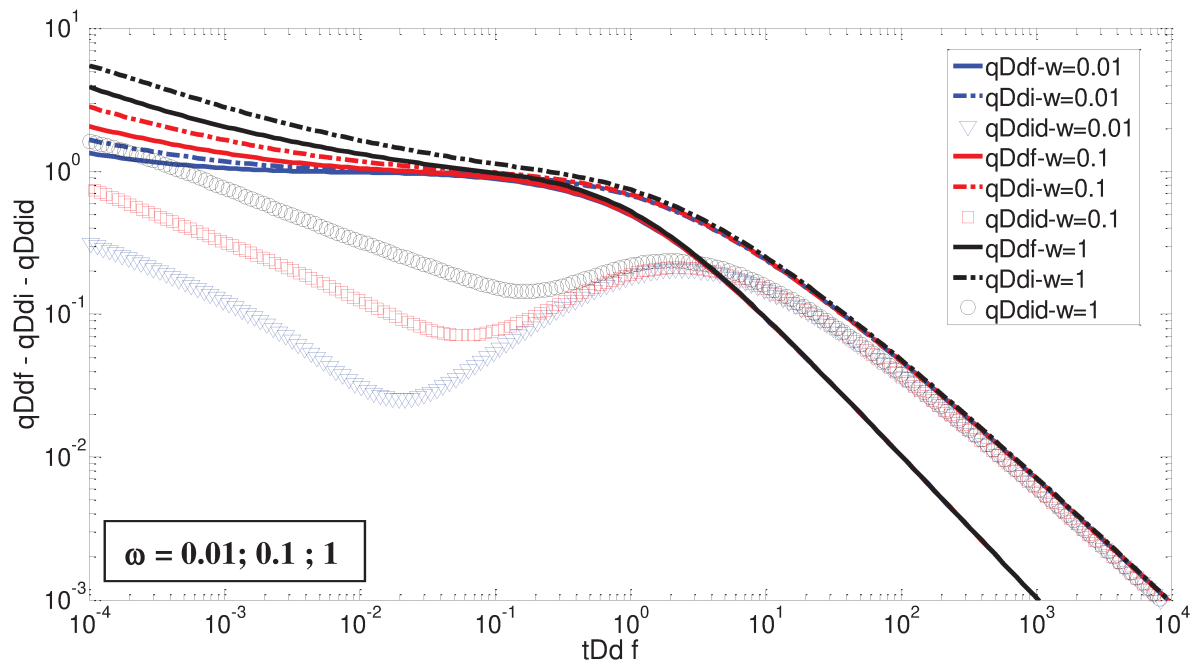


Figure D.1 – Decline type curves for dual porosity systems. $r_{eD} = 100$; $\lambda = 1 \times 10^{-4}$.

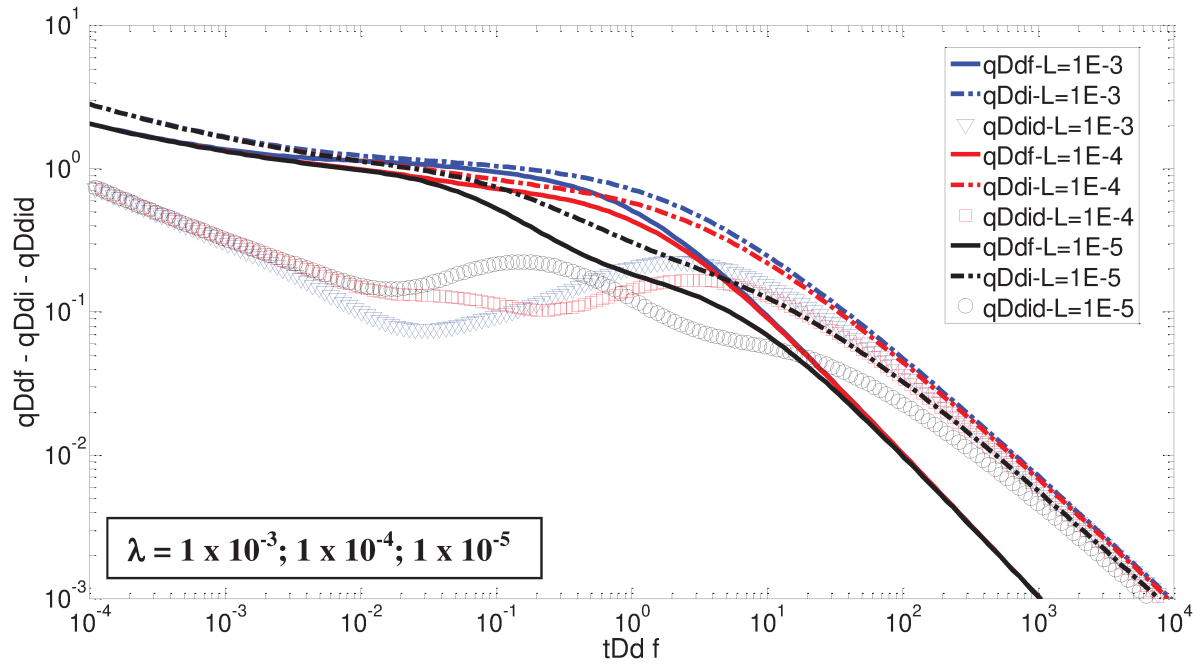


Figure D.2 – Decline type curves for dual porosity systems. $r_{eD} = 100$; $\omega = 0.1$.

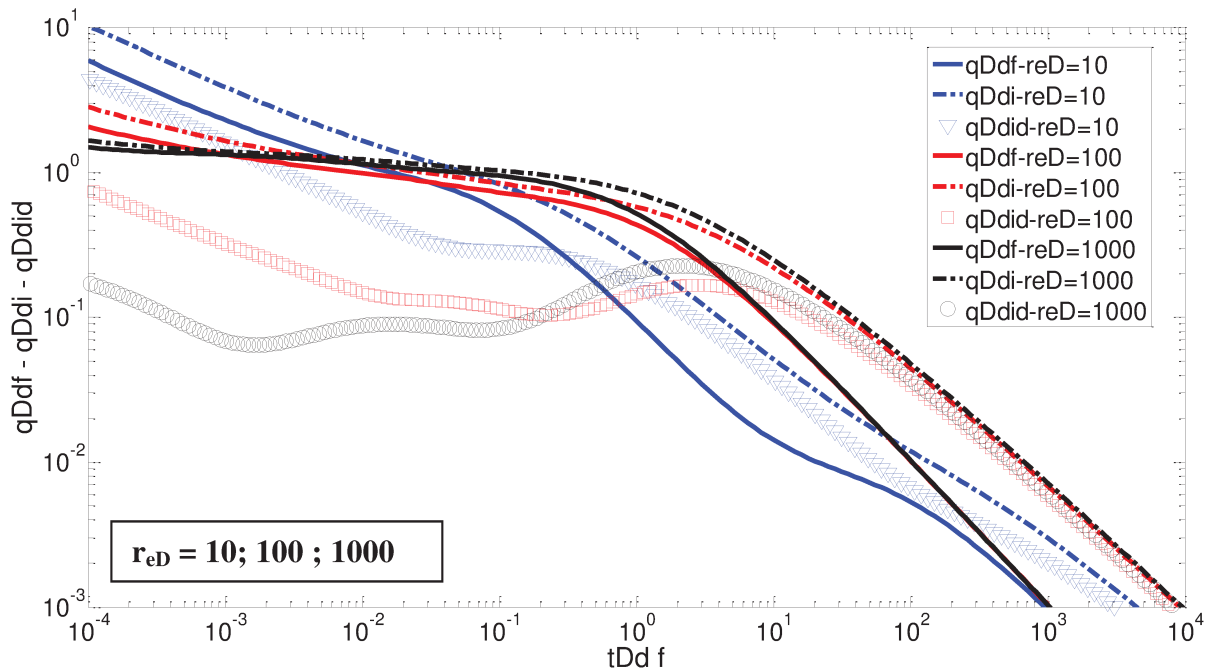


Figure D.3 – Decline type curves for dual porosity systems. $\omega = 0.1$; $\lambda = 1 \times 10^{-4}$.

In **Fig. D.1**, we presents a sensibility of storativity ratio (ω), where unity corresponds to the homogeneous reservoir case. **Fig. D.2** presents different values of interconnectivity coefficient (λ). **Fig. D.3**, shows the sensibility of dimensionless drainage radius (r_{eD}). As can

be seen, the dimensionless decline rate integral derivative ($q_{Dd_{id}}$) is the variable que visually assist in the identification of determined system characteristics.

Derivation of dimensional variables:

The dimensional real variables derivation is the same as described for DMB method, until **Eq. C-17** cited in this appendix as **Eq. D-10**. Blasingame type curve requires the same iterative procedure, to determine the material balance pseudo-time (t_{ca}) for the total fluid volume, as described for DMB.

For total system:

$$\frac{P_{p_i} - P_{p_{wf}}}{q_g} = m_{f+m} t_{ca} + \tilde{b}_{pss} \dots\dots\dots (D-10)$$

Where:

$$m_{f+m} = \frac{1}{G c_{t_i}} \dots\dots\dots (D-11)$$

$$\tilde{b}_{pss} = \frac{142.2 q_{g_i} \mu_{g_i} B_{g_i}}{k_f h} \left[\ln \left(\frac{r_e}{r_{wa}} \right) - \frac{3}{4} + \frac{2(1-\omega)^2 r_{wa}^2}{\lambda r_e^2} \right] \dots\dots\dots (D-12)$$

Eq. D-10 can also be written as **Eq. D-13**, and then reduced to the **Arps (1945)** harmonic decline curve format (**Eq. D-14**) by defining additional dimensionless variables can be defined: dimensionless decline rate (q_{Dd_f}) and dimensionless decline time (t_{caDd}).

$$\frac{q_g}{P_{p_i} - P_{p_{wf}}} \tilde{b}_{pss} = \frac{1}{1 + \frac{m_{f+m} t_{ca}}{\tilde{b}_{pss}}} \dots\dots\dots (D-13)$$

$$q_{Dd_{f+m}} = \frac{1}{1 + t_{caDd}} \dots\dots\dots (D-14)$$

Where:

$$q_{Dd_{f+m}} = \frac{q_g}{P_{p_i} - P_{p_{wf}}} \tilde{b}_{pss} \dots\dots\dots (D-15)$$

$$t_{caDd} = \frac{m_{f+m}}{\tilde{b}_{pss}} t_{ca} \dots\dots\dots (D-16)$$

This means that when pseudo-pressure and the material balance pseudo-time are used to model gas flow, the data trend must decline along the harmonic stem on Fetkovich liquid type curve. Consequently, as \tilde{b}_{pss} is a constant, a match between the Log-Log plot of $\frac{q_g}{P_{pi}-P_{pwf}}$ vs. t_{ca} , and the analytical type curves (q_{Ddf} vs. t_{Ddf}), allows the calculation of the OGIP and formation properties (**Palacio and Blasingame 1993**).

To smooth noisy production data, the normalized pseudo-pressure rate $\frac{q_g}{P_{pi}-P_{pwf}}$ (or q_{Ddf+m}) can be integrated (**Eq. D-17**) and then derived to obtain typical reservoir behavior (**Eq. D-18**).

$$\left(\frac{q_g}{P_{pi}-P_{pwf}} \right)_i = \frac{1}{t_{ca}} \int_0^{t_{ca}} \left(\frac{q_g}{P_{pi}-P_{pwf}} \right) dt_{ca} \dots \dots \dots (D-17)$$

$$\left(\frac{q_g}{P_{pi}-P_{pwf}} \right)_{id} = -t_{ca} \frac{d}{dt_{ca}} \left[\left(\frac{q_g}{P_{pi}-P_{pwf}} \right)_i \right] \dots \dots \dots (D-18)$$

The matching process:

The quantity of independent variables of the type curve plot (ω , λ and r_{eD}), makes difficult the matching process, for this reason we propose the following manual matching process. First the type curves are generated for different values of interporosity flow coefficient (λ), **Fig. D.2**. It provides the behavior of the total system production.

Next, we generate curves for different storativity ratio (ω) values, **Fig. D.1**, for the value of λ found in the previous plot. It helps to differentiate the behavior of a dual porosity from a single porosity system.

Finally, the last type curve sensibility would be the dimensionless drainage radius (r_{eD}), **Fig. D.3**, for the previous values of ω and λ .

Once the match is achieved with production data variables, the type curve plot and the Log-Log plot provides the following information: q_{Ddf} , $\left[\frac{q_g}{(P_{pi}-P_{pwf})} \right]$, t_{Ddf} , t_{ca} , r_{eD} , ω and λ .

The fracture permeability can be calculated from **Eq. D-15**:

$$k_f = \frac{142,2 \mu g_i B g_i}{h} \frac{\left[\frac{q_g}{(P p_i - P p_{wf})} \right]_{MP}}{(q_{Dd_f})_{MP}} \left(\ln(r_{eD}) - \frac{1}{2} + \frac{2(1-\omega)^2 r_{wa}^2}{\lambda r_e^2} \right) \dots\dots\dots (D-19)$$

Wellbore skin is calculated from **Eq. D-20** once the dimensionless external radius (r_{eD}) is obtained from the matching process:

$$S = \ln \left(\frac{r_w}{r_{wa}} \right) \dots\dots\dots (D-20)$$

Where:

$$r_{wa} = \frac{r_e}{r_{eD}} \dots\dots\dots (D-21)$$

The OGIP is obtained from **Eq. D-16**:

$$G = \frac{1}{c_{ti}} \frac{t_{ca}}{t_{Dd_f}} \frac{\left[\frac{q_g}{(P p_i - P p_{wf})} \right]_{MP}}{(q_{Dd_f})_{MP}} \dots\dots\dots (D-22)$$

VITA

Name: Pedro Marcelo Adrian Herbas

Born: December 21, 1983

Place of Birth: Cochabamba, Bolivia

Parents: Julio Adrian Gutierrez
Clery Herbas Salazar

Permanent Address: Los Pororos Street, 2585
Santa Cruz de la Sierra
Bolivia

Education: Universidad Autónoma Gabriel René Moreno (UAGRM)
Department of Petroleum Engineering
B.Sc. in Petroleum Engineering
April, 2008.

Universidade Estadual de Campinas (UNICAMP)
Department of Petroleum Engineering
M.Sc. in Petroleum Engineering
December, 2015.

Technical Interest: Pressure Transient Analysis
Production Data Analysis
Reservoir Engineering

Affiliation: Society of Petroleum Engineers (SPE)
Sociedad de Ingenieros de Bolivia (SIB)